ABSTRACT

Title of Dissertation:	SULFUR ISOTOPE CHARACTERIZATION OF MANTLE RESERVOIRS SAMPLED BY OCEAN ISLAND BASALTS
	James Wosley Dottin III, Doctor of Philosophy, 2020
Dissertation directed by:	Dr. James Farquhar, Department of Geology and Earth System Science Interdisciplinary Center

Ocean islands are volcanic islands in the middle of oceans that are formed when magma deep inside the Earth buoyantly rises to the surface and erupts as basaltic lava (termed Ocean Island Basalt, OIB). Geochemical characterization of OIB have identified multiple chemical reservoirs that reside in the deep Earth, including primordial, recycled, and convective mantle components that contribute material to OIB systems. Stable sulfur isotope compositions of these reservoirs provide an opportunity to constrain the types of material that contribute to this heterogeneity and processes involved in the production of the respective reservoirs. In this dissertation, I present sulfur isotope compositions of basalts from two OIB localities: the Samoan islands and Mangaia (an island in the Cook-Austral suite). Samoa is unique in that it preserves evidence for sampling all identified mantle reservoirs and Mangaia is unique in that it preserves evidence for hosting Archean/early-Proterozoic related sulfur as a result of

mantle recycling. I use sulfur isotopes to constrain how the mantle plume plumbing system beneath Mangaia and Samoa affect the S-isotope compositions erupted at individual islands and identify the prevalence of anomalous S-isotope compositions in different mantle components that reflect a common link to surface material recycled throughout Earth's history. I constrain the primordial sulfur isotope composition of the mantle ($\Delta^{33}S$= 0‰) through analyses of basalts from Ofu, Samoa and show that it is similar to estimates from meteoritic materials. I also test whether Samoa shows geographical zonation for geochemical components through the eruption of multiple isotopically distinct recycled sulfur components that are delivered to specific groups of islands within the island chain. I find that Sulfur isotope compositions of Samoan basalts are unique to each grouping of islands, where HIMU-related and rejuvenated lavas show the most distinct compositions, revealing positive and negative $\Delta^{33}S$ compositions respectively. At Mangaia (extreme HIMU), I test whether isotopically distinct sulfur reservoirs exist within the Mangaia mantle plume. The sulfur isotope compositions measured at Mangaia demonstrate an increased level of S-isotope heterogeneity in the Mangaia mantle plume from previous measurements and point to an additional recycled compositional endmember that is potentially younger than the Archean/early-Proterozoic recycled component previously identified.

SULFUR ISOTOPE CHARACTERIZATION OF MANTLE RESERVOIRS SAMPLED BY OCEAN ISLAND BASALTS

by

James Wosley Dottin III

Dissertation submitted to the Faculty of the Graduate School of the
University of Maryland, College Park, in partial fulfillment
of the requirements for the degree of
Doctor of Philosophy
2020

Advisory Committee:
Dr. James Farquhar, Chair
Dr. Jabrane Labidi
Dr. Matthew Jackson
Dr. Richard Walker
Dr. Vedran Lekic

Preface

In this dissertation, chapter 2 ("Sulfur isotope characterization of primordial and recycled sources feeding the Samoan mantle plume") is that of a previously published work in *Earth and planetary Science Letters* of which I was lead author. I collected all sulfur isotope data. I received aid in interpretation and manuscript writing/revising primarily from Dr. James Farquhar and Dr. Jabrane Labidi. The samples were provided by Dr. Matthew Jackson, who also provided aid in data interpretation manuscript writing/revising. Dr. Vedran Lekic is also included as an author for his help in placing the project into context of geodynamic models and for building a statistical model to test for relationships in the data set. Citation: D**ottin III, J.W.,** Labidi, J., Lekic, V., Jackson, M.G., Farquhar, J. (2020) Sulfur isotope characterization of primordial and recycled sources feeding the Samoan mantle plume. *Earth and Planetary Science Letters*. **534** DOI: 10.1016/j.epsl.2020.116073

Chapter 3 ("Sulfur isotope evidence of geochemical zonation of the Samoan mantle plume") was written with the expectation that it will be prepared for submission to a peer reviewed journal. I improved methods for bulk rock digestions and collected all sulfur isotope data presented. I received aid in writing/revising and data interpretation of Dr. James Farquhar and Dr. Matthew Jackson. Samples analyzed were provided by Dr. Matthew Jackson and Dr. Marcel Regelous.

Chapter 4 ("Bulk sulfur isotope characterization of HIMU mantle feeding the Mangaia mantle plume: Evidence for multiple recycled sulfur reservoirs") is work that has been submitted to *Geochemistry, Geophysics, Geosystems* for publication. Dr.

Jabrane Labidi and I performed the sulfur isotope measurements. I received aid in writing/revising from Dr. James Farquhar, Dr. Jabrane Labidi, and Dr. Matthew Jackson. Samples were provided by Dr. Matthew Jackson and Dr. Jon Woodhead.

Acknowledgements

It goes without saying, that the work presented in this thesis would not have been possible without the love, prayers, hard work, and scientific contributions from so many during my time at UMD. Firstly, I would like to thank my advisors Dr. James Farquhar and Dr. Jabrane Labidi for all their hard work and contributions to this work. From the time I entered the program until my departure, their teaching and mentorship had a significant impact in developing me into the geochemist I am today.

To my wife, Dr. Ruth Y. Dottin, thank you for being by my side and continuously holding me up throughout the ups and downs of my graduate student journey. Without your prayers, endless love, and encouragement, I could not have completed any of the work here. Your constant reminder of my ability to succeed made each workday that much more tolerable. I love you and I appreciate you.

To my family, both the Dottins (James Jr., Sartreina, Tatjana, Janiece, and Sharai) and the Youngs (Curt, Dianne, Issac and Mary, Luke and Dani, Rachel and Seth, Joe and Caitlin), you are endlessly thanked for you love, prayers and encouragement. To my church family and community group, you are thanked for you love and prayers.

I would like to acknowledge members Farquhar Lab group (both past and current) for their support and aid in my development (Daniel Eldridge, Brian Harms, Joost Hoek, Nivea Magalhaes, Maddy Turner, Elizabeth Peters, Aumary Bouyon, Mojhgan Haghnegahdar, Rumya Ravi, and Nanping Wu).

The faculty, postdocs, and graduate students are thanked for their support during my time at UMD. Many of the students and postdocs were willing to take the

time and work closely with me on interdisciplinary project issues. For them (Chao Gao, Katherine Bermingham, Andi Mundl-Petermeier, Phil Piccoli, Vedran Lekic, and Richard Walker), I am grateful.

To my close friends outside of the realm of geology (Paul Deo Jr., Julia Frieze, Lia Monti, Priyanka Moondra, Ryan Sheldon), thank you for listening, supporting and expressing enthusiasm in my work. The love, care, and support were always appreciated and helped fuel interest in the work presented. To my best friend, Alex Ray, thank you for being there every single step of the way. Words cannot express my gratitude.

I owe much thanks to Marth Gilmore and James Greenwood. You both were essential in my road to develop for graduate school. Thank you for believing in me and your investing time to ensure my success. Much gratitude is also due to Suzanne O'Connell for inspiring me to be a geologist. Our time on class field trips (and in class) with Brighty will never be forgotten.

To Lisa Tuitt, thank you for reading my dissertation and providing constructive edits.

I acknowledge support for my projects including conference attendance and travel from the University of Maryland, Ronald E. McNair Graduate Fellowship, National Science Foundation, National Aeronautics and Space Administration, and the Geochemical Society.

Table of Contents

List of Tables

List of Figures

Chapter 1: Introduction

The process of solar system formation started with dust grains orbiting the proto-sun. These grains collided, and in some cases, stuck together. Particles thus formed continued to collide with other particles and grew into larger particles and eventually to form planetesimals that orbited the proto-sun (e.g. Dauphas and Morbidelli, 2014 and citations within). Planetary embryos began to form, gravitationally drawing in these planetesimals to form larger planetary bodies. These processes and residual radioactivity generated enough heat to melt the rocky material, resulting in differentiation into core, mantle, and (in some cases but, not all) a crust. Our planet, Earth, is one of the planets in our solar system that has undergone differentiation (Figure 1).

Our planet's lithosphere (the crust and uppermost mantle) is uniquely divided into segments, termed tectonic plates, that move! These movements, combined with the continuous process of crust formation in parts of the ocean (called mid ocean ridges) and the returning of plates to the mantle at places where plates converge (called subduction), is termed plate tectonics. These plate movements are also one of the major causes of earthquakes, mountain building, and volcanism on our planet. Of the three, volcanism is particularly useful to geologists who want to receive chemical information about material far beneath the ground we stand on, and further, how the reservoirs these rocks reside in have evolved through geologic time.

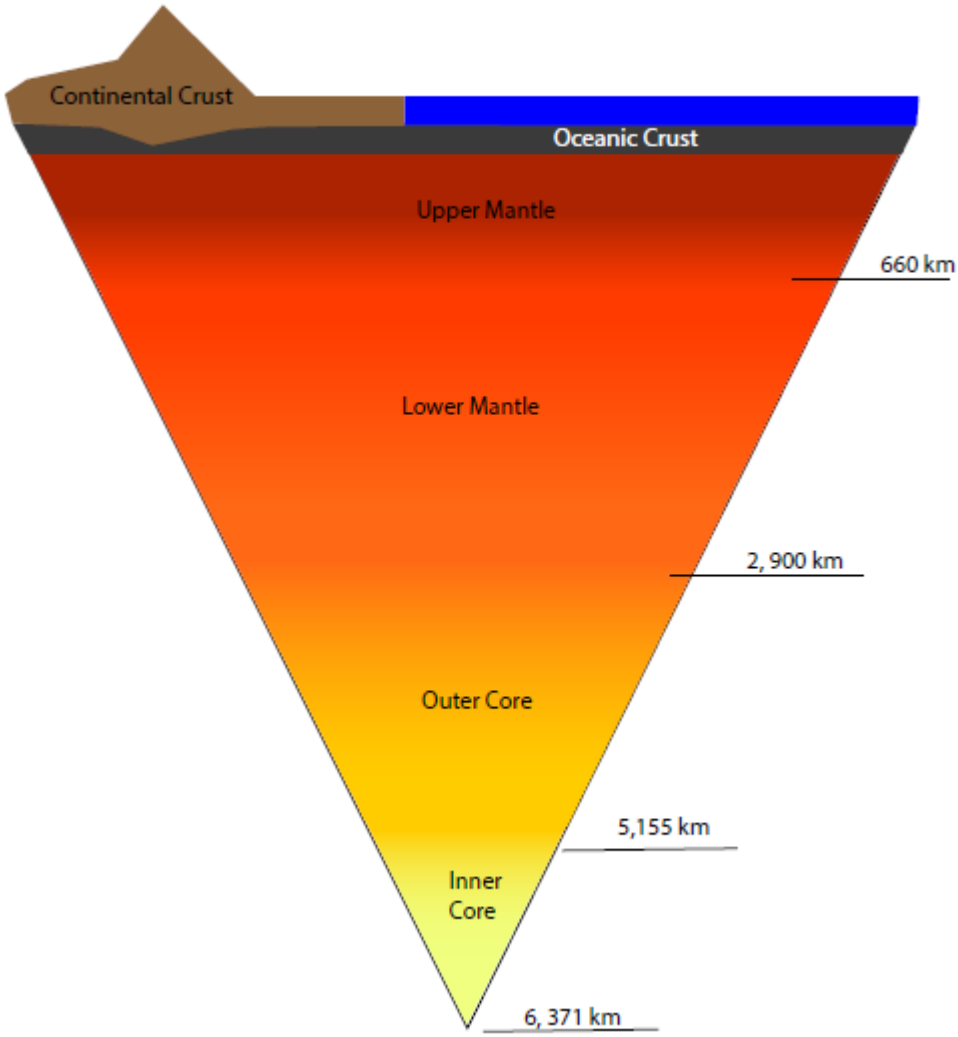

Figure 1. Schematic of the Earth's layers. The core is metal and dense and forms from the gravitational separation of metal from immiscible silicate liquids. The inner core has crystallized and is solid, whereas as the outer core is liquid and convects. The lower mantle and upper mantle are made of silicate minerals and are solid but at depths greater that 100-150 km are hot enough to have deform and convect. The outer most layer of the Earth is the Earth's crust (beginning at the base of the continental/oceanic lithosphere) that is also silicate, but forms more rigid, dynamically shifting tectonic plates. Material from these plates is recycled to the mantle and includes material containing sulfur. Sulfur has a chemical affinity for the Earth's core, resulting in ~ 97% of Earths sulfur sequestered into the core (Dreibus and Palme, 1996), but significant amounts of sulfur are also present in the mantle and crust. The origin of this sulfur and its transfer of sulfur between core, mantle, and crust are a focus of this dissertation.

Volcanoes are formed as springs of molten rock (magma) from deep within the Earth. With volcanic eruptions come hot (and many cases odorous) gases, fire, earthquakes, destruction, and sometimes, a new home for humans and other organisms. Islands, like those in Hawaii, Samoa, and the Cook-Australs were constructed by volcanoes in the middle of oceans where eruptions of molten rock are continuously added to an area until the volcanic pile breaks the ocean's surface. By studying the elemental abundances and isotopic compositions within the rocks from these islands, we know that the magmas preserve signals from the deep Earth and the early Earth; such signals come from right underneath the crust and reach to the Earth's core.

This dissertation explores these ancient messages from the deep Earth using "isotope geochemistry"[1]. Specifically, the dissertation reveals new information from the element sulfur and its isotopic composition preserved in volcanic rocks from the volcanic ocean islands of Samoa and Mangaia. Variations in the sulfur isotope composition of earth materials trace processes that occurred in the past.

Sulfur, the 16th element on the periodic table, is unique in that it has four stable isotopes (or in laymen's terms 3 slightly heavier versions of itself that don't doesn't decay by radioactivity). As the Earth evolves, chemical processes cause the isotopes to fractionate the proportions of the four isotopes in sulfur-bearing compounds which can be incorporated into the rock record. In some cases, sulfur with isotopic signatures of processing at Earth's surface are transferred into the mantle through subduction at

[1] Isotopes are atoms of the same element with a different mass as a result of a different number of neutrons in the nucleus.

convergent plate margins. Analyses of volcanic rocks suggest that some of this subducted sulfur is returned to Earth's surface by volcanoes that form ocean islands.

A variety of processes can fractionate sulfur isotopes that yield variable S-isotope compositions which allows different localities on Earth to host unique S-isotope compositions in the rocks. Materials that are subducted into the mantle can possess different S-isotope compositions, and depending on where they are returned to the surface, different signatures can be produced at different ocean islands. The variable signatures observed among different islands in this dissertation provide insight into the types of compositions that are recycled through the mantle and also insight into rock from the ancient deep earth reservoir that is brought to the Earth's surface for the first time. These different compositions ultimately tell about how various sulfur reservoirs interact with one another in the mantle and further, how mantle dynamics play a role in the S-isotope compositions observed at ocean islands.

1.1 Overview of this study's research findings

Sulfur isotope data for a suite of whole rock samples of basalts from Samoa (Chapter 2) reveal a relationship between the isotopic compositions of sulfur (S), radiogenic tungsten (W), radiogenic helium (He), and radiogenic lead (Pb) that points to a contribution from a deep, ancient, primordial mantle reservoir. Recent studies (Mundl et al., 2017; Mundl-Petermeier et al., 2020) have argued that tungsten and helium data reflect interactions with the Earth's core, early differentiation of silicate reservoirs, or late accretion. The observed relationships with sulfur place constraints on the primordial S-isotope composition of the mantle, and further, the S-isotope composition of other deep mantle reservoirs. The relationships between S, W, He, and

Pb support a plumbing system of the mantle plume feeding Samoa with at least four sulfur reservoirs.

Chapter 3 examines connections with these mantle reservoirs and the plume system by study of S geochemistry of a variety of islands associated with Samoa. Previously published work by Jackson et al. (2014) identified unique radiogenic Pb isotope compositions associated with separate grouping of islands at Samoa, that the called the Vai trend, the Malu trend, the Upo trend, and a rejuvenated signature. Each of these groups display Pb isotope compositions that allude to dilute contributions from the archetypal mantle reservoirs: EM I (rejuvenated basalts), EM II (Malu Trend), HIMU (Vai Trend), and Depleted MORB (Upo trend). By characterizing the S-isotope composition of the various compositional Pb isotope trends at Samoa, the data reveal unique S-isotope compositions associated with each of the various compositional trends and affirm suggestions of multiple ancient recycled and present day crustal sources feeding the Samoan mantle plume.

Chapter 4 presents S-isotope data on olivine and pyroxene mineral phenocrysts (mineral crystals that formed in a magma chamber at depth) from the island Mangaia, part of the Cook-Austral islands, that characterize sulfur from a heterogeneous source area that included multiple melts and multiple sources of melts. At least three distinct compositional endmembers are identified and are observed because the phenocrysts act as capsules that trapped sulfur during the process of mixing. These sources represent different types of oceanic crust that were recycled to the mantle.

Prior to this work, a study by Cabral et al. (2013) documented sulfur mass-independent fractionation at Mangaia (S-MIF, a unique signature in S-isotopes that is

very ancient-see section 1.7) in individual sulfide grains using Secondary Ion Mass Spectrometry (SIMS) and from one bulk sulfide measurement from an olivine separate using the SF_6 method. Their observations suggest sulfur hosted in oceanic crust with S-MIF from the Archean (> ~2.5 Ga) is subducted and recycled through the mantle, where it is preserved, incorporated into the mantle plume, and erupted at Mangaia. This dissertation provides data from phenocrysts of 5 basalt flows from Mangaia. Samples analyzed here show evidence for at least two exotic sulfur isotope compositions that are mixed in the Mangaia mantle plume, and one could be the endmember identified by Cabral et al. (2013). Using relationships between sulfur and radiogenic lead, it is argued that the two sources of sulfur are recycled and are potentially distinct from one another in terms of age, where the mixing component identified in this study is potentially younger than the component identified by Cabral et al. (2013). The chapter discusses possible reason for the multiple S components and outlines how each hypothesis can impact the observed compositions.

1.2 An introduction to sulfur isotope notation

The research presented in this dissertation is primarily focused on measurements of sulfur and its 4 stable isotopes: ^{32}S, ^{33}S, ^{34}S, and ^{36}S. ^{32}S, ^{33}S, ^{34}S, and ^{36}S have solar system abundances of 95%, 0.75%, 4.21%, and 0.02% respectively. By convention the isotope ratios are reported using the following (reported in units of ‰):

$$\delta^{34}S = [((^{34}S/^{32}S)_{sample} / (^{34}S/^{32}S)_{CDT}) - 1]$$

$$\delta^{33}S = [((^{33}S/^{32}S)_{sample} / (^{33}S/^{32}S)_{CDT}) - 1]$$

$$\delta^{36}S = [((^{36}S/^{32}S)_{sample} / (^{36}S/^{32}S)_{CDT}) - 1]$$

The notation above is used to describe mass-dependent fractionations and data are normalized to Canyon Diablo Troilite (CDT) to facilitate direct comparison with meteorite analyses[2]. Repeat analyses on a single reservoir of standard gas (IAEA-S1) yields the following: -0.401‰, 0.116‰, and -0.796‰ for $\delta^{34}S$, $\Delta^{33}S$, and $\Delta^{36}S$. A second set of notations, Δ-notation (Figure 2), was devised to differentiate mass-dependent from mass-independent fractionation and are defined as (in units of ‰):

$$\Delta^{33}S = [(^{33}S/^{32}S)_{sample}/(^{33}S/^{32}S)_{CDT}] - [(^{34}S/^{32}S)_{sample}/(^{34}S/^{32}S)_{CDT}]^{0.515}$$

$$\Delta^{36}S = [(^{36}S/^{32}S)_{sample}/(^{36}S/^{32}S)_{CDT}] - [(^{34}S/^{32}S)_{sample}/(^{34}S/^{32}S)_{CDT}]^{1.9}$$

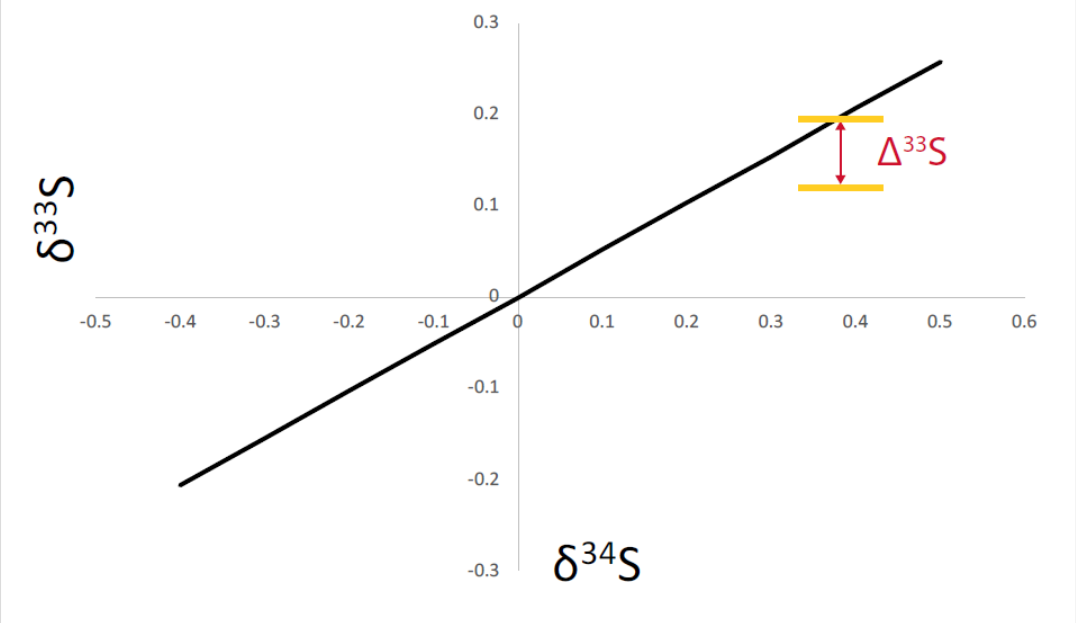

Figure 2. Schematic illustration of how the Δ notation is determined. In this plot, $\Delta^{33}S$ is shown as a deviation from a mass-dependent fractionation array between $\delta^{33}S$ and $\delta^{34}S$.

The exponents of 0.515 and 1.9 are used to define the mass-dependent relationships of $\delta^{33}S$ and $\delta^{36}S$ where $\delta^{33}S = 0.515 \times \delta^{34}S$ and $\delta^{36}S = 1.9 \times \delta^{34}S$ (Hulston and Thode, 1965).

[2] Note that $\delta^{34}S$ relative to V-CDT is -0.3 (Robinson, 1995)

These relationships approximate equilibrium mass-dependence that reflect the role of mass in fractionation of isotopes. $\delta^{33}S$ varies as approximately one half (≈ 0.515) the variation of $\delta^{34}S$ because the difference in mass between ^{33}S and ^{32}S is 1 amu, which is one half the mass difference of ^{34}S and ^{32}S, 2 amu. The same rule applies for $\delta^{36}S$ seeing that it varies as approximately two times (≈ 1.9) the variation of $\delta^{34}S$ because the mass difference between ^{36}S and ^{32}S is 4 amu. The exponent values are not exactly .5 and 2 due to the way that energy scales with mass as described by statistical mechanics (Hulston and Thode, 1965). From $\Delta^{33}S$ and $\Delta^{36}S$, an isotopic value for a mass dependent process would have $\Delta^{3x}S \approx 0‰$ and $\delta^{3x}S \approx 0.515 \times \delta^{34}S$. Correspondingly, samples with enrichments or depletions in an isotope that were produced by chemical or physical processes that reflect properties other than mass (e.g. electron spin, chance overlap between electronic states, and external controls such as non-uniform (selectively shielded) UV spectra) can yield $\Delta^{33}S$ values that are not equal to zero and is thus non-mass-dependent or mass-independent. The focus of this thesis is related to evaluating both mass-dependent and mass-independent sulfur isotope signals from deep mantle derived rocks.

1.3 S-isotope fractionation mechanisms

1.3.1 Mass dependent effects

Equilibrium isotope effects (EIE) occur in equilibrium chemical reactions where the reaction is reversible. The EIE work by distributing the isotopes among the reactants and products in such a way that it minimizes the total energy in the system, where the energy in the system is dependent upon the vibrational frequencies of the isotopologues.

The amount of fractionation governed by the equilibrium isotope effect scales with temperature, mass, and bond stiffness. The magnitude of fractionation normally decreases with increasing temperature (proportional to $1/T^2$ at its high temperature limit) and increases for elements with larger mass ratios ($(m_h+m_l)/(m_h*m_l)$, *where* m_h *= the mass of the heavy isotope and* m_l *=the mass of the light isotope)*. The heavy isotope is concentrated in the phase with the stiffest bond. Reversals in equilibrium fractionations between phases can occur when vibrational modes differ by a significant amount, for instance if high frequency vibrations are associated with bonds involving hydrogen in one phase, but only lower frequency modes occur for the partner phase.

The minimization of energy in the system is directly related to the total energy of each molecule, defined as $E_{total}= E_{vibrations}+E_{rotations}+E_{translations}$. The various energy types exist at multiple quantum states that can be defined as the partition function $Q=\Sigma g_i e^{-E/KT}$, where (g is a statistical term to account for possible degeneracy, k is Boltzmann's constant $1.380658x10^{-23}$J/K, i represents the possible quantum states, and T is temperature in K) and the total partition function is defined as $Q_{total}= Q_{vibrations}+Q_{rotations}+Q_{translations}$.

The vibrational partition function can be illustrated by considering a diatomic molecule, where each isotope in the molecule has some amount of potential energy, illustrated by the potentially energy well (Figure 3).

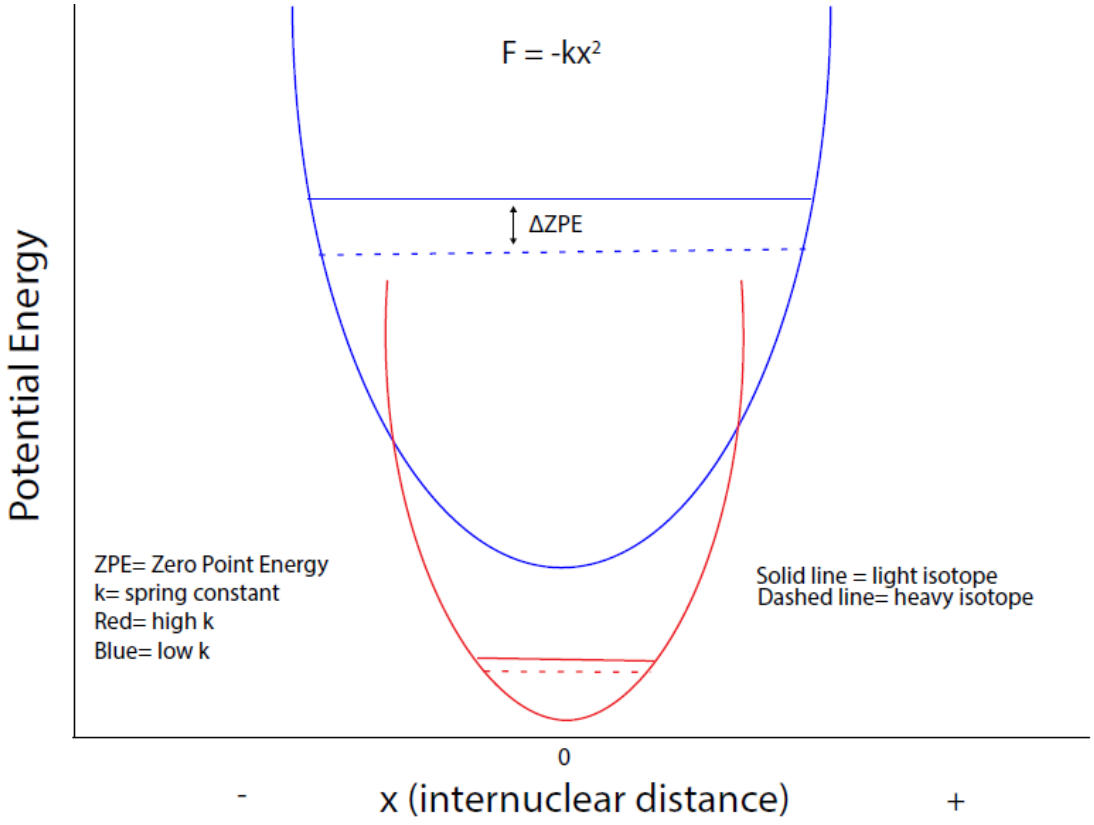

Figure 3. Zero Point Energy (ZPE) differences shown on a graph of potential energy vs. displacement from classical resting position between heavy and light isotopologues of the same element in two different bonds. The tighter (red) bond results in larger ZPE differences between the heavy and light isotopologues. From a simple spring relationship, the heavy isotope will preferably partition into the tighter potential energy well, as a greater ZPE difference indicates a tighter bond.

The molecules will have an average spacing between one another as a result of repulsive and forces of the bond that are imposed by the molecular orbitals. The energy difference that describes this distance is defined as $E=(n+1/2)h\nu$. where n is the vibrational energy level (n = 0, 1, 2, etc.), h = Planck's constant (6.62608×10^{-34} J·sec, ν= frequency ($(1/2\pi)(k/\mu)^{0.5}(sec^{-1})$). Thus, even at the ground state, the molecules have Zero Point Energy, which is related to the strength of the bonds within the molecule. The frequency of the molecule can be expressed as $\nu=(1/2\pi)*\sqrt{(k_s/\mu)}$, where

$\mu=m_1m_2/(m_1+m_2)$ and K_s is the spring constant. The equation for frequency, thus, states that when the heavier isotope is partitioned into the molecule, the frequency decreases resulting in a vibrational level with lower potential energy, where in turn, it becomes more difficult to break the bond of the molecule. Near the energy minimum, the potential well approximates a simple harmonic oscillator, $Q_{vib}=\Sigma e^{-(n+1/2)h\nu/kT}$, this equation can be simplified to $Q_{vib}=e^{-U/2}\Sigma e^{-(n)U}$ where $U=h\nu/kT$. For further simplification, an approximation can be applied where $\Sigma x^n=1/(1-x)$, and $0<x<1$. As a result, the final equation for the vibrational partition function is $Q_{vib}=e^{-U/2}*(1/(1-e^{-U}))$. The translational and rotational partition function are dependent on a number of terms that eventually cancel, but are simpler and can be expressed as $Q_{2\ tr}/\ Q_{1\ tr}=(M_2/M_1)^{3/2}$ and $Q_{2\ rot}/\ Q_{1\ rot}=(\sigma_1 I_2)/\ (\sigma_2 I_1)$. Ultimately, the partition function ratio can be expressed as $[Q_2/\ Q_1]=[(M_2/M_1)^{3/2}]*[(\sigma_1 I_2)/\ (\sigma_2 I_1)]*\ [(e^{-U*/2}(1/(1-e^{-U})))/(e^{-U/2}(1/(1-e^{-U*})))]$. All terms in the partition function ratio equation have mass terms and this is where the mass dependence arises for isotopic exchange reactions.

Kinetic isotope effects (KIEs) occur in unidirectional reactions and are described in Bigeleisen and Wolfsberg (1958), Thornton and Thornton (1970), Melander and Saunders (1980). Many KIE involve a transition state that sits in between the reactant and product states. The rate of reaction for specific isotopes reflects the 'commitment' to the product state of a proportion of the population that occupies the transition state at any given time. The isotopic makeup of this population in the transition state depends on isotopic mass and associated vibrational frequencies in both the transition state and the reactant state, but not on products states generated unidirectionally by commitment from the transition state. A simple way to think about

KIE is that there is a reversible exchange (equilibration) between the reactant states and the transition state, and that the isotope ratios of the transition state are then transferred directly via a leak to the product states. There can be a small correction related to tunneling that links reactant state more directly to the product state or if the product states feed back to the transition or reactant states.

The process of kinetic isotope fractionation has been described using:

$$\frac{K_2}{K_1} = \left(\frac{V_{\ddagger}^*}{V_{\ddagger}}\right)\left[\left(\frac{Q_2}{Q_1}\right)_{tunneling}\left(\frac{Q_{vib}^*}{Q_{vib}}\right)_{TS} / \left(\frac{Q_{vib}^*}{Q_{vib}}\right)_{RS}\right]$$

K_2/K_1 is the ratio of forward reactant rates for different isotopic species. Translations, rotations, and vibrations that describe movements of atoms or groups of atoms in the reactant state (RS) and transition state (TS) are embedded in the partition function ratios in the same way as they are for EIE. The additional term $\left(\frac{V_{\ddagger}^*}{V_{\ddagger}}\right)$ describes the translation of atoms along the reaction coordinate (bond breaking/making) that passes through the transition state to the product state in terms of an imaginary frequency since the path across transition state crests an energy maximum that can be treated with similar physics to the vibrations that are bound by the energy minima of the bound states. The term $\left(\frac{Q_2}{Q_1}\right)_{tunneling}$ is referred to as a tunneling connection which is the probability of tunneling through the PE barrier. Tunneling refers to paths that do not pass over the top of the PE barrier but 'pass through it'. Tunneling corrections are typically related in part to the energy tails and a treatment of the reaction coordinate by classical mechanics (Melander and Saunders, 1980).

Typically, the transition-state has broader (more weakly bound) real frequencies than the reactant state. This results in closer spacing of energy levels, lower ΔZPE, resulting in an enrichment of the lighter isotope in the TS compared to the RS and leads to a light isotope enrichment in the products. In cases where the TS is a deep, tight well, an inverse kinetic isotope effect that yields an enrichment of the heavier isotope in the TS and products is possible. Given that the terms in KIE are the same as those for EIE and all depend on mass, a similar mass dependence arises. Note that when KIE are treated solely in terms of $\left(\frac{V_{\ddagger}^{*}}{V_{\ddagger}}\right)$ (ignoring the tunneling correction) that the mass dependence yielded is proportional to the square root of the masses (Young et al., 2002) rather than the relationships typically given by EIE[3].

1.3.2 Mass-independent effects (MIF)

KIEs are also responsible for mass-independent isotope signatures. Such is the case when the effect is governed by factors such as electron spin, molecular symmetry, or overlap between multiple energy states versus mass-dependent factors. EIEs can also be responsible for MIF when factors such as nuclear volume influence bond energies (Bigeleisen, 1996; Schauble, 2007)

For S isotopes, mass-dependent fractionation processes yield variations in $\delta^{34}S$, but not significant variations in $\Delta^{33}S$. However, MIF can produce large variations for $\Delta^{33}S$. Small $\Delta^{33}S$ variations can be produced when EIE and KIE are linked in network

[3] The square root mass relationship approach is commonly seen in the geochemical literature and give the false impression that KIE have a distinctly different mass dependence than EIE. The mass dependence of KIE is intermediate between that given by the square root mass relationship and that given by the quantum mechanical treatment of the real vibrational frequencies.

through (1) mass conservation effects such as isotope mixing (Farquhar et al., 2007) and Rayleigh distillation (Ono et al., 2006). Isotope mixing can produce small shifts in $\Delta^{33}S$. Mixing occurs when two discrete sulfur-bearing reservoirs (or pools) mix and subsequently experience the removal of one endmember composition from the other endmember composition involved. Significant effects are observed, however, from fractionations associated with metabolic processing of sulfur, resulting in large $\delta^{34}S$ fractionations. Additional effects such as the magnetic-spin effect (Oduro et al., 2011) and those associated with small temperature gradients (~100 degrees) can also produce variations in $\Delta^{33}S$ (Sun and Bao, 2011). Effects associated with spin, however, require a difference in pairing of electron and nuclear spin and are also known as odd (as in odd vs even mass) isotope anomalies.

The most commonly seen type of MIF are associated with gas phase photochemistry. Photochemistry is used here to describe any chemistry initiated by absorption of light to produce photoexcited products. In some cases, the absorption is directly the species that exhibits the isotopic fractionation. In other cases, the absorption produced species that initiate a reaction sequence that produces the isotopic fractionation in other species. In all cases, the reactions involve electronically-excited states[4]. When a gas phase molecule is exposed to a light source, the absorbed energy (λ) drives an electronic excitation to higher electronic orbitals and forms a new state for the molecule. The jump in energy levels results in a change in shape of the molecule, the position of atoms, and the PE well. These changes can cause further reactions

[4] The term state refers to the electronic configuration of a molecule. If the electrons are in different sets of orbitals due to excitation, they are in one of potentially many excited states. If electrons are in their lowest energy levels the molecule is said to be in its ground state.

through photoexcitation or crossing over to other states, an isotopically selective process that can depend on factors such as electron spin or the chance of overlap between states. During photo-absorption and excitation, molecules can experience the Frank Condon effect, which describes the probability of molecules transitioning from one state to another state and its dependence on the nuclear coordinates which are describe by probability density functions of the two states. As isotope mass increases, there are changes in the vibrational frequencies. The changes in vibrational frequency will affect the overlap of nuclear position and the probability of further photoexcitation, which ultimately impacts the overall reaction rate. Processes such as self-shielding or mutual shielding have also been invoked for the production of S-MIF. This is a process in which vibrational features of an isotopologue (e.g. $^{32}SO_2$) are shifted an absorbed electromagnetic wavelengths, leaving the remaining isotoplogues susceptible to photodissociation (e.g. Lyons, 2007).

1.4 Geochemistry of the mantle

A major objective in deep-earth geochemistry is to develop a model that defines the origin and evolution of the chemical reservoirs in the mantle. The variability and endmember compositions presented in isotope and trace element data from Ocean Island Basalts and Mid-Ocean Ridge Basalts have provided the foundation for identifying these chemical reservoirs. With associated chronometers, timescales on which these reservoirs formed and evolved yield added insight into the origin and evolution of the various reservoirs.

This dissertation aims to constrain the origin and evolution of deep Earth mantle reservoirs through S-isotope analyses of Ocean Island Basalts (OIBs). Ocean Island

Basalts (OIBs) are basaltic rocks that are found on volcanic islands or where volcanic islands are forming in the ocean. Generally, OIBs are located on oceanic crust and they form away from tectonic plate boundaries (with the one exception of Iceland where volcanism is produced at a spreading center in the Atlantic Ocean). The volcanic islands formed from ocean island basalt occur in places where there is upwelling of hot magma from within the mantle and are typically associated with mantle plumes. The exact origin of most plumes has been a subject of debate but may be resolvable with the combination of seismological and geochemical observations.

1.4.1 Radiogenic isotope compositions of Earth's mantle

Work using radiogenic isotopes of strontium (Sr), neodymium (Nd), and lead (Pb) isotope compositions of Mid-Ocean Ridge Basalts (MORB) and Ocean Island Basalts (OIB) define four distinct, isotopically extreme, geochemical endmembers of the mantle (Figure 4). One endmember, the Depleted MORB Mantle (DMM) is defined by relatively low $^{206,207,208}Pb/^{204}Pb$ and $^{87}Sr/^{86}Sr$ that is associated with high $^{143}Nd/^{144}Nd$ and is argued to have formed as a result of melt extraction during the formation of the Earth's crust. Another endmember, Enriched Mantle I (EM I) is defined by its low $^{143}Nd/^{144}Nd$, high $^{87}Sr/^{86}Sr$, low $^{206}Pb/^{204}Pb$, and high $^{208}Pb/^{204}Pb$ as a result of recycling either delaminated subcontinental lithosphere (McKenzie and O'nions, 1983) or ancient pelagic sediment (Hawkesworth et al., 1986; Mahoney et al., 1991; Milner and le Roex, 1996). An additional enriched mantle reservoir, Enriched Mantle II (EM II) is characterized as having high $^{87}Sr/^{86}Sr$ and high $^{208}Pb/^{204}Pb$ for a given $^{206}Pb/^{204}Pb$ that is argued to reflect the recycling and incorporation of terrigenous sediments from

continental crust (e.g. Jackson et al., 2007a; Workman et al., 2008). HIMU (high μ, $\mu=^{238}U/^{204}Pb$) is generally thought to have formed from recycling oceanic crust that experienced Pb loss upon subduction into the mantle (e.g. Chauvel et al., 1992; Kelley et al., 2005), but has also been argued to be the result of incorporating delaminated metasomatized subcontinental lithospheric mantle in the plume source (e.g. Weiss et al., 2016).

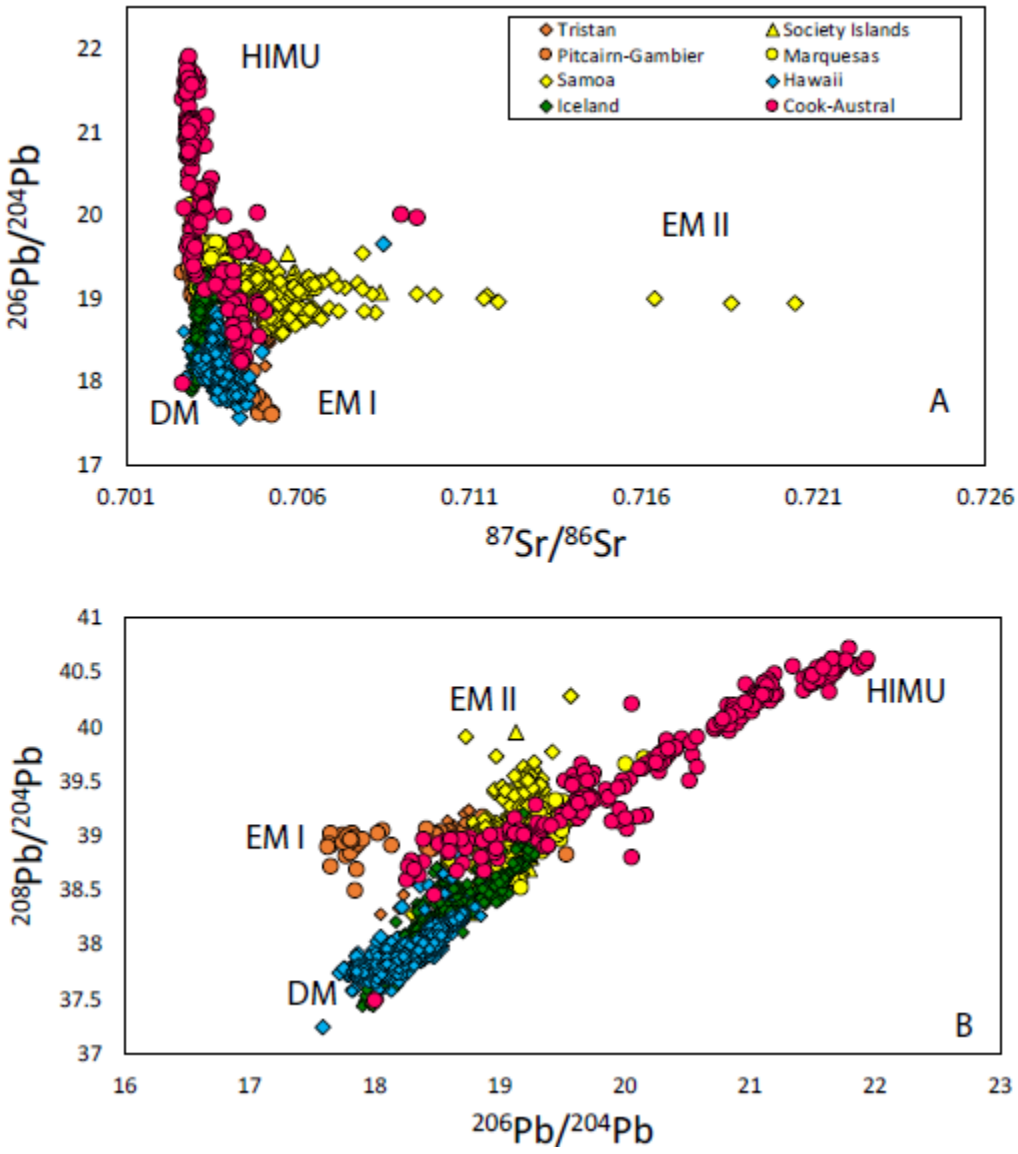

Figure 4. (A) $^{87}Sr/^{86}Sr$ vs. $^{206}Pb/^{204}Pb$ and (B) $^{206}Pb/^{204}Pb$ vs. $^{208}Pb/^{204}Pb$ for OIB sources as an exemplary illustration of geochemical compositions that define the extreme mantle endmembers. Data are from the GeoRoc database.

In addition to recycled components and a depleted upper mantle from crust formation, studies that report radiogenic isotope compositions of OIB argue that reservoirs of *primordial* (early formed and undisturbed) material are preserved. Evidence is provided through high $^{3}He/^{4}He$ ratios in Hawaii (Kurz et al., 1982; Honda et al., 1993; Valbracht et al., 1997), Samoa (Jackson et al., 2007b; Jackson et al., 2009a), Iceland (Kurz et al., 1985; Graham et al., 1998; Hilton et al., 1999; Trieloff et al., 2000; Macpherson et al., 2005), the Galapagos (Graham et al., 1993; Kurz and Geist, 1999; Saal et al., 2007), and Baffin Island (Stuart et al., 2003). Additional evidence for early-formed "primordial" mantle domains is observed through excess ^{20}Ne and ^{21}Ne in Terceria Island (Madureira et al., 2005) and the Galapagos (Kurz et al., 2009), and negative $\mu^{182}W$ values in Samoa and Hawaii (Mundl et al., 2017; Mundl-Petermeier et al., 2020). The formation of these primordial domains is a subject of debate, but may be related to a reservoir at the base of the mantle that underwent core-mantle exchange (Mundl-Petermeier et al., 2020).

As it stands, determining whether ocean islands host primitive components has employed measurements from He and W isotope systems. Measurements from these systems can be used as a proxy for identifying samples with primordial components and when used in conjunction with stable isotope systems, such as that for sulfur, the primordial isotope compositions can be further defined for other elements that cannot show isotope compositions that directly link to the very early, unprocessed mantle.

1.5 History of S-isotopes in Earth's mantle

The S-isotope composition of the mantle was first interpreted to be homogenous in $\delta^{34}S$, with values showing on average 0.5 ± 0.6 ‰ and 0.5 ± .05 ‰ for Mid Ocean Ridge Basalts (MORB) and Ocean Island Basalts (OIB) respectively (Kanehira et al., 1973; Sakai et al., 1982; Sakai et al., 1984). Work by Labidi et al., (2012, 2013, 2014) reassessed the S-isotope composition of MORB with modified digestion techniques and higher analytical precision and showed that the upper mantle sample by MORB was depleted in ^{34}S, with $\delta^{34}S$ averaging (-0.91‰ ±0.2). The depletion is argued to be a relict of core-formation where ^{34}S is preferentially partitioned into the core relative to the mantle.

Recent analyses of OIB have also demonstrated that the S-isotope composition of mantle is heterogeneous. However, unlike MORB, the heterogeneity in S-isotopes of OIB is the result of recycling oceanic and continental crust.

At Samoa, the type locality for the EM II mantle reservoir, $\delta^{34}S$ of reduced and oxidized sulfur species measured at Vailulu'u, Malumalu, and Tau'u is heterogeneous with $\delta^{34}S$ values ranging from +0.11‰ to +2.79‰ in sulfide and from +4.19‰ to +9.71 ‰ in sulfate (Labidi et al., 2015). The $\delta^{34}S$ values of reduced sulfur were found to be positively correlated with $^{87}Sr/^{86}Sr$ and the positive correlation is argued to reflect the incorporation of continental crust with positive $\delta^{34}S$.

At Mangaia, an island in the Cook-Austral suite of islands and the type locality for the HIMU mantle reservoir, individual sulfide grains analyzed using Secondary Ion Mass Spectrometry (SIMS) are shown to preserve mass-independent $\Delta^{33}S$ (down to

$\Delta^{33}S$ = -0.34‰ ±0.07), that has been confirmed with a bulk sulfide measurement that reveals a $\Delta^{33}S$ of -0.12‰ ±0.04. In addition, $\delta^{34}S$ values range from -3.25‰ (±2‰) to -17.25‰ (±0.61‰) (including measurements from SIMS and the bulk sulfide measurement). The nature of the anomalous $\Delta^{33}S$ led to arguments that the values reflect the incorporation of recycled Archean components associated with subducted oceanic crust.

Similarly, at Pitcairn, the type locality for EM I, S-isotope compositions of individual sulfides show negative $\delta^{34}S$ (down to -5.94‰ ± 0.15) and negative $\Delta^{33}S$ (down to -0.85‰ ± 0.13) that is also argued to be a reflection of recycled Archean sulfur. For both Mangaia and Pitcairn, what remains unanswered is the cause of the negative $\delta^{34}S$. Further exploration of this problem is discussed in Chapter 4.

1.6 S-isotope composition of primitive meteorites

This dissertation focuses on sulfur isotope geochemistry of the Earth's mantle and not those of other solar system bodies. One aspect of this geochemistry is understanding the S-isotope composition of the bulk earth. As a community, we use meteorites and other solar system materials to constrain the bulk Earth sulfur isotope composition.

Meteorites are broken up pieces of planets, planetesimals, and other solar system materials that make their way to Earth. They preserve information related to isotope compositions of the early solar system and processes that occur on solar system bodies. Although meteorite work is not the focus of this dissertation, work in this dissertation uses the primitive meteorite record as a reference point when

normalizing data and as a source of context when evaluating primordial compositions that may be preserved on Earth (Chapter 2). Context for the primitive meteorite record partially reflects meteorite work I have completed in parallel with this dissertation research (Dottin et al., 2018b; Wu et al., 2018).

Meteorites can generally be divided into two classifications: chondrites and achondrites. Chondrites are stony, broken up pieces of primitive asteroids that host chondrules which are condensates from the early solar system. Achondrites don't have chondrules and include iron meteorites (representative of cores from differentiated asteroids) and stony-iron meteorites, in addition to stony meteorites. Note a subset of these, basaltic achondrites, represent surface material from differentiated planetessimals and planets (e.g. Mars and the moon) and asteroids (e.g., Vesta).

Sulfur isotope compositions of different meteorite groups vary in systematic ways that provide information about their formation and processing and associations. Bulk S-isotope compositions in ordinary and enstatite chondrites range from $\delta^{34}S$= -0.4±0.04 to 0.6 ±0.04 (1σ) (Gao and Thiemens, 1993b) and carbonaceous chondrites have $\delta^{34}S$ values that range from -0.70±0.15 to +0.18 ± 0.15 (Labidi et al., 2017); also see Gao and Thiemens, 1993a) and an average $\Delta^{33}S$ of +0.021±0.071 (1σ) (Labidi et al., 2017). Iron and stony-iron meteorites have $\delta^{34}S$ values that extend from -0.799 ±0.3 to 0.888 ±0.3 (2 SD) (Antonelli et al., 2014; Dottin et al., 2018b) and $\Delta^{33}S$ variation that ranges from -0.027 ± 0.002 (average for IIIF group) to +0.022± 0.002 (2 SE) (average from IVA group) . The Howardite-Eucrite-Diogenite group also shows variability in S-isotope composition with values ranging from -0.22 ± 0.18 to

0.81 ± 0.18 (2 SD) in $\delta^{34}S$ and 0.006 ± 0.008 to 0.024 ± 0.008 (2 SD) in $\Delta^{33}S$ (Wu et al., 2018).

Overall, both the chondrite and achondrites show S-isotope variability, but it is important to note that these variations are small relative to Earth materials (see next section). Although the $\delta^{34}S$ variability of the different meteorite groups is explained with different parent body processes such as sulfur loss during evaporation (e.g. Wu et al., 2018), the $\Delta^{33}S$ variability in meteoritic materials is uniformly argued to reflect complex photochemistry in the early solar nebula. The homogeneity observed among large bodies is argued to reflect homogenization of sulfur via widespread generation of iron sulfides and averaging processes that occur during processing of protoplanetary materials.

Other solar system materials like Mars also show evidence for S-MIF. Martian meteorites reveal $\Delta^{33}S$ values that range from +0.260 ± 0.008 to -0,76 ± 0.15 (Franz et al., 2014; Dottin et al., 2018a; Franz et al., 2019) as a result of assimilating MIF from surface into the overriding lava flows, but the bulk $\Delta^{33}S$ of Mars is within error of 0 (Franz et al., 2014; 2019). Comparatively, the Earth (convective mantle and primordial mantle) and the moon also have compositions that are within uncertainty of zero, which is normalized to Canyon Diablo troilite, where $\Delta^{33}S = 0$ (Labidi et al., 2014; Wing and Farquhar, 2015; Dottin III et al., 2020)[5].

[5] Note that the recycling of continental slabs into the Earth's mantle has resulted in the contamination of this value with components that have $\Delta^{33}S \neq 0$ and the partitioning of sulfur into the core (resulting in ~2 wt% sulfur in the core and ~0.5% for bulk silicate earth (Dreibus and Palme, 1996) yielded an upper mantle $\delta^{34}S$ of -0.9‰ (Labidi et al., 2014).

1.7 The Archean sulfur isotope record and its relationship to recycled components

Ocean island basalts reveal evidence for recycled oceanic and continental crustal components that are generally dated using long-lived radiogenic isotope systems. Localities such as Mangaia and Pitcairn have had sulfur isotopes analyzed in their basalts. The analyses from Mangaia (Cabral et al., 2013) and Pitcairn (Delavault et al., 2016) demonstrate evidence for S-MIF that is linked to an Archean origin. The leading hypothesis for generation of this signal at these hot spot localities is that subducting oceanic crust with Archean related sulfur into the mantle is subsequently entrained into the mantle plume feeding the ocean islands. In order to provide context, below I outline some of the major findings related to S-isotope compositions for the Archean rock record and the rock record that extends through the Proterozoic and into the Phanerozoic. Sedimentary features on continents are not the focus of this dissertation. However, the information within these rocks provides context for the types of isotope signatures that can be transferred from the surface and into the Earth's mantle through subduction. These sedimentary features typically host a wealth of information related to Earth's geologic history and particularly historical events that occurred on Earth's surface and in the Earth's atmosphere.

In localities such as south Africa, western Australia, Canada, and Greenland, the rock record displays large variations in $\Delta^{33}S$, ranging from ~ -3‰ to + ~14‰ (see compilation in Killingsworth et al. (2019)) throughout the Archean into the earliest Proterozoic (Figure 5).

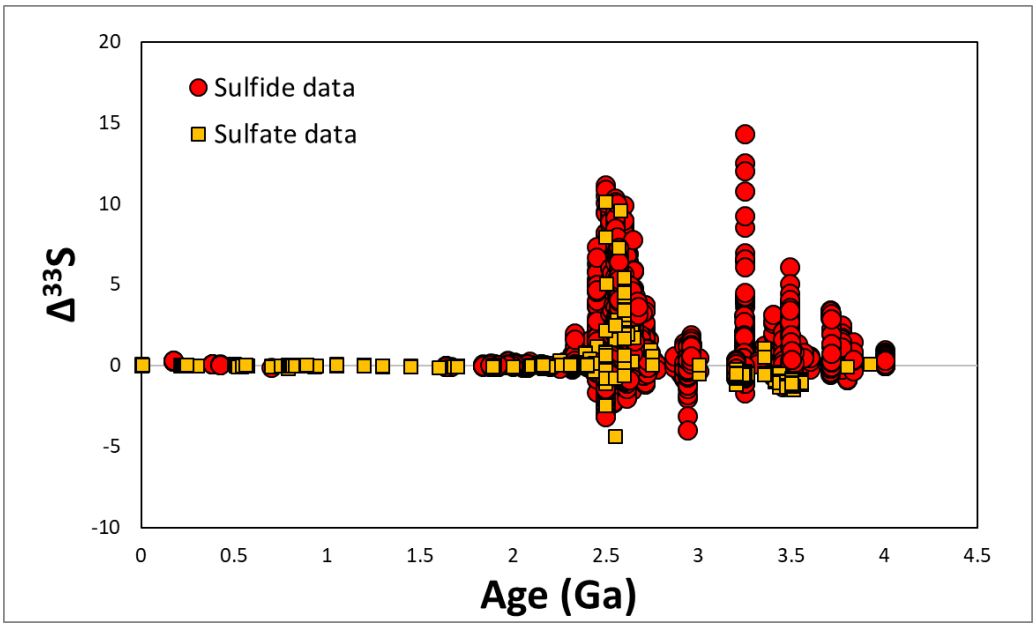

Figure 5. Data compilation of age (Ga) vs. $\Delta^{33}S$ for sulfide and sulfate fractions. The figure presented is produced by the data compilation provided in Killingsworth et al. (2019).

The production of these excursions is thought to reflect the process of wavelength-specific photochemistry on sulfur-bearing molecules in an essentially oxygen-free atmosphere (Farquhar et al., 2000; Farquhar et al., 2001). Note that the S-MIF discussed for the meteorite record is not the same as that produced on earth. On earth, the Archean rock record reveals an array between $\Delta^{33}S$ vs. $\Delta^{36}S$ with a slope of -1 to -2. Other solar system bodies (and even S-MIF produced relatively recently on Earth) do not follow this relationship. It is also important to note the periodic attenuation of the $\Delta^{33}S$ throughout the Archean that is argued to reflect periodic changes in the composition of the atmosphere (Ohmoto et al., 2006), that has led to additional research of using the $\Delta^{33}S$ signal to model atmospheric evolution in the Archean (Domagal-Goldman et al., 2008; Zerkle et al., 2012). As a comparison, Archean oceanic crust exposed at ISUA Greenland lacks major S-isotope variations in both $\delta^{34}S$ and $\Delta^{33}S$

linking the majority of the signal to magmatic mantle derived sulfide (Siedenberg et al., 2016). There are however relatively small $\Delta^{33}S$ variations (-0.17‰ to +0.26‰) that are linked to mixing with a S source with MIF such as seawater sulfate, ocean floor sediments, or recycled components (Siedenberg et al., 2016).

From the earliest Proterozoic into the phanerozoic, $\Delta^{33}S$ is minimized to values hovering around $\Delta^{33}S \neq 0$, indicative of the major onset of oxygenation on Earth. Importantly, $\delta^{34}S$ also changes, showing a range from < 30 ‰ in the Archean to >80 ‰ post 1 Ga (Farquhar et al., 2014). The change in $\delta^{34}S$ values is attributed to the increased concentration of sulfate in the oceans and in turn in increased amount of sulfate reduction (a process known to fractionate $\delta^{34}S$). A signature of post Archean rocks near Earth's surface is highly variable in $\delta^{34}S$ (Figure 6).

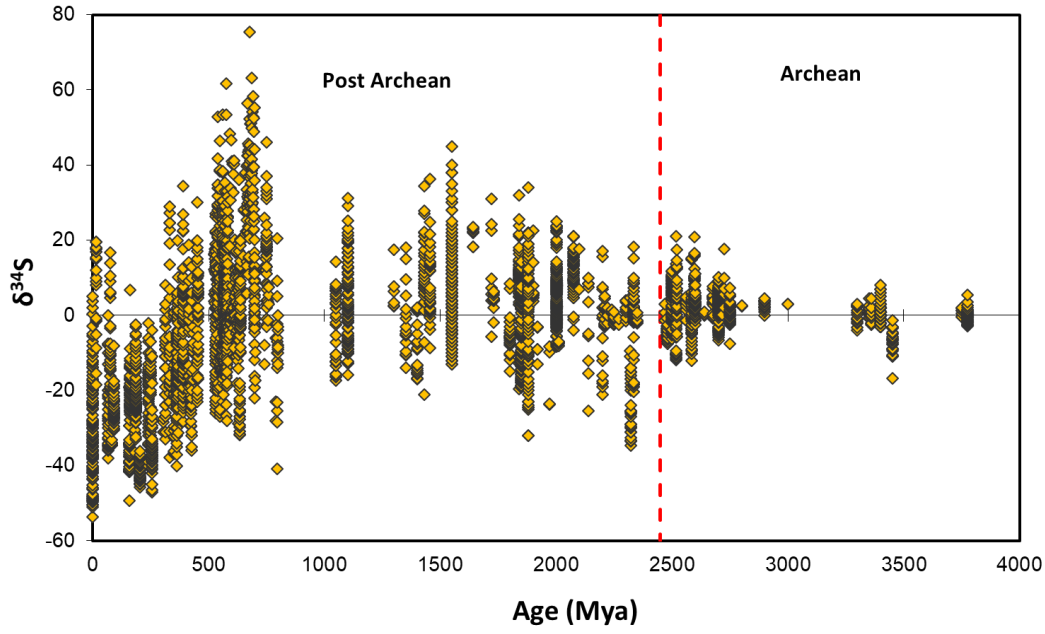

Figure 6. Data compilation of Age (Mya) vs.$\delta^{34}S$ that highlights the increased variability post – Archean age. Data compilation from (Canfield and Farquhar, 2009).

1.8 List of terms and abbreviations

Table 1. List of terms and abbreviations in Chapter 1

Term	Symbol	Definition
Mass dependent fractiation	$\delta^{3x}S$	$[(({}^{3x}S/{}^{32}S)_{sample} / ({}^{3x}S/{}^{32}S)_{CDT}) - 1]$, x=3,4,or 6; CDT=Canyon Diablo Troilite standard
Mass Independent Fractionation	$\Delta^{33}S$	$[({}^{33}S/{}^{32}S)_{sample}/({}^{33}S/{}^{32}S)_{CDT}]- [({}^{34}S/{}^{32}S)_{sample}/({}^{34}S/{}^{32}S)_{CDT}]^{0.515}$
	$\Delta^{36}S$	$=[({}^{36}S/{}^{32}S)_{sample}/({}^{36}S/{}^{32}S)_{CDT}]- [({}^{34}S/{}^{32}S)_{sample}/({}^{34}S/{}^{32}S)_{CDT}]^{1.9}$
Mass of element	m_h,m_l (or M)	Atomic (or molecular for M) mass of element involved in isotope exchange
Energy	E	Energy associated with movements of the molecule
Partition function	Q	$\Sigma g_i e\text{-}E/KT$
g	g	statistical degeneracy term
Boltz's Constant	k	$1.380658x10^{-23}$J/K
Zero Point Energy	ZPE	$E=(n+1/2)h\nu$
Planck's constant	h	$6.626x10^{-34}$ J·sec
Vibrational frequency	ν	$(1/2\pi)(k_s/\mu)^{0.5}(sec^{-1})$
Spring constant	k_s	Spring stiffness
Reduced mass	μ	$m_1m_2/(m_1+m_2)$
U	U	$h\nu/kT$
Symmetry number	σ	Number of ways to orient a molecule
Moment of inertia	*I*	μr^2, r=average interatomic distance

Chapter 2: Sulfur isotope characterization of primordial and recycled sources feeding the Samoan mantle plume

This chapter has previously been published in *Earth and Planetary Science Letters*.

D**ottin III, J.W.,** Labidi, J., Lekic, V., Jackson, M.G., Farquhar, J. (2020) Sulfur isotope characterization of primordial and recycled sources feeding the Samoan mantle plume. *Earth and Planetary Science Letters*. **534** DOI: 10.1016/j.epsl.2020.116073

Abstract

Understanding present-day mantle heterogeneity is key to understanding the geochemical evolution of our planet. The Samoan islands are the type locality for the Enriched Mantle (II) reservoir that is thought to be produced from the subduction and recycling of marine sediment from upper continental crust. In addition to hosting extreme radiogenic isotope compositions from the EM II reservoir, Samoa also exhibits contributions from other mantle reservoirs in a dilute form including the EM (I) (recycled continental material), HIMU (recycled oceanic crust), and DMM (depleted upper mantle) mantle reservoirs. The plume system feeding the Samoan islands sits above a seismically imaged Large Low Shear Velocity Province (LLSVP) and an Ultra-Low Velocity Zone (ULVZ) that is thought to contribute, in addition to recycled components, the recently discovered early-formed (primordial) components with negative $\mu^{182}W$ and high $^{3}He/^{4}He$. Recent work measuring sulfur isotopes in ocean island basalts has established that recycled oceanic and continental crust host unique S-isotope compositions that can be identified at various hotspot localities. Here we document previously unknown relationships between $\Delta^{33}S$ and radiogenic tungsten, helium and lead isotopes from 7 Samoan basalts (from the islands of Ofu, Vailulu'u

and Malumalu) that suggest mixing between several endmembers. One, a HIMU influence that has slight positive $\Delta^{33}S$ and positive $\delta^{34}S$; another, related to EM II that has near zero $\Delta^{33}S$ and positive $\delta^{34}S$; a third, which is primordial with negative $\mu^{182}W$, high $^{3}He/^{4}He$, that has $\Delta^{33}S = 0$ ‰ and negative $\delta^{34}S$. From this, we conclude that the indistinguishable ^{33}S of the primordial endmember from that of the convective mantle indicates that sulfur isotopes were homogenized early in Earth's history. The Vailulu'u sample with HIMU characteristics, carries a small but resolvable $\Delta^{33}S$ that allows, but does not require mass-independent Archean $\Delta^{33}S$ to shift the $\Delta^{33}S$. The observed correlations involving $\Delta^{33}S$ support arguments linking Pb, He, and W geochemistry to a deep mantle process and places constraints on questions related to the sources of mantle geochemical heterogeneity.

1. Introduction

Basalts erupted at ocean islands (OIBs) are thought to sample both the deep and convective mantle, and provide insight into the diversity of mantle reservoirs. Long-lived radiogenic isotope com-positions of strontium (Sr), neodymium (Nd), and lead (Pb) from OIBs reveal compositional heterogeneity of the mantle and have formed the basis for identifying distinct mantle reservoirs produced by melt removal and incorporation of recycled components over time (Zindler and Hart, 1986). The process of core formation and further planetary differentiation allowed for the production of an early formed reservoir (from here forward in this paper, we refer to this as a primordial reservoir). Components of this reservoir are observed in modern mantle plume basalts such as Samoa, and are manifested as isotopic anomalies in the short lived radiogenic

isotope composition of tungsten (W) (Rizo et al., 2016; Mundl et al., 2017; Mundl-Petermeier et al., 2019; Mundl-Petermeier et al., 2020; also see Kruijer and Kleine, 2018) and noble gas signatures of helium (He), neon (Ne), xenon (Xe), and argon (Ar) (e.g. Kurz et al., 2009; Mukhopadhyay, 2012). The isotopic observations that identify primordial components in mantle plume systems have suggested links to Large Low Shear Velocity Provinces (LLSVPs) and Ultra Low Velocity Zones (ULVZs) in the deep mantle (Williams et al., 2019).

Here, we present new bulk rock quadruple sulfur isotope data on (n = 7) basalts from three Samoan volcanoes–Ofu, Vailulu'u and Malumalu (**Figure 7**)–to explore whether sulfur isotopes provide insight into the primordial signatures described above.

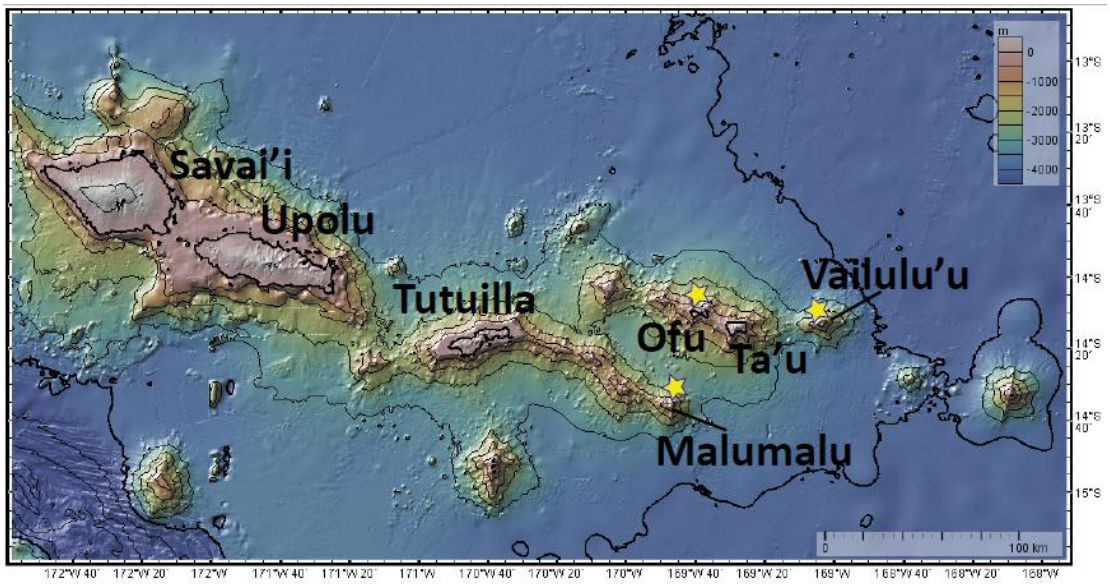

Figure 7. Shown is a map of the Samoan volcanoes. Gold stars denote the localities sampled for this study. The map was configured using the GeoMapApp program.

So far sulfur isotopes have been used to track recycling of exogenic sulfur into plume systems (Cabral et al., 2013a; Labidi et al., 2015; Delavault et al., 2016), to identify an

isotopic imprint of planetary differentiation (Labidi et al., 2013), and to trace magmatic processes such as degassing (Beaudry et al., 2018). The observation of mass-independent ($\Delta^{33}S$ = 0 ‰) and mass-dependent ($\Delta^{33}S$ = 0 ‰, variable $\delta^{34}S$) signatures of sulfur in mantle samples highlights its potential value for study in other mantle systems. The samples studied here yield a relationship between $\mu^{182}W$ and $^{3}He/^{4}He$ that illustrate a contribution from a primordial component (negative $\mu^{182}W$ anomalies associated with high $^{3}He/^{4}He$) and a non-primordial component. This offers an opportunity to place constraints on the primordial sulfur isotope composition of the mantle and to offer insight into the source of non-primordial W and He isotope compositions.

2. Geologic context/background

2.1. Samoan radiogenic isotopic geochemistry

Samoa is historically seen as sampling the archetypical Enriched Mantle-II (EMII) mantle source (e.g. Zindler and Hart, 1986). More recent work on radiogenic isotope signatures of lead (Pb) argues that the various Samoan volcanoes receive contributions from multiple mantle endmember sources (Jackson et al., 2014) including a depleted component, recycled components, and a primordial component, and these are sampled in the Vai, Malu, and Upo volcanic lineaments. Radiogenic isotopic compositions of strontium (Sr), neodymium (Nd), and lead (Pb) for samples from Samoa reveal signatures of recycled, subducted oceanic and continental crust in endmembers such as: the Enriched Mantle 1 (EMI) component in rejuvenated Samoan

lavas, the Enriched Mantle 2 (EMII) component at Malumalu seamount and Savai'i submarine lavas, and the dilute HIMU (high $\mu = {}^{238}U/{}^{204}Pb$) component at Ta'u island and Vailulu'u seamount (Jackson et al., 2014). The EMI endmember is characterized by relatively low $^{143}Nd/^{144}Nd$ and $^{206}Pb/^{204}Pb$ at high $^{87}Sr/^{86}Sr$, and high $^{208}Pb/^{204}Pb$ at a given $^{206}Pb/^{204}Pb$. The EMII source is characterized by the highest $^{87}Sr/^{86}Sr$ and $^{208}Pb/^{204}Pb$ at a given $^{206}Pb/^{204}Pb$ and its origin is argued to reflect the subduction and recycling of continental sediments (Jackson et al., 2007a; Workman et al., 2008). The HIMU endmember is thought to reflect recycled oceanic crust after it experienced Pb loss during subduction, hence leading to ingrowth of radiogenic $^{206}Pb/^{204}Pb$ (e.g. Kelley et al., 2005 and references within).

Studies of ocean island basalts, including Samoa, also suggest various ocean islands host primordial mantle components. Evidence for this comes from high $^{3}He/^{4}He$ ratios in Hawaii (e.g. Kurz et al., 1983; Valbracht et al., 1997 and references within), Samoa (Jackson et al., 2007b; Jackson et al., 2009b), Iceland (e.g. Macpherson et al., 2005 and references within), Galapagos (Graham et al., 1993; Kurz et al., 2009), and Baffin Island (Stuart et al., 2003; Starkey et al., 2009). Additional evidence for early-formed "primordial" mantle domains is observed through the association of primitive Ar and Ne, and ancient Xe isotope signatures in mantle plumes with high $^{3}He/^{4}He$ (e.g. (Kurz et al., 2009; Mukhopadhyay, 2012), negative $\mu^{182}W$ associated with high $^{3}He/^{4}He$ in Samoa and Hawaii (Mundl et al., 2017), and positive $\mu^{182}W$ in Baffin island and Ontong Java Plateau (Rizo et al., 2016; also see Kruijer and Kleine, 2018).

2.2. Unique seismic structures beneath Samoa

In addition to the isotopic heterogeneity observed in the mantle, seismic evidence for compositional heterogeneity in the deep mantle has been mounting. Recent studies confirm that at the largest scales, the pair of Large low Shear Velocity Province (LLSVPs) appear to be associated with both low shear wavespeed and high density, a telltale signature of compositional heterogeneity (Moulik and Ekström, 2016; Lau et al., 2017). At smaller scales, Ultra Low Velocity Zones (ULVZs), whose properties have been interpreted to represent either partial melt (Williams and Garnero, 1996) or very high iron enrichment (Wicks et al., 2010), have now been detected beneath Samoa (Thorne et al., 2013), Hawaii (Cottaar and Romanowicz, 2012), and Iceland (Yuan and Romanowicz, 2017). High resolution global tomographic models constructed using full waveform inversion have been interpreted to require the presence of compositional heterogeneity within plume conduits themselves (French and Romanowicz, 2015). Importantly, efforts in mantle geochemistry have begun to associate mantle reservoirs that host primordial components, such as that sampled by Samoa, to Large Low shear Velocity Provinces (e.g. Williams et al., 2019) and Ultra Low Velocity Zones (e.g. Mundl et al., 2017) that reside at the base of the mantle. These observations continue to contribute evidence that mantle plumes are sampling reservoirs that are both deep and compositionally distinct from the ambient mantle.

3. Methods

Splits (1 to 3 gram aliquots) of the same fine crushed powder from Mundl et al. (2017) were placed into Teflon reactors for acid digestion as described by Labidi et al. (2012). These samples are a different type from those studied by Labidi et al. (2015) in that the samples are not glasses but, are rather the same powder from the interiors of the sampled flows used by Mundl et al. (2017). Prior to digestion, the setup was degassed with N2 for ~ 15 min. After degassing, the samples were acidified and digested in heated (70-80 ˚C) 3.2M $CrCl_2$, 12M HCl, and 29M HF in the amounts of 10 ml, 5 ml, and 5 ml respectively. The amount of solution was doubled for larger samples (>2 grams of powder). Sulfides were released as H_2S that is then bubbled (pulsed bubbling of ~3-5 bubbles every ~1-2 s) through a water trap and lastly trapped as Ag_2S in an acidic $AgNO_3$ trap solution. The captured Ag_2S subsequently transferred to a 1.5 ml Eppendorf centrifuge tube where it was then rinsed, agitated with a vortex machine for 10 s, and centrifuged with Milli-Q water. The supernatant was pipetted off and the rinsing procedure was repeated 6 times. After rinsing, the Ag_2S was dried at 70 ˚C. The dried Ag_2S was then weighed to determine sulfur concentration and the Ag_2S (0.3 mg to 5 mg) reacted with 3-5 times excess F_2 in heated (~250 ˚C) nickel reaction tubes for at least 8 h. Note, some samples yielded greater than 5 mg of Ag_2S (up to 15 mg). For these samples, 3-5 mg splits were taken and used for isotopic analyses. The resulting SF_6 was transferred to a liquid nitrogen cooled trap and the residual F_2 was passivated by a reaction with ~110 ˚C KBr salt. After passivation, the liquid nitrogen trap was replaced by an ethanol slush (~−108 ˚C to −115 ˚C) in an effort to separate HF from the remaining SF_6. Once separated, the SF6 was transferred to a liquid nitrogen cooled injection loop of a gas chromatograph (GC). Next, the SF_6 was simultaneously thawed

and injected into the gas chromatograph with flowing helium at a rate of 20 mL/min. The gas chromatograph allows for a final SF_6 purification using a 1/8-inch diameter, 20-foot long Haysep-Q™ GC column. The SF_6 was monitored while passing through the (GC) and captured from the helium flow in liquid nitrogen cooled spiral metal tubes. Lastly, the captured purified SF_6 was measured manometrically to determine procedural yields and preserved in individual sample fingers of glass manifolds. Yields determined from fluorination range from 70% to 106%. The glass manifold was then attached to an additional liquid nitrogen cooled manifold that is used to introduce SF6 into the sample bellows of a Thermo Finnigan MAT 253 dual-inlet mass spectrometer.

3.1. Mass spectrometry

Sulfur has four stable isotopes (^{32}S (95.2%), ^{33}S (0.75%), ^{34}S (4.25%), and ^{36}S (0.02%)), and isotopic variations of sulfur isotopes were determined using mass spectrometry of purified SF6. The purified SF6 was measured by monitoring SF+ 5 ion beams at m/z of 127, 128, 129, and 131. Data are reported in per mil using the following notation:

$$\delta^{33}S = [((^{33}S/^{32}S)_{sample}/(^{33}S/^{32}S)_{CDT}) - 1]$$

$$\delta^{34}S = [((^{34}S/^{32}S)_{sample}/(^{34}S/^{32}S)_{CDT}) - 1]$$

$$\delta^{36}S = [((^{36}S/^{32}S)_{sample}/(^{36}S/^{32}S)_{CDT}) - 1]$$

$$\Delta^{33}S = [((^{33}S/^{32}S)_{sample}/(^{33}S/^{32}S)_{CDT})) - ((^{34}S/^{32}S)_{sample}/(^{34}S/^{32}S)_{CDT})^{0.515}]$$

$$\Delta^{36}S = [((^{36}S/^{32}S)_{sample}/(^{36}S/^{32}S)_{CDT})) - ((^{34}S/^{32}S)_{sample}/(^{34}S/^{32}S)_{CDT})^{0.91}]$$

All analyses were normalized to analyses of a large, single reservoir of SF_6 gas produced by fluorination of IAEA-S1 undertaken in the same session as the sample analyses. This normalization was conducted during each analytical session to account for changes in the composition of different aliquots of mass spectrometer reference gas. We developed this approach for studies of meteorite samples and found that the approach yields more accurate and reproducible $\Delta^{33}S$ (Antonelli et al., 2014). The data are then normalized to the value measured for Canyon Diablo Troilite (CDT) using the same approach and calibration in Antonelli et al. (2014) and Dottin et al. (2018). This places IAEA-S1 at a value of $\delta^{33}S = -0.091$ ‰, $\delta^{34}S = -0.401$ ‰, $\delta^{36}S = -1.558$ ‰, $\Delta^{33}S = 0.116$ ‰, $\Delta^{36}S = -0.796$ ‰. Estimates of uncertainty can be assigned on the basis of measured long-term reproducibility of independent fluorinations of a variety of reference materials. These uncertainties include contributions from mass spectrometry and chemical preparation and, for $\Delta^{33}S$, vary depending on the mass spectrometry counting times. For $\delta^{34}S$ and $\Delta^{36}S$ the long-term reproducibility on reference materials is ±0.3 and ±0.3 ‰ (2σ). For $\Delta^{33}S$, the long-term reproducibility is ±0.008 ‰, and ±0.016 ‰ (2σ), for mass spectrometry analyses made using 9 and 3 analytical cycles, respectively. The reproducibility reported in Table *2* of 2 (SE) represents the in-run precision from mass spectrometry and renormalization determined by Monte Carlo error propagation. The reproducibility (SE) for $\delta^{34}S$ and $\Delta^{36}S$ is smaller than seen from the long-term reproducibility on IAEA-S1 due to factors associated with the chemical procedures in preparing the SF6 ($\delta^{34}S$) and interferences ($\Delta^{36}S$). The reproducibility (SE) is comparable to that seen for $\Delta^{33}S$ on the basis of long-term reproducibility on IAEA-S1. This suggests greatest contributor to

reproducibility for $\Delta^{33}S$ comes from mass spectrometry. Estimates of precision (total uncertainty) are assumed to be the larger of the long-term reproducibility of reference materials and the propagated, normalized mass spectrometry data. These are presented in Table *2*. For figures we plot estimated uncertainty. We use a Bayesian approach (details given in Table 7) to assess match between data and models for relationships between sulfur isotope data and other geochemical systems.

4. Results

Data from 7 Samoan basalts are presented in Table *2* and *Figure 8*.

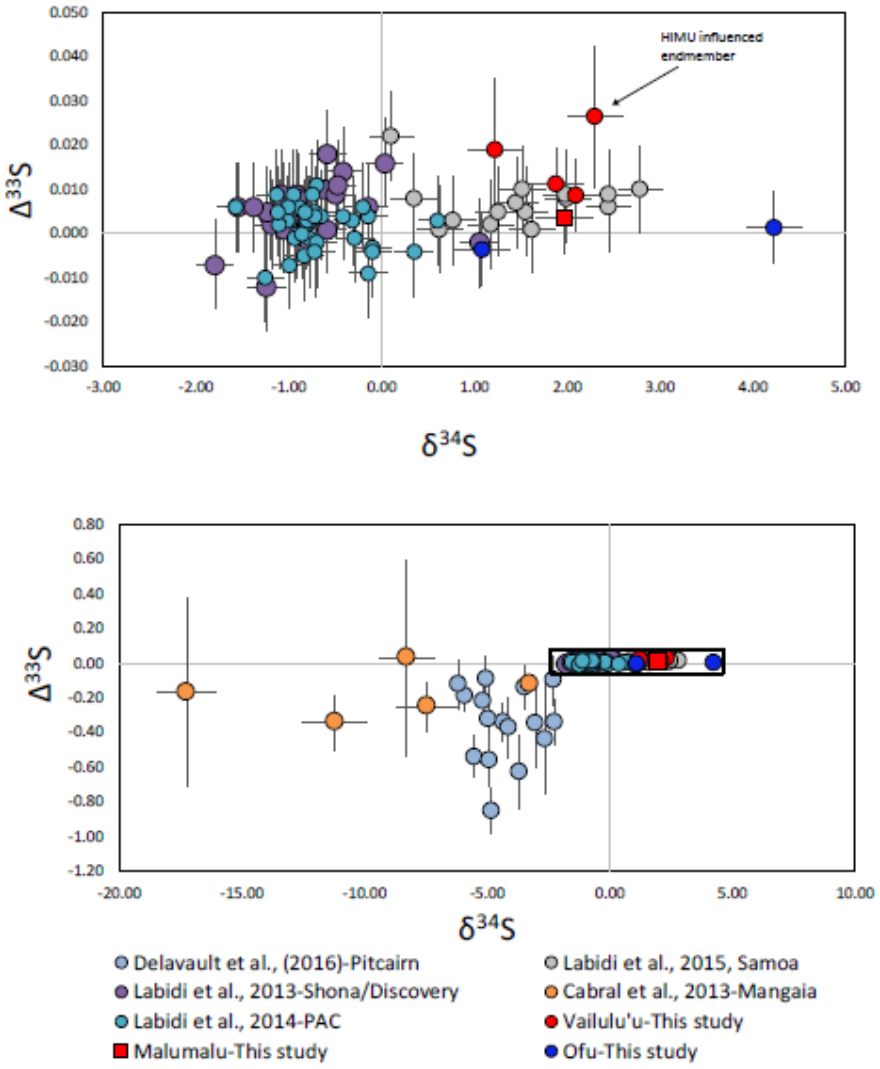

Figure 8. Compilation of new and existing S-isotope data ($\delta^{34}S$ vs. $\Delta^{33}S$) for various OIB and MORB sources. New data plotted are from bulk rock powders (blue and red symbols) from the Vailulu'u, Malumalu, and Ofu volcanoes of Samoa. The remaining data is collected either as glass (Labidi et al. 2013, 2014, 2015) or as individual sulfides using Secondary Ion Mass Spectrometry (SIMS) (Cabral et al., 2013; Delavault et al., 2016. The data we report fall within the range of values reported on glasses by Labidi et al., 2015 with the exception of 1 data point from Ofu (Ofu-04-15). Note, the values shown from Labidi et al., (2013, 2014, 2015) are not shifted to the CDT scale in $\delta^{34}S$ and the UMD-CDT scale for $\Delta^{33}S$. This shift in normalization yields a -0.1 ‰ shift in $\delta^{34}S$ and a +0.01 ‰ shift in $\Delta^{33}S$. The error bars on $\delta^{34}S$ are an estimate from the long-term reproducibility on standards that takes into account the uncertainty associated with sample processing. Error bars on $\Delta^{33}S$ represent estimates from the long-term reproducibility on standard materials (see methods).

Sulfur concentrations of the bulk rock phase represent a lower limit, as a small amount of S could be lost in the sample preparation (rinsing and weighing procedure). Concentrations range from 30 ppm to 800 ppm S and isotopic compositions extend from +1.08‰ to +4.23‰ (± 0.3), −0.004‰ to +0.027‰ (± 0.008), and −0.29‰ to +0.22‰ (± 0.3) in $\delta^{34}S$, $\Delta^{33}S$, and $\Delta^{36}S$ respectively. With the exception of sample Ofu-04-15 ($\delta^{34}S$ = +4.23‰), the $\delta^{34}S$ data are within the range of compositions previously reported (+0.11‰ to +2.79‰, Labidi et al., 2015). The $\Delta^{33}S$ and $\Delta^{36}S$ are all within the previously reported range, +0.001‰ to +0.022‰, and −0.063‰ to +0.271‰, for $\Delta^{33}S$ and $\Delta^{36}S$ respectively[6]. The compositions we observe are within the range of bulk sulfur isotope compositions reported for the global dataset of glasses from ocean island and mid ocean ridge basalts where values range from ~ −3‰ to +3‰ in $\delta^{34}S$ and −0.01‰ to +0.01‰ in $\Delta^{33}S$ (Labidi et al., 2015; 2014; 2013). However, the observed compositions are not as extreme as the isotopic data obtained on individual sulfides via secondary ion mass spectrometry (SIMS), at localities such as the Canary Islands that reveal large negative $\delta^{34}S$ variations (up to −8.2‰) assigned to degassing with strictly mass dependent $\Delta^{33}S$ (Beaudry et al., 2018) and Mangaia and Pitcairn that show large negative $\delta^{34}S$ variations (−17.25‰ to −2.25‰) associated with sub-permil $\Delta^{33}S$ variations (0 ‰ to −0.85 ‰) (Cabral et al., 2013; Delavault et al., 2016). These SIMS measurements resolve isotopic difference on a granular scale, which is different from bulk measurements presented here, and have larger uncertainties. Our data reveal

[6] The compositions reported here are not shifted to the CDT scale in $\delta^{34}S$ and the UMD-CDT scale for $\Delta^{33}S$. This shift in normalization yields a −0.1 shift in $\delta^{34}S$ and a +0.01 shift in $\Delta^{33}S$ which would convert to +0.01‰ to +2.69‰, +0.011‰ to +0.032‰, and −0.063‰ to +0.271‰ for $\delta^{34}S$, $\Delta^{33}S$, and $\Delta^{36}S$ respectively.

relationships between $\Delta^{33}S$ and radiogenic isotopic compositions of W, Pb, and He. The data do not, however, preserve a relationship between $\delta^{34}S$ and radiogenic isotopic compositions of W, Pb, and He. In order to assess the significance of these relationships, we employed a Bayesian model selection approach to quantify the relative probability that the underlying relationship is represented by a line (M1) versus a constant value (i.e. line with zero slope; M2). We explicitly marginalize out the extra tunable parameter (slope of the line) present in M1, and assume that the errors in both composition estimates are normally distributed and uncorrelated. We find that the radiogenic W, Pb, and He vs. $\Delta^{33}S$ data strongly prefer M1 over M2 (>99% chance of being true).

Table 2. Compilation of new S-isotope data and previously published radiogenic isotope data

Location	Sample	Dredge depth (bars)	S (ppm)	$\delta^{34}S$ (‰)			$\Delta^{33}S$ (‰)			$\Delta^{36}S$ (‰)		
					†	‡		†	‡		†	‡
Samoa												
Vailulu'u	AVON3-63-2	92	809	1.23	0.028	0.3	0.019	0.010	0.016	-0.47	0.02	0.3
	AVON3-70-9	113	201	2.30	0.015	0.3	0.027	0.012	0.016	-0.22	0.03	0.3
	AVON3-71-22	417	603	2.09	0.005	0.3	0.009	0.006	0.008	0.08	0.03	0.3
	AVON3-73-1	96	214	1.88	0.003	0.3	0.01	0.004	0.008	-0.02	0.02	0.3
Malumalu	AVON 3-77-1	361	393	1.97	0.007	0.3	0.004	0.006	0.008	-0.01	0.02	0.3
Ofu	OFU-04-15	0	64	4.23	0.009	0.3	0.001	0.004	0.008	0.22	0.07	0.3
	OFU-05-18**	0	29	1.08	0.015	0.3	-0.004	0.004	0.008	0.13	0.03	0.3

†Reproducibility (2 Standard Error) determined using a monte-carlo error propagation that takes into account the in-run precision on measurements of IAEA-S1 during the analytical session and the sample. ‡ Estimated uncertainty from long-term reproducibility on standard materials. †† The reported $\mu^{182}W$ values reported is an average of two analyses from Mundl et al. (2017). The error reported here and shown in figure 2 and 3 is the long-term external reproducibility reported in Mundl et al. (2017). (a) (Mundl et al., 2017), (b) (Jackson et al., 2007), (c) (Jackson et al., 2014), (d) (Workman et al., 2004), (e) (Horan et al., 2018). **Note that Ofu-05-18 is a resampling of the same dike as sample Ofu-04-06 in Jackson et al. (2007).

Table 1. Continued

Location	Sample	$\mu^{182}W$			$^{3}He/^{4}He$ (R_A)			$^{206}Pb/^{204}Pb$		
			2 SE			2σ			2σ	
Samoa										
Vailulu'u	AVON3-63-2	-4.9	2.1	a	10.06	0.1	c	19.3578	0.0018	c
	AVON3-70-9	-5.8	5.2	a	8.05	0.2	d	19.3960	0.0004	c
	AVON3-71-22	-2.8	4	a	9.64	0.2	d	19.358	0.0194	d
	AVON3-73-1	-7.7	3.8	a	8.1	0.2	d	19.2299	0.0002	c
Malumalu	AVON 3-77-1	-7.45	4††	a	13.45	0.2	d	19.2683	0.0003	c
Ofu	OFU-04-15	-13.7	4	e	29.6	0.4	b	19.1410	0.00190	b
	OFU-05-18**	-13.8	3.3	a	33.7	0.4	b	19.1890	0.00190	b

5. Discussion

5.1. Preservation of mantle sulfur in interiors of pillow basalts?

We report sulfur concentrations in the interior of pillow basalts erupted at Ofu, Vailulu'u and Malumalu that range from 30 to 800 ppm. These are lower than concentrations seen in glasses erupted at these islands (600 to 2000 ppm S, Labidi et al., 2015). Typically, samples of glass, erupted at ocean depths greater than 1000 meters have the greatest chance of preserving the sulfur concentrations and isotopic compositions of the erupted melt (Moore and Fabbi, 1971). The bulk rock samples from Vailulu'u and Malumalu are from submarine eruptions (they were collected at water depths of ≥92 bars) and preserve slightly higher sulfur concentrations, but are at the low end (600-800 ppm) of the S concentrations reported for samples of glass from the same localities by Workman et al. (2006) and Labidi et al. (2015) and in some cases (see Table *2, Figure 32*) reveal even lower concentrations (~200 ppm) than the lowest value (~600 ppm) reported by Labidi et al. (2015). Bulk rock samples with the lowest S concentrations (30 and 60 ppm S) are subaerial lavas from Ofu. Sulfur loss can also be associated with isotopic shifts in $\delta^{34}S$, but not $\Delta^{33}S$ or $\Delta^{36}S$.

The sulfur isotope compositions of Samoan basalts (from this study and Labidi et al., 2015) are ^{34}S-enriched relative to the composition of mantle sulfur proposed by Labidi et al. (2013; 2014) of −1‰ ±0.5. These ^{34}S-enrichments could be caused by recycling of ^{34}S-bearing subducted components (Labidi et al., 2015), or by syneruptive

or post-eruptive sulfur loss. While sulfur loss could be accounted for by episodes of sulfide segregation, as seen in some Samoan melts (Labidi et al., 2015), we argue that the lowest sulfur concentrations observed here illustrate sulfur loss through an event(s) of sulfur degassing and that the loss of sulfur (^{32}S) could account for the increasing ^{34}S-enriched characteristic of the Ofu samples ($\delta^{34}S$ = +1.8‰ and +4.3‰). A similar shift in $\delta^{34}S$ from degassing cannot be ruled out for the samples from Vailulu'u and Malumalu, however, some of these samples still overlap the range of sulfur isotopic compositions seen for Samoan glasses by Labidi et al. (2015) (Figure *8*).

Sulfur loss through degassing can occur as an equilibrium fractionation, a kinetic fractionation, or a combination of both. At the Quartz-Fayalite-Magnetite reaction buffer, SO_2 dominates the gas phase (Gaillard and Scaillet, 2009; Burgisser et al., 2015), and degassing is expected for melts erupting at less than 100 bars pressure (∼1000 m depth) (Gaillard and Scaillet, 2009). At 1200 ◦C, sulfur dioxide is ^{34}S-enriched by ∼1.5‰ to 3‰ relative to the dissolved sulfide in the melt (e.g. Mandeville et al., 2009), and equilibrium degassing of sulfur dioxide drives the melt to more negative $\delta^{34}S$ compositions. If instead the S were degassed as H_2S, S loss would result in a negligible fractionation of ^{34}S (Mandeville et al., 2009) but H_2S loss is not supported by degassing models of melts with these compositions and oxygen fugacities (Burgisser et al., 2015). The alternative, kinetic degassing, results upon rapid loss of S and generates a ^{34}S heavy residual melt, rather than depletion, driving the melt towards positive $\delta^{34}S$ (e.g. de Moor et al., 2013 and references within). Note, positive $\delta^{34}S$ can be achieved during decompression degassing in highly oxidizing conditions (>QFM +3, (Fiege et al., 2014). Degassing almost certainly occurred, however our data do not

allow for a single process with a singular fractionation to be identified (Figure *31*). This limits our ability to project back to the $\delta^{34}S$ of an initial magma. We note that oxidative weathering of the crystalline interiors may have induced the loss of reduced S. Studies of isotope effects associated with low temperature oxidation by Heidel et al. (2013) show no change in the $\delta^{34}S$ of the residual sulfides from oxidation, but, reveal a fractionation for the product sulfate which they attribute to formation of more than one product. Thus, in the event of oxidative weathering, it is expected that the $\delta^{34}S$ of sulfide would still reflect that of its parental melt.

5.2. Recycled sulfur in Samoa

The submarine erupted samples we analyzed from Vailulu'u and Malumalu have higher S concentrations than the analyzed Ofu samples and we suggest (see above) that sulfur degassing may have only minimally modified the isotopic composition. These samples have $\delta^{34}S$ values (+1.23‰ to +2.30‰) that fall within the range of values previously reported on glassy Samoan basalts by Labidi et al. (2015) and exhibit similar radiogenic isotope compositions for Pb, Sr, and He (Figure *9*).

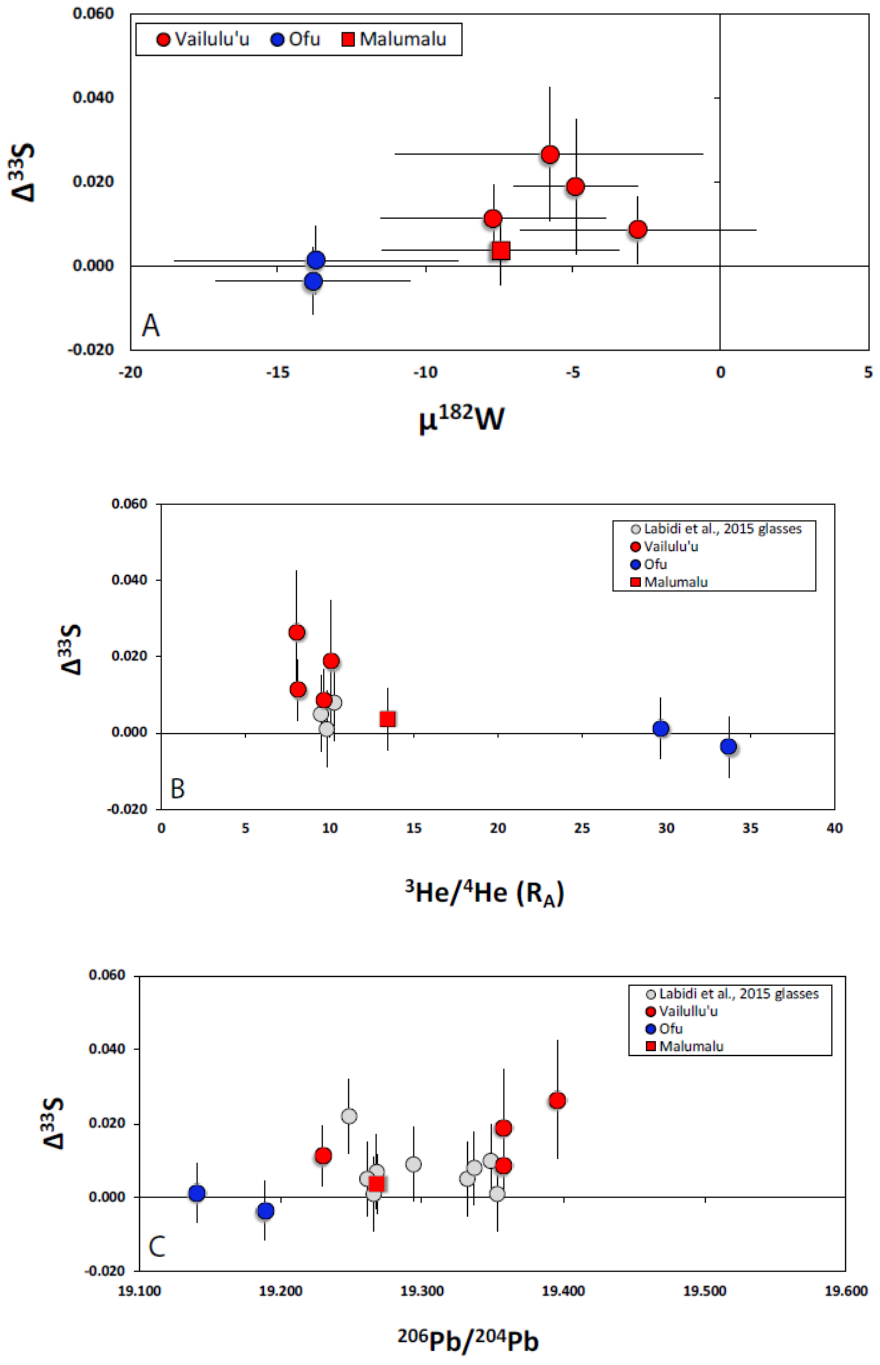

Figure 9. This figure illustrates a relationship in (A) $\mu^{182}W$ vs. $\Delta^{33}S$, (B) $^{3}He/^{4}He$ vs. $\Delta^{33}S$, and (C) $^{206}Pb/^{204}Pb$ vs. $\Delta^{33}S$. $\mu^{182}W$ data are from Mundl et al. (2017) and Mundl-Petermeier et al. (2020). $^{3}He/^{4}He$ data are from Jackson et al. (2007a) and Jackson et al. (2014). $^{206}Pb/^{204}Pb$ are from Jackson et al. (2007a, 2007b), Jackson et al. (2014), and Workman et al. (2004). Error for $^{3}He/^{4}He$ and $^{206}Pb/^{204}Pb$ are reported in Table 1 and are within the plotted symbols.

Even though the sulfur concentrations are generally lower than that observed by Labidi et al. (2015) (Figure *32*), the geochemical similarity between the samples suggests they are part of the same population. Thus, we defer to the study by Labidi et al. (2015) for insight into the $\delta^{34}S$ of the primary magma, where they identified a mixing array between a lower $^{87}Sr/^{86}Sr$ mantle domain with negative $\delta^{34}S$, and an EMII endmember with positive $\delta^{34}S$.

The relationship between $\Delta^{33}S$ and other geochemical systems such as tungsten, helium and lead isotopes reflects mixing of mantle reservoirs sampled by the Samoa mantle plume, including a recycled component with dilute HIMU characteristics (Jackson et al., 2014), an EMII sulfur component that has been documented by Labidi et al. (2015) and a primordial endmember defined by negative $\mu^{182}W$ and high $^{3}He/^{4}He$ (Mundl et al., 2017). Below, we explore in greater detail various scenarios for interpreting the relationships between sulfur and other geochemical systems. We start by discussing the connection with the recycled component and then discuss the connection with the primordial endmember in the context of its suggested origin and placement this endmember.

Our data from Vailulu'u and Malumalu occupy the same field for $\delta^{34}S$ and $^{87}Sr/^{86}Sr$ (Figure *10*) and also the same field for $\delta^{34}S$ vs $\Delta^{33}S$ (Figure *8*) as defined for volcanic glasses of the Samoan volcanic chain reported by Labidi et al. (2015).

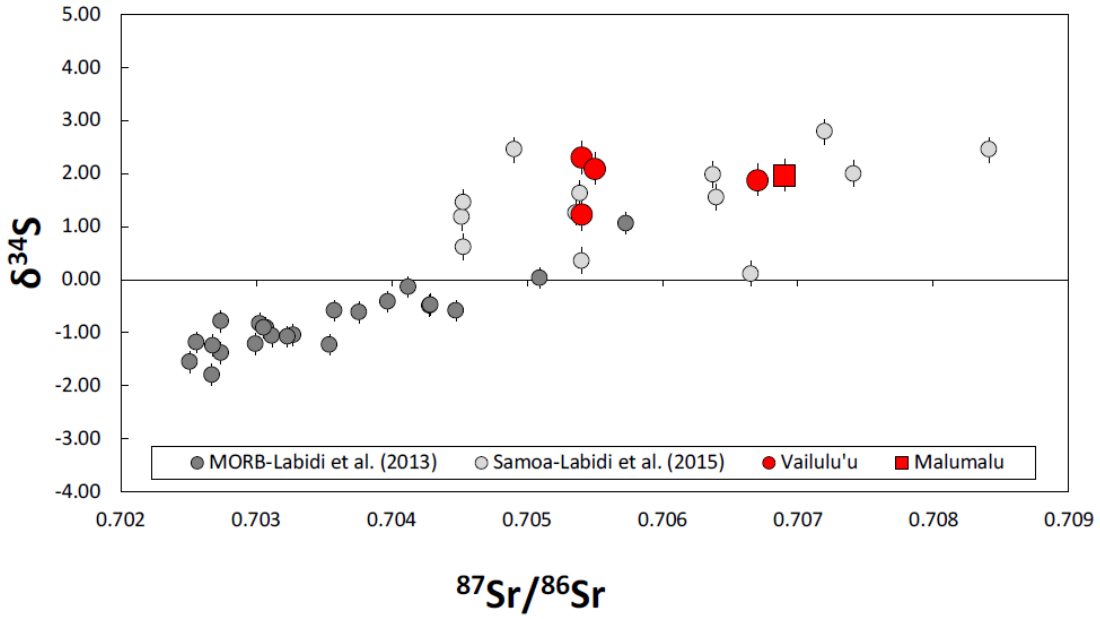

Figure 10. Plot of $^{87}Sr/^{86}Sr$ versus $\delta^{34}S$ for data presented in this study (red, we exclude data from Ofu because these samples are from subaerial eruptions and likely reflect compositions affected by degassing) and data reported by (Labidi et al., 2015; 2013) (light and dark grey). Note, Labidi et al., 2015 propose the increasing $\delta^{34}S$ and $^{87}Sr/^{86}Sr$ relationship is the result of mixing with S-enriched upper continental crust with the conditions of either S/Sr = 50, $\delta^{34}S$ = +5‰ or S/Sr = 17, $\delta^{34}S$ = +10‰.

Labidi et al. (2015) argue that these relationships between $\delta^{34}S$ and $^{87}Sr/^{86}Sr$ reflect mixing between an EMII mantle endmember with positive $\delta^{34}S$ (+10 ‰ ± 3) and radiogenic $^{87}Sr/^{86}Sr$ and a mantle domain with negative $\delta^{34}S_{V\text{-}CDT}$ (−0.89 ‰ ± 0.11 (1σ)) and less radiogenic $^{87}Sr/^{86}Sr$. Minor scatter in the $\Delta^{33}S$ of the combined data allows for other components with different $\Delta^{33}S$, such as HIMU, as underplating of HIMU enriched material to the crust below Samoa has been proposed as the outcome of the earlier passage of the Cook-Austral plumes (Workman et al., 2004); however, the HIMU component may also be indigenous to the Samoan plume (Jackson et al., 2014).

Jackson et al. (2014) argue that the Vailulu'u lavas reveal characteristics suggestive of a dilute HIMU signature. The slightly elevated $\Delta^{33}S$ in Vailulu'u lavas is interpreted to reflect a dilute contribution from a HIMU component that possess variable anomalous $\Delta^{33}S$. A similar observation is observed in lavas from Vailulu'u in Labidi et al. (2015). Given the data from Malumalu (EM II) and Vailulu'u (dilute HIMU) occupy different fields for $\delta^{34}S$ and $^{87}Sr/^{86}Sr$ and a slightly different field for $\delta^{34}S$ vs $\Delta^{33}S$ (Figure *10*), the case may be that the sources of sulfur are indeed different for the Vai and Malu volcanic lineament. The high $^{87}Sr/^{86}Sr$ in EM II Malumalu lavas (and possibly the Vailulu'u lavas, which also have moderately elevated $^{87}Sr/^{86}Sr$), combined with observed $\delta^{34}S$ vs $\Delta^{33}S$, allows for a potential mixture of both Proterozoic and Archean sediments (Labidi et al., 2015). In this type of mixture, the small magnitude $\Delta^{33}S$ signature could also be contributed by Proterozoic sediments (See Johnston (2011) for data compilations showing such characteristics for early to middle Proterozoic sediments). Such small-magnitude positive and negative shifts of $\Delta^{33}S$ are a natural outcome of biological and biogeochemical cycling (Ono et al., 2006) and are seen in sulfide and sulfate from a wide range of sedimentary and hydrothermal systems (Johnston, 2011).

5.3. Sulfur from the primordial mantle

The plume component with which this recycled endmember is mixed hosts a heterogeneous radiogenic Pb isotopic composition. The data from Samoa define four arrays in $^{206}Pb/^{204}Pb$ vs. $^{204}Pb/^{204}Pb$ that all converge on a small range of values (19.0-19.3 in $^{206}Pb/^{204}Pb$, 39.0-39.4 in $^{208}Pb/^{204}Pb$) (Jackson et al., 2014) that are associated

with the high $^{3}He/^{4}He$ ratios of the "common component" (20-33.8 RA). Samples from Samoa with high $^{3}He/^{4}He$ also preserve negative $\mu^{182}W$ (Mundl et al., 2017). Such ^{182}W deficits require a separate evolution from mantle-hosted ^{182}Hf, which went extinct within the first 60 million years of solar system history. ^{182}W deficits are thus signatures formed early in Earth's accretionary history that were immediately isolated from mantle convection and mixing (Mundl et al., 2017).

The observed relationships between S with He and W (Figure *9*) suggests the contribution of sulfur from an undegassed, early-formed mantle reservoir. Our data establish that materials linked to the deep primordial component have $\Delta^{33}S \approx 0‰$, similar to the average MORB value of 0.008 ‰ ± 0.006 (n = 80, 1 s.d., Labidi and Cartigny, 2016). A homogeneous mantle $\Delta^{33}S$ with variable $\mu^{182}W$ supports a process that homogenized $\Delta^{33}S$ prior to the ingrowth of $\mu^{182}W$ signatures in different reservoirs. In Samoan lavas, the recycled components bring materials with $\Delta^{33}S = 0‰$ associated with the recycled component with HIMU characteristics (**Figure *33***) (Jackson et al., 2014) and the observed relationship is apparent because this component has a different $\Delta^{33}S$ than the endmember with negative $\mu^{182}W$. It was shown that the convective mantle is defined by $\Delta^{33}S$ and $\mu^{182}W$ both equal to zero (e.g. Willbold et al., 2011; Labidi et al., 2014). We therefore expect future analyses will fill in a three-component mixing field for $\Delta^{33}S$ and $\mu^{182}W$ (though, hints of this field may already be present in Fig. 5); endmember 1 is a primordial component, endmember 2 is a recycled component, endmember 3 is the convecting mantle.

To allow for an early segregated metal-rich reservoir with a ^{182}W deficit, Mundl et al. (2017) suggest a connection to deep mantle reservoirs such as the seismically-

defined Large Low Shear Velocity Province (LLSVP) or Ultra Low Velocity Zone (ULVZ) beneath Samoa which have been suggested to host Fe-rich metals (e.g. Zhang et al., 2016) and/or may have interacted with the core (Rizo et al., 2019). Work by Frost et al. (2004) suggests the formation of such metal could have occurred via an Fe^{2+} disproportionation pathway driven by formation of bridgmanite early in Earth's history. This process has the potential to yield a reservoir of deep mantle metal with moderate W abundances and low HSEs (Mundl et al., 2017). Zhang et al. (2016) point out that S will concentrate in this metal phase, which in turn will mute the expression of the equilibrium metal/silicate fractionation (>1: Labidi et al., 2016) and yield an isotopic composition similar to that of the mantle in which it formed (negative $\delta^{34}S$ and $\Delta^{33}S = 0$). This composition is consistent with the composition of sulfur we infer for the endmember with negative $\mu^{182}W$.

An alternative proposed mechanism for producing negative $\mu^{182}W$ variations involve high-pressure episodes of core formation that are recorded and preserved in the deep mantle (Jackson et al., 2018). At high pressure, sulfur remains a siderophile element (Suer et al., 2017) but the isotopic effect remains unconstrained. There is a potential for changes in the mass dependent fractionation of $^{34}S/^{32}S$ (see discussion in Labidi et al., 2016), but we consider it unlikely that the $\Delta^{33}S$ would be affected in the formation of the deep mantle reservoir.

Mundl et al. (2017) discount the possibility that physical core metal entrainment was the source of primordial (negative) $\mu^{182}W$ because HSEs are not sufficiently enriched in Samoan lavas and are uncorrelated with negative $\mu^{182}W$. In consideration of the mantle nature of sulfur in samples with increasingly negative $\mu^{182}W$ from

Vailulu'u and Malumalu,2 the data suggest the primordial component likely has negative $\delta^{34}S$, which would be inconsistent with the core being the source of the sulfur that was later diluted with recycled sediments. Labidi et al. (2013) and Labidi and Cartigny (2016) argue that the $\delta^{34}S$ of the bulk Earth, if chondritic, must be between −0.27‰ and +0.04‰. In this case, the mantle and core bracket this value with the mantle having strongly negative $\delta^{34}S$ (−0.89‰ ± 0.11 (1σ)) while the core is slightly ^{34}S-enriched. Further support for the Mundl et al. (2017) suggestion that the $\mu^{182}W$ anomalies did not originate from entrainment of core material, may be provided by the lack of significant curvature in the $\Delta^{33}S$ – $\mu^{182}W$ array (Figure *11*) and the prevalence of near zero or slightly positive $\Delta^{33}S$ for early solar system materials (Antonelli et al., 2014). Significant curvature would be expected if the mantle mixed with core material to generate the $\Delta^{33}S$ – $\mu^{182}W$ array (Figure *11*) observed here, due to different W/S ratios in the mantle and core. The lack of curvature also implies the W/S concentration ratio is not much different in the mixing endmembers and, unless the primordial reservoir has negative $\Delta^{33}S$, the negative $\mu^{182}W$ endmember may not be significantly more negative (e.g. if it was a direct core contribution) than the most negative values that have been measured thus far.

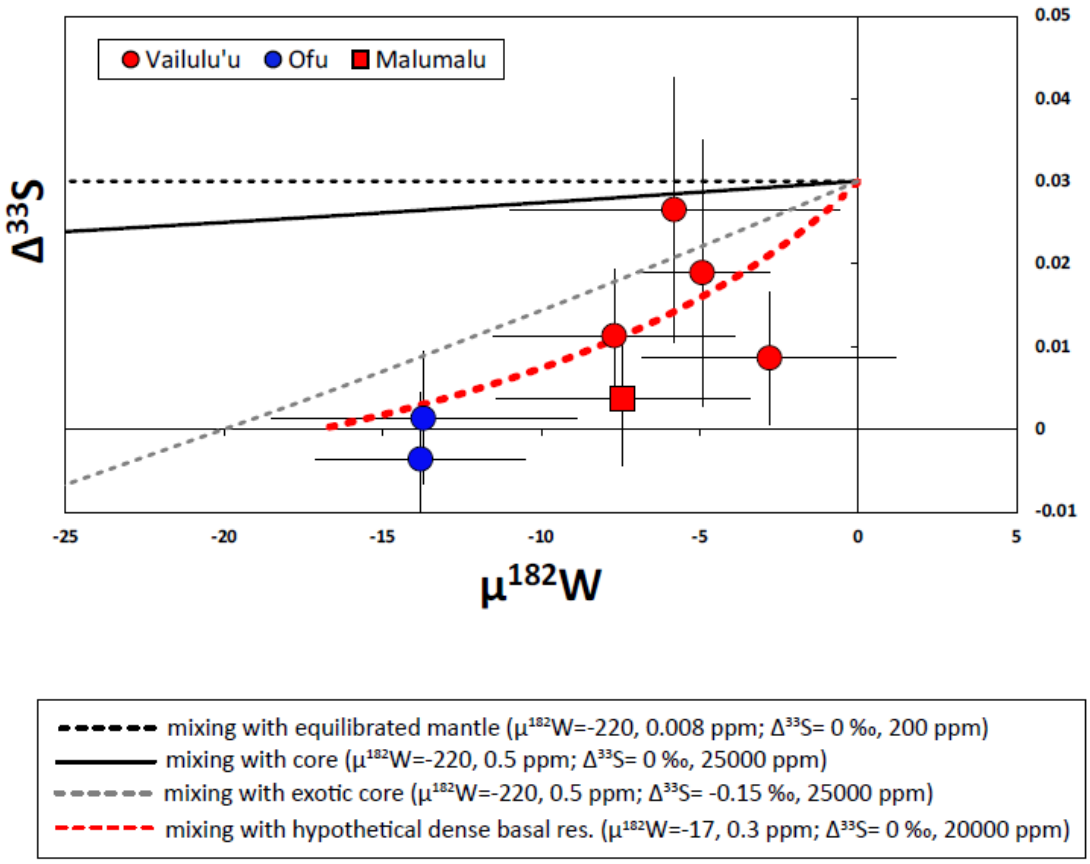

Figure 11. Plot of $\mu^{182}W$ vs. $\Delta^{33}S$ illustrating scenarios for mixing of sulfur and tungsten between a primordial reservoir and a recycled component. Compositions for the primordial reservoir are denoted in parenthesis. We assign the recycled mantle endmember composition for all scenarios to be $\mu^{182}W = 0$, 0.008 ppm; $\Delta^{33}S = 0.03$, 200 ppm. This composition is chosen to illustrate how various models evolve from a composition matching the most ^{33}S-enriched sample in our data set.

More recent work by Mundl-Petermeier et al. (2020) introduce an argument for anomalous $\mu^{182}W$ that involves a chemical and isotopic equilibration process for W between a basal silicate layer and the core. Mundl-Petermeier et al. (2020) argue that the best candidate reservoirs are seismically imaged ULVZs. An equilibration process that generates a reservoir with $\mu^{182}W$ of ~-17 for a $\Delta^{33}S$ ~0 would explain our data (Mundl-Petermeier et al., 2020). The resulting reservoir would mix with a recycled

endmember with $\Delta^{33}S$ =0 to produce the arrays that are seen. Using simple mixing calculations, the data are well fit with this model assuming the amount of tungsten mixed into the basal silicate reservoir yields a $\mu^{182}W$ of ~−17.

6. Conclusions

The Samoan islands are the type locality for the EM (II) reservoir but also receive dilute contributions from EM (I), HIMU, and DMM related components. Furthermore, Samoa sits above a seismically imaged LLSVP and ULVZ that is thought to be the source of material that exhibit primordial isotope compositions, seen as high $^{3}He/^{4}He$ and negative $\mu^{182}W$. We have characterized the nature of sulfur in primordial and recycled mantle sources using multiple sulfur isotopes of bulk rock Samoan basalts by focusing on Samoan islands with high $^{3}He/^{4}He$ and negative $\mu^{182}W$. Relationships between $\Delta^{33}S$ and other geochemical systems such as radiogenic tungsten, helium and lead isotopes is observed and suggests mixing between a component with HIMU characteristics (slight positive $\Delta^{33}S$ and positive $\delta^{34}S$) with a primordial endmember (negative $\mu^{182}W$, high $^{3}He/^{4}He$, $\Delta^{33}S$ = 0‰ and negative $\delta^{34}S$). The antiquity of the primordial endmember is indicated by ^{182}W deficits that require a separate evolution from mantle-hosted ^{182}Hf within the first 60 million years of solar system history. The similar indistinguishable $\Delta^{33}S$ from that of the convective mantle indicates that sulfur isotopes were thus homogenized early in Earth's history. The small but resolvable $\Delta^{33}S$ in the recycled endmember reflects sulfur that is contributed by a Samoan plume component with HIMU characteristics (with a possible mixture of Proterozoic sulfur from continental crust sediments). Although a contribution from mass-independent

Archean $\Delta^{33}S$ could be associated with HIMU, it is not required to explain the $\Delta^{33}S$ variation because younger (Proterozoic) contributions may also have small positive and negative deviations from $\Delta^{33}S = 0$. The correlations between sulfur, Pb, He, and W are most easily reconciled with a deep mantle process linked to a dense, undegassed basal reservoir such as a ULVZ. Although our data do not support a reservoir with $\mu^{182}W = -220$ and $\Delta^{33}S = 0$, the relationship between sulfur and tungsten could reflect W isotope equilibration through a core-mantle equilibration process, where a diluted core W isotope composition having less negative $\mu^{182}W$ is incorporated into the plume that also hosts recycled sediments having $\Delta^{33}S = 0$. Ultimately, our work identifies relationships between sulfur and radiogenic Pb, He, and W that provide a means of continuing to unravel the complexities of geochemical heterogeneity of the mantle. With this work, we further the understanding of how the subduction and recycling of oceanic and continental crust can influence geochemical signatures observed at ocean islands and how well dispersed the various reservoirs are in the mantle.

Chapter 3: Sulfur isotope evidence of geochemical zonation of the Samoan mantle plume

James W. Dottin III[*1], Jabrane Labidi[3], Matthew G. Jackson[4], James Farquhar[1,2]

[*]Corresponding author: jdottin@umd.edu
[1]Department of Geology, University of Maryland, College Park, MD 20742, United States
[2]Earth System Science Interdisciplinary Center, College Park, MD 201742, United States
[3]Universite de Paris Institut de physique du globe de Paris, CNRS, F75005 Paris, France
[4]Department of Earth Science, University of California, Santa Barbara, CA 93106, United States

Marcel Regelous and Matthew Jackson are thanked for providing the samples analyzed in this chapter.

Abstract

The radiogenic Pb isotope composition of Samoan basalts reveals a geometry of the Samoan plume revealed by geochemical data that suggests dilute forms of the various mantle compositional endmembers contribute compositionally distinct material to lavas erupted at different islands. Recent work on the S-isotope composition of Samoan basalts demonstrates that HIMU-related material carry a small positive $\Delta^{33}S$ that is distinct from the primordial mantle. Here, whole rock multiple sulfur isotope data on basalts from Malumalu, Malutut, Upolu, Savaii, and Tutuilla that sample the full range of geochemical heterogeneity at Samoa and allow for assessment S-isotope compositions associated with specific islands. We observe variable S concentrations

(10-1000 ppm) and $\delta^{34}S$ values (-0.29‰ to +4.84‰ ± 0.3, 2σ) that reflect a combination of mixing with recycled components and degassing. We show negative $\Delta^{33}S$ (-0.018‰ ±0.008, 2σ) from a rejuvenated basalt (later-stage basalts erupted after a period of quiescence following the main island-shield stage volcanism) on Upolu island that is distinct from all $\Delta^{33}S$ measured in this study and those published to date. We also identify an outlier among basalts from the Malu trend with slightly positive $\Delta^{33}S$ (+0.028‰ ± 0.008, 2σ) whose origin remains unreconciled but may be related to terrigenous sediment of marine origin. The majority of samples reveal $\Delta^{33}S$ within uncertainty of $\Delta^{33}S=0$, suggesting $\Delta^{33}S$ is relatively well mixed in the Samoan mantle plume. Furthermore, Upolu one of the older islands with DM-like compositions also has $\Delta^{33}S =0$ which establishes an estimate of the initial $\Delta^{33}S$ erupted at the Samoan islands. The small but resolvable $\Delta^{33}S$ values associated with the Vai Trend (a group of islands with lavas that exhibit contributions from HIMU components) and the rejuvenated basalts establish the basis for arguments related to specific recycled components that have distinct isotope compositions that we can directly link to the geochemical trends among the Samoan islands.

1. Introduction

Ocean island basalts (OIB) are volcanic rocks associated with hotspots erupted at intraplate locations in the world's ocean basins. Through the geochemical characterization of OIB and mid-ocean ridge basalts (MORB) with long lived-radiogenic isotopes of strontium (Sr), Neodymium (Nd), and Lead (Pb), four chemically distinct reservoirs have been identified in the mantle that are thought to be

the products of melt removal and recycled crust. These reservoirs are Depleted MORB Mantle (DMM), Enriched Mantle 1 (EM I), Enriched Mantle 2 (EM II), and HIMU (high $\mu=^{238}U/^{204}Pb$). DMM is produced from removal of melt at the base of lithosphere and is typically characterized as basalt with La/Sm <1 (e.g. Hofmann, 1988). The EM II reservoir hosts the highest $^{87}Sr/^{86}Sr$ and $^{208}Pb/^{204}Pb$ at a given $^{206}Pb/^{204}Pb$ and is produced from recycling continental crust (Jackson et al., 2007a; Workman et al., 2008). The HIMU reservoir is produced from recycling of oceanic crust where Pb is lost during subduction, resulting in the high radiogenic Pb isotope compositions (e.g. high $^{206}Pb/^{204}Pb$). EM I is characterized by relatively low $^{143}Nd/^{144}Nd$ and $^{206}Pb/^{204}Pb$ at high $^{87}Sr/^{86}Sr$, and high $^{208}Pb/^{204}Pb$ at a given $^{206}Pb/^{204}Pb$ and although controversial, is generally thought to be produced from the subduction and recycling of continental material (e.g. McKenzie and O'nions, 1983; Hawkesworth et al., 1986; Milner and le Roex, 1996).

Ocean island basalts also sample a fifth (or more) component, the primordial mantle (termed the common component (C) hereafter after Hanan and Graham, 1996), that is early formed and relatively undisturbed by processes of mantle mixing. Primordial mantle components have been identified through observations of primitive Ar and Ne, and Xe isotope compositions of mantle plume with high $^{3}He/^{4}He$ (Kurz et al., 2009; Mukhopadhyay, 2012). Recently, primordial components have been observed through correlations between $^{3}He/^{4}He$ and $\mu^{182}W$ at localities such as Samoa, Hawaii and, Iceland (Mundl et al., 2017; Mundl-Petermeier et al., 2020), and as negative $\mu^{182}W$ from younger rock material from Reunion and the Deccan flood basalts (Rizo et al., 2019). A unique feature of the identified primordial reservoirs is their

association with the seismically imaged Large Low Shear Velocity Provinces (LLSVPs) and Ultra Low Velocity Zones (ULVZs) (e.g. French and Romanowicz, 2015); mantle domains that reside at the base of the mantle that may host material that is chemically distinct from the convective mantle as they illustrate properties such as partial melt (Williams and Garnero, 1996) or high-iron enrichment (Wicks et al., 2010). With the observation of these seismically imaged reservoirs beneath localities such as Samoa (Thorne et al., 2013), Hawaii (Cottaar and Romanowicz, 2012), and Iceland (Yuan and Romanowicz, 2017), models have invoked processes such as chemical equilibration between the core and deep reservoirs such as a ULVZ to explain the negative $\mu^{182}W$ and high $^{3}He/^{4}He$ at locations such as Samoa (e.g. Mundl et al., 2020).

Sulfur isotope compositions of OIBs have been used to trace and identify various sources of sulfur that have been recycled into the mantle. At Mangaia[7], the type locality for the HIMU mantle reservoir, work by Cabral et al. (2013) identified anomalous S isotope compositions in the form of negative $\delta^{34}S$ and negative $\Delta^{33}S$ that are argued to reflect the recycling of Archean S stored in oceanic crust. Similarly, at Pitcairn[8], the type locality for the EM I mantle reservoir, Delavault et al. (2016) observe negative $\delta^{34}S$ and negative $\Delta^{33}S$ in individual sulfide grains and argue that the compositions originate from recycled Archean S. Samoa, the type locality for the EM II mantle reservoir, generally hosts positive $\delta^{34}S$ and $\Delta^{33}S$ that averages within uncertainty of the origin ($\Delta^{33}S = 0$) (Labidi et al., 2015) that is argued to reflect the recycling of continental crust. Recent work by Dottin et al. (2020) has however,

[7] Mangaia sits south east of Samoa and is approximately 1800 km away.
[8] Pitcairn sits south east of Samoa and is approximately 4600 km away.

identified positive $\delta^{34}S$ in Samoan basalts that reflect a signature from degassing and slightly positive $\Delta^{33}S$ at the Vailulu'u island that is associated with a diluted recycled HIMU component. With the type localities for the extreme mantle endmembers characterized for S-isotope, we can test whether the signatures are entrained into the Samoan mantle plume, and further whether there is a commonality to the S at type localities and the S in recycled components contributing to the radiogenic Pb isotope heterogeneity.

The Samoan islands, collectively called Samoa, are a group of islands located in the south Pacific Ocean, north of the northern terminus of the Tonga trench. In Samoa, the type locality for the Enriched Mantle II mantle signature, the highest $^{87}Sr/^{86}Sr$ from recycled continental crust are seen; however, the various islands within exhibit geochemically distinct trends for $^{206}Pb/^{204}Pb$ vs. $^{208}Pb/^{204}Pb$ that have been linked to dilute contributions from other mantle endmembers including HIMU (recycled oceanic crust) and Depleted MORB Mantle (Jackson et al. 2014). Some of the islands at Samoa have also experienced rejuvenated volcanism (volcanism after a period of quiescence); erupting geochemically distinct material with dilute EM I type compositions that have been linked to recycled continental material.

In addition to hosting recycled components, Samoa also exhibits a contribution from a deep primordial component. This primordial material was initially identified by high $^{3}He/^{4}He$ (Jackson et al., 2007) and later associated with negative $\mu^{182}W$ (Mundl et al., 2017; Mundl-Petermeier et al., 2020), linking the reservoir to one that likely formed as a result of chemical equilibration between the core and the deep mantle. In Pb isotope space, the various geochemical trends identified at Samoa converge on Pb isotope

compositions associated with high $^{3}He/^{4}He$ (Jackson et al., 2014), termed the Common "C" Component (Hanan and Graham, 1996), providing evidence for a complex geochemical system that involves mixing between primordial mantle and multiple recycled components.

Here, were present new bulk rock quadruple sulfur isotope analyses on n=18 basalts from Malumalu, Malutut, Savaii, Upolu, and Tutuila (*Figure 12*).

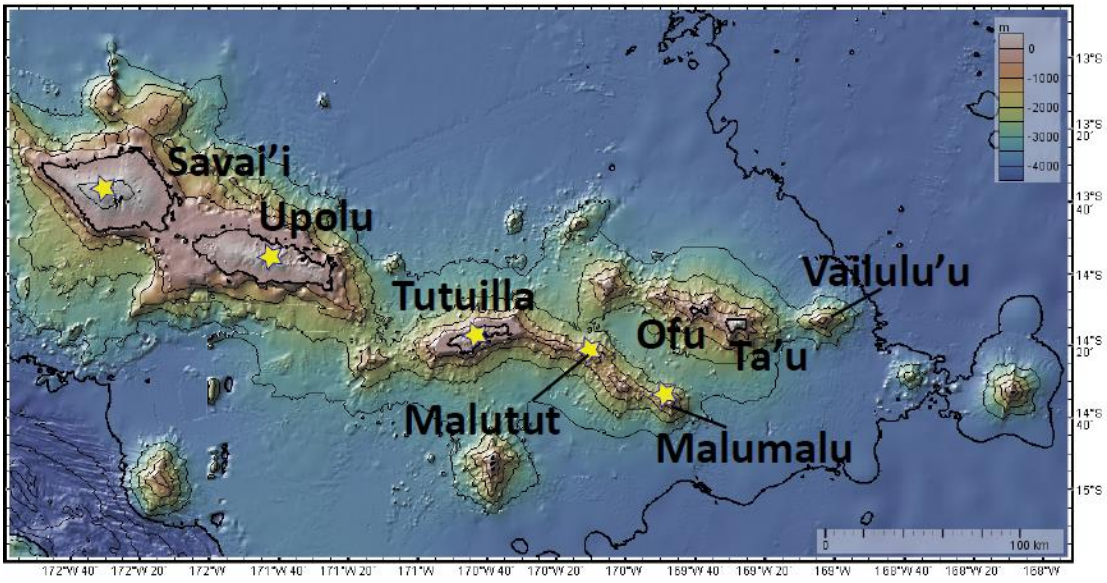

Figure 12. Map of Samoa. Stars denote islands or seamounts of samples characterized in this project. This map was generated using the GeoMap App.

We explore whether there are distinct S-isotope compositions revealed by basalts from the various geochemical trends and the implications for the S-isotope composition of the different mantle reservoirs. To date, the sulfur isotope analyses of OIB demonstrate distinct S-isotope compositions for the type localities of HIMU (Mangaia) (Cabral et al., 2013), EM I (Pitcairn) (Delavault et al., 2016), EM II (Samoa) (Labidi et al., 2015; Dottin III et al., 2020), and for DMM (Labidi et al., 2012; Labidi et al., 2013; Labidi et

al., 2014). With these distinctions, we explore how the complicated plumbing system plays a role in defining the S-isotope compositions erupted at specific localities and potentially draw connections between S-isotope compositions recycled and erupted elsewhere.

2. Methods

In preparation for acid digestion, ~ 3-6 grams of whole rock chips were crushed in a steel mortar and pestle and sieved to <56 microns. Aliquots of ~ 3 grams of homogenized powder were then placed into Teflon reactors with stir bars. The Teflon reactors were subsequently connected to a water trap with plastic tubing and the water trap was connected to an $AgNO_3$ trap were released sulfide would eventually precipitate as Ag_2S. Prior to acidification, the digestion set-up (similar to that presented in Labidi et al., 2012) was purged with N_2 for approximately 10 to 15 minutes. After purging 20 ml of $CrCl_2$, 10 ml of HCl, and 10 ml of HF was injected into the Teflon reactors through a two-way valve with flowing N_2 through a separate port. After acidification, the sample and reagents were heated to ~80 degrees C and stirred with a magnetic stir bar for better powder digestion and to avoid the formation of fluorides which can inhibit the release of sulfide. During this reaction sulfides in the powder are released as H_2S, that is then carried through the water trap to trap acid, lastly bubbled through the $AgNO_3$ trap to precipitate sulfide as Ag_2S. The reaction ran for ~3 hours. Once the reaction was complete, samples were stored in the dark for a minimum of three days and subsequently rinsed and centrifuged in 1.5 ml Eppendorf 6 times with

Milli-Q water. After rinsing, samples were dried for ~2 hours at 70 degrees C, weighed (to calculate S concentration), and wrapped in foil in preparation for fluorination.

2.1 Fluorination

Samples in foil packets were placed into nickel reaction tubes and reacted with 3-5 times excess fluorine overnight to produce SF_6. Briefly, SF_6 was first frozen into a liquid nitrogen trap and excess fluorine was passivated through a heated KBr salt. The remain frozen gas was thawed with an ethanol slush (~-108 to -110 degrees C) to separate SF_6 from HF (also produced during the overnight fluorination). The separated SF_6 was frozen into a separate coil and injected into a gas chromatograpgh with He flow. Using peak monitoring software, we were able to trap the purified SF_6 with liquid nitrogen in metal coils. After trapping, we monometrically calculated yields (78% to 108% for this study) of fluorination.

2.2 Mass Spectrometry

The purified SF_6 was next analyzed using a ThermoFinnigan MAT 253 dual-inlet gas source mass spectrometer. All samples, apart from one (ALIA 108-01), were analyzed as nine sets of eight 26-second cycles of measurements of both the reference gas and the sample gas and bracketed with analyses of a single reservoir of IAEA-S1 standard materials. ALIA 108-01 was analyzed 8 sets of 8 26-second cycles of measurements of both the reference gas and the sample gas. An analysis of IAEA-S1 was conducted only at the beginning of the session for ALIA108-01. During the analysis a pump failed on the mass spectrometer causing the analysis to end early. After

careful inspection of the analyses, the data presented do not appear to have been affected prior to pump failure. All samples were first normalized to IAEA-S1 conducted during the analytical session and subsequently renormalized to IAEA-S1 relative to CDT that places IAEA-S1 at -0.401, 0.116, 0.796 for $\delta^{34}S$, $\Delta^{33}S$, and $\Delta^{36}S$ respectively (Antonelli et al., 2014). Our estimated uncertainty on measurements (all 2σ) is 0.3, 0.008, and 0.3 for $\delta^{34}S$, $\Delta^{33}S$, and $\Delta^{36}S$ respectively and is estimated from the long-term uncertainty on measurements of IAEA-S1. We note that the in-run uncertainty on measurements of $\delta^{34}S$ and $\Delta^{36}S$ are smaller than values reported. The uncertainty reported on $\delta^{34}S$ and $\Delta^{36}S$ includes uncertainty associated with sample processing through wet chemistry and fluorination.

3. Results

Whole rock S-isotope data and S concentrations from basalts that sample the various Samoan Islands are presented in Figure 13 and Table *3*. Sulfur concentrations range from ~ 10 to 1000 ppm. Although subaerial lavas typically have lowers S concentrations relative to the S concentrations from submarine lavas, indicative of sulfur loss, there is no clear relationship between eruption depth versus S concentration (see appendix Figure 35). The new data are from Malumalu, Malutut, Savaii, Upolu, and Tutuila. Samples from Malumalu (n=2) have S-isotope compositions that are within the range (including uncertainty) of previously reported data on Malumalu ($\delta^{34}S$= 1.45 ‰ to 2.69‰ ± 0.2 relative to CDT, $\Delta^{33}S$= 0.004‰ to 0.01‰ ± 0.1, and $\Delta^{36}S$ = -0.01‰ to 0.271‰ ± 0.2) which have been reported for sulfur from fresh glass (Labidi et al., 2015) and whole rock powders (Dottin et al. 2020). The data from

Malutut, related to Malumalu, extend to more positive $\delta^{34}S$ (up to +4.89 ‰ ± 0.3) and higher $\Delta^{33}S$ (up to +0.028 ‰ ± 0.008). Data for samples from Savaii, Tutuila, and Upolu have S- isotope compositions that are within the range of previously reported data on Samoan Basalts by Labidi et al. (2015) and Dottin et al. (2020). Rejuvenated volcanism from Tutuila, Savaii and Upolu show a slightly different S-isotope composition with values ranging from -0.28‰ to 1.99‰ in $\delta^{34}S$, -0.018‰ to 0.017‰ in $\Delta^{33}S$, and -0.52‰ to 0.33‰ in $\Delta^{36}S$. The samples from rejuvenated volcanism show the largest range in $\Delta^{33}S$ for a single group of Samoan basalts reported thus far.

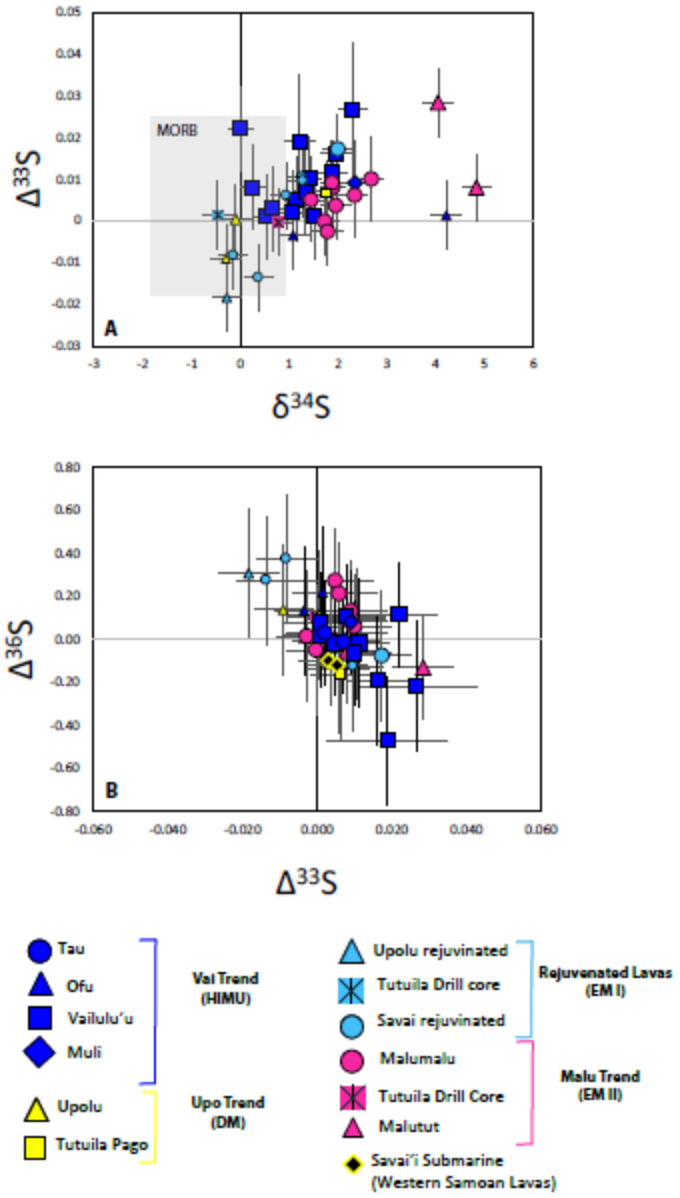

Figure 13. S-isotope compositions of basalts measured for this chapter and from previous publications by Labidi et al. (2015) and Dottin et al. (2020). A.) $\delta^{34}S$ vs. $\Delta^{33}S$ relative to CDT MORB data field represents data from Labidi et al. 2013;2014. Large symbols indicate data from submarine lavas. Small symbols indicate data from subaerial lavas. B.) $\Delta^{33}S$ vs. $\Delta^{36}S$ of basalts measured in this chapter.

Table 3. Compilation of S-isotope compositions for Samoan basalts

Sample	Dedge Depth (m)	Location	S (ppm)	$\delta^{34}S$	2σ	$\Delta^{33}S$	2σ	$\Delta^{36}S$	2σ
Rejuvenated Lavas									
UPO-7A	0	Upolu	45	-0.28	0.30	-0.018	0.008	0.31	0.30
S 11	0	Savai'i	28	0.94	0.30	0.006	0.008	-0.14	0.30
S 15	0	Savai'i	15	1.26	0.30	0.011	0.008	0.03	0.30
S 12	0	Savai'i	31	0.37	0.30	-0.014	0.008	0.27	0.30
S 32M	0	Savai'i	83	1.28	0.30	0.010	0.008	-0.13	0.30
S 26S	0	Savai'i	52	-0.15	0.30	-0.008	0.008	0.38	0.30
ALIA 116-04	2510	Savai'i	655	1.99	0.30	0.017	0.008	-0.08	0.30
Upo Volcanic Lineament									
U 16	0	Upolu	11	-0.09	0.30	0.000	0.008	0.12	0.30
U19	0	Upolu	9	-0.29	0.30	-0.009	0.008	0.14	0.30
TUT 99-01	0	Tutuila	69	1.76	0.30	0.006	0.008	-0.17	0.30

Table 4 continued. Compilation of S-isotope compositions for Samoan basalts

	Sample	Dedge Depth (m)	Location	S (ppm)	$\delta^{34}S$	2σ	$\Delta^{33}S$	2σ	$\Delta^{36}S$	2σ
Malu Volcanic Lineament										
	AVON3-78-1	2264	Malumalu	361	1.73	0.30	0.000	0.008	-0.05	0.30
	AVON3-76-9	2393	Malumalu	449	1.79	0.30	-0.003	0.008	0.01	0.30
†	AVON3-77-1	3605	Malumalu	393	1.97	0.30	0.004	0.008	-0.01	0.30
*	AVON3-76-11	2393	Malumalu	1693	2.79	0.24	0.010	0.010	0.059	0.18
*	AVON3-76-13	2393	Malumalu	1289	1.55	0.24	0.005	0.010	0.271	0.18
*	AVON3-76-3	2393	Malumalu	1348	2.00	0.24	0.008	0.010	0.099	0.18
*	AVON3-76-6	2393	Malumalu	1514	2.45	0.24	0.006	0.010	0.211	0.18
*	AVON3-76-8	2393	Malumalu	1435	1.98	0.24	0.009	0.010	0.129	0.18
	ALIA108-01	3200	Malutut	167	4.05	0.30	0.028	0.008	-0.13	0.30
	ALIA108-04	3200	Malutut	81	4.84	0.30	0.008	0.008	-0.06	0.30
Vai Volcanic Lineament										
	OFU-04-15	0	Ofu	64	4.23	0.30	0.001	0.008	0.22	0.30
	OFU-04-06	0	Ofu	29	1.08	0.30	-0.004	0.008	0.13	0.30
	AVON3-71-22 (Avg)	4170	Vailulu'u	1038	1.97	0.30	0.016	0.008	-0.19	0.3
†	AVON3-63-2	920	Vailulu'u	809	1.23	0.30	0.019	0.016	-0.47	0.30
†	AVON3-70-9	1130	Vailulu'u	201	2.30	0.30	0.027	0.016	-0.22	0.30
†	AVON3-73-1	960	Vailulu'u	214	1.88	0.30	0.01	0.008	-0.02	0.30
*	AVON3-71-13	4170	Vailulu'u	1755	1.52	0.24	0.010	0.010	-0.063	0.18
*	AVON3-71-11	4170	Vailulu'u	1794	1.62	0.24	0.001	0.010	0.017	0.18
*	AVON3-71-2	4170	Vailulu'u	1768	1.26	0.24	0.005	0.010	-0.020	0.18

Table 5 continued. Compilation of S-isotope compositions for Samoan basalts

	Sample	Dedge Depth (m)	Location	S (ppm)	$\delta^{34}S$	2σ	$\Delta^{33}S$	2σ	$\Delta^{36}S$	2σ
*	AVON3-68-3	780	Vailulu'u	800	0.35	0.24	0.008	0.010	0.106	0.18
*	AVON3-73-12	960	Vailulu'u	600	0.11	0.24	0.022	0.010	0.112	0.18
*	AVON3-75 2	2675	Ta'u	651	1.18	0.24	0.002	0.010	0.030	0.18
*	AVON3-75-10	2675	Ta'u	819	0.62	0.24	0.001	0.010	0.072	0.18
*	AVON3-75-15	2675	Ta'u	945	1.45	0.24	0.007	0.010	-0.013	0.18
*	AVON3-74-2	2544	Ta'u	1575	0.77	0.24	0.003	0.010		
*	AVON3-79-4	3484	Muli	880	2.45	0.24	0.009	0.010	0.080	0.18
	Submarine western Samoan lavas									
	ALIA 114-03	2510	Savai'i submarine	32	1.62	0.30	0.003	0.008	-0.10	0.30
	ALIA 128-21	2560	Savai'i submarine	219	4.23	0.30	0.005	0.008	-0.12	0.30
	Tutuila Island Drill Core									
	TGA-3 164.5	0	Tutuila	11	-0.47	0.30	0.001	0.008	-0.01	0.30
	TGA-3 1457	0	Tutuila	12	0.77	0.30	0.000	0.008	0.11	0.30

† Data from Dottin et al., 2020; * Data from Labidi et al., 2015

4. Discussion

4.1. The effect of degassing on $\delta^{34}S$ and S concentrations

Degassing is well documented as an agent responsible for altering both $\delta^{34}S$ and S concentrations (e.g. Moore and Fabbi, 1971; Mandeville et al., 2009), including compositions and concentrations recorded for basalts from Samoa (Dottin et al. 2020) and the Canary Islands (Beaudry et al., 2018). At the Quartz-Fayelite-Magnetite reaction buffer SO_2 dominates the gas phase with significant loss at pressures less than 100 bars (Gaillard and Scaillet, 2009; Burgisser et al., 2015). At 1200 degrees C, SO_2 is ^{32}S-enriched by ~1.5 to 3 ‰, resulting in a decrease in $\delta^{34}S$ of residual sulfide as SO_2 is degassed. When gas is rapidly lost, other open system kinetic processes affect the $\delta^{34}S$ of SO_2 and residual sulfide can be enriched in ^{34}S (e.g. de Moor et al., 2013). We therefore interpret both the $\delta^{34}S$ data and the S concentrations (of sulfide) (~10 to ~1000 ppm S) to reflect sulfur loss and note that it is problematic to attribute either directly to the original value of the source. The compositions rather reflect a combination of degassing and mixtures with recycled components.

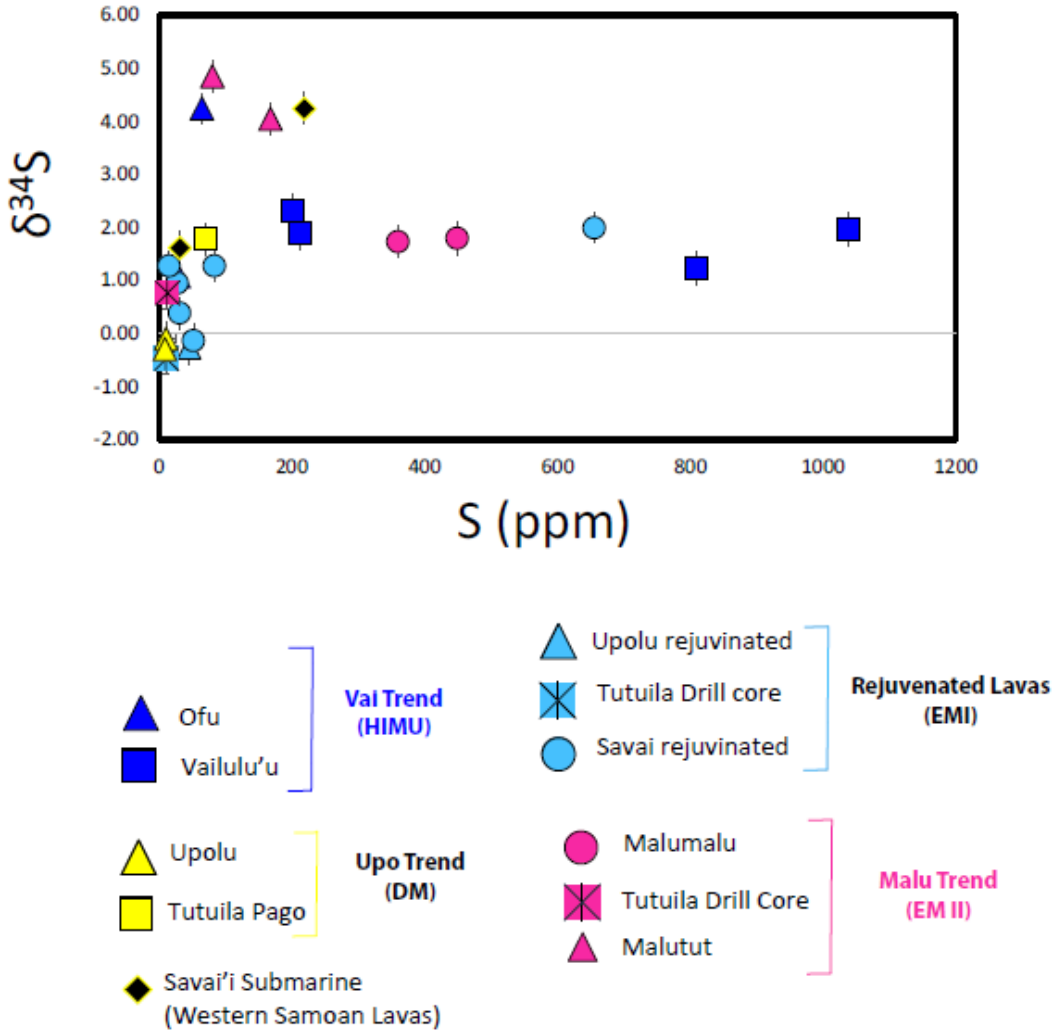

Figure 14. S (ppm) vs. $\delta^{34}S$ for bulk rock analyses from Samoan basalts including data from Dottin III et al. (2020). The data show variable $\delta^{34}S$ at lowers S concentrations, indicative of complex degassing and mixing.

We note that $\Delta^{33}S$ is little affected by degassing and provides an opportunity to explore whether the proposed distinct recycled components at Samoa can be identified with unique $\Delta^{33}S$. In a plot of $\Delta^{33}S$ for each sample, the data appear to present possible differences in composition when grouped according to criteria described in Jackson et

al., (2014), making it plausible that relationships may exist between sulfur and the geochemical mixing trends identified in that study.

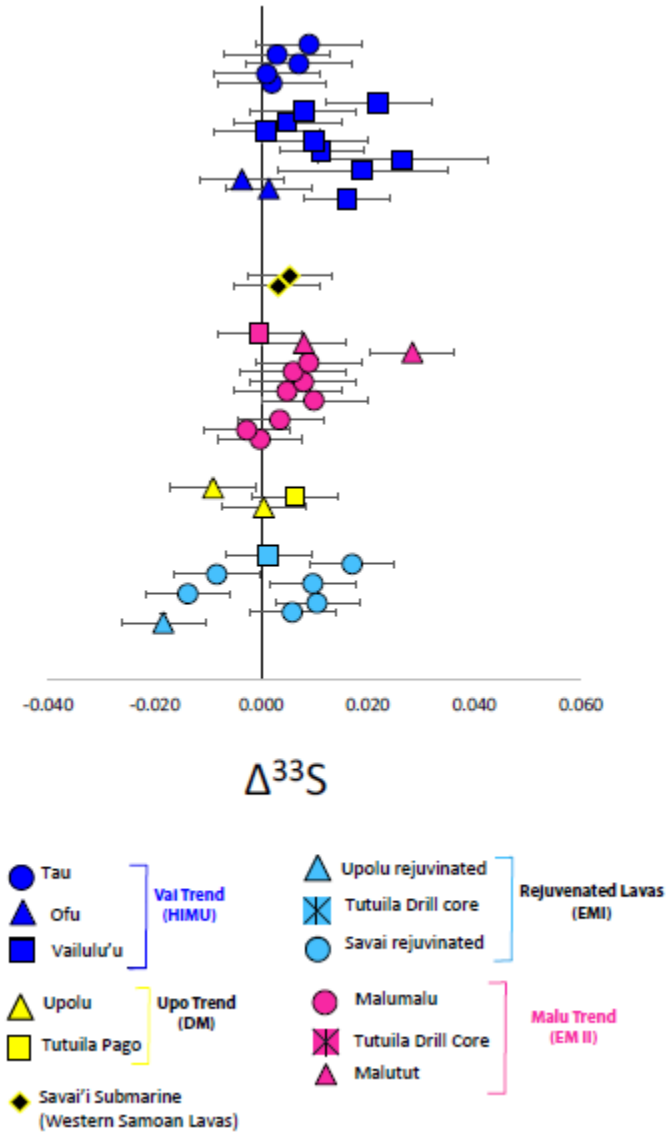

Figure 15. $\Delta^{33}S$ of each sample and their associated Geochemical trend. Data from the Vai Trend and Malu trend include data collected in Labidi et al. (2015) and Dottin III et al. (2020).

4.2 A discussion of the volcanic trends

Jackson et al., (2014) group the islands of Samoa into geochemically-defined volcanic trends: the Vai trend, the Malu trend, and the Upo trend (*Figure 16*). Note that three of the Samoan islands (Savai'i, Upolu, and Tutuila) have also experienced varying amounts of rejuvenated volcanism. The Vai trend is captured by the youngest chain of volcanic islands in Samoa and displays the highest $^{206}Pb/^{204}Pb$ (Workman et al., 2004) that is argued to reflect compositional influence from HIMU-related components. The Malu tend captured by the second youngest group of islands is argued to reflect compositional influence from EM II-related components that is reflects in higher $^{208}Pb/^{204}Pb$ for a given $^{206}Pb/^{204}Pb$. The Upo trend (Jackson et al., 2014), has low $^{206}Pb/^{204}Pb$ ratios consistent with mixing between C and a DM component (Workman et al., 2004). The rejuvenated basalts from Upolu, Savai'i and Tutuila also have low $^{206}Pb/^{204}Pb$ (but higher $^{208}Pb/^{204}Pb$ at a given $^{206}Pb/^{204}Pb$ than the Samoan Upo component) linked to the incorporation of EM I related components (Jackson et al., 2014). These four distinct compositional trends have been argued to reflect mixing between a common component and geochemically-distinct and geographically-spaced recycled components in the mantle plume (source) (Jackson et al., 2014). Their distinct lead geochemistry provides an ideal framework evaluating the way sulfur from various sources is distributed in this plumbing system.

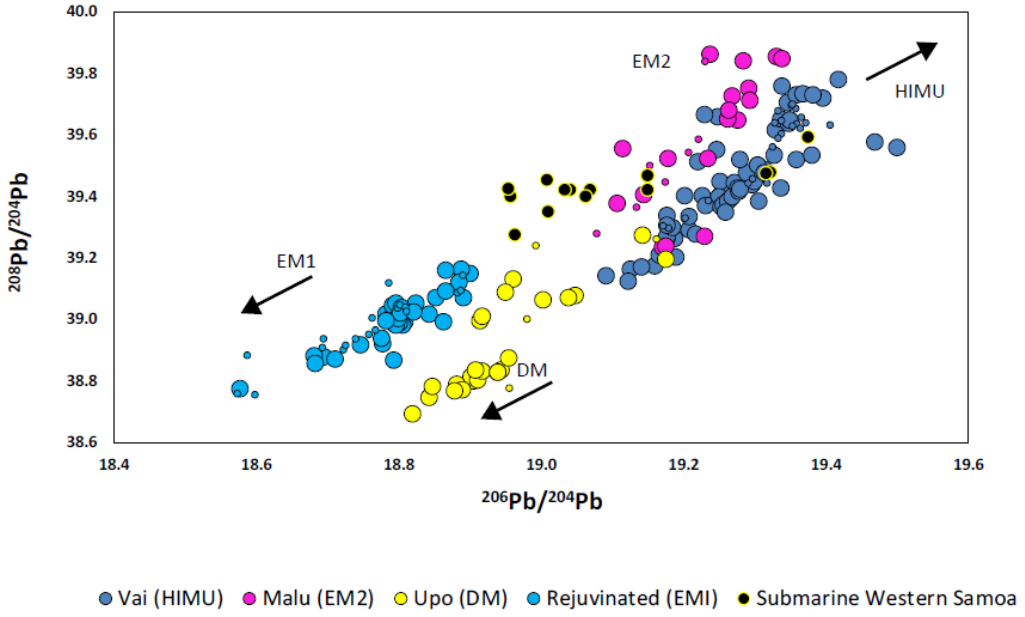

Figure 16. Compilation of Pb isotope compositions adapted from Jackson et al., (2014) that illustrate the geochemical characterization of each volcanic trend.

4.2.1 The Vai trend

Sulfur isotope compositions of basalts from the Vai trend were reported in Labidi et al. (2015) and Dottin et al. (2020). Samples from the Vai trend preserve evidence of mixing between a primordial component ($\Delta^{33}S=0$, negative $\mu^{182}W$, high $^{3}He/^{4}He$) and a recycled HIMU component (slightly positive $\Delta^{33}S$, convective mantle compositions of $\mu^{182}W$ and $^{3}He/^{4}He$, and relatively high $^{206}Pb/^{204}Pb$ isotope compositions). Dottin et al. (2020) argue that the relationship between positive $\Delta^{33}S$ and high $^{206}Pb/^{204}Pb$ (Figure 9, Chapter 2) reflects recycled sulfur associated with HIMU. In Jackson et al. (2014), it was argued that the Vai trend receives a distinct contribution of recycled HIMU-related material from the east, in contrast to EM II

components at the Malu trend from west (discussed in next section). The $^{206}Pb/^{204}Pb$ vs. $^{208}Pb/^{204}Pb$ compositions from the Vai trend (and other trends) radiate from a small range of values associated with high $^{3}He/^{4}He$, termed the common component (Hanan and Graham, 1996; Jackson et al., 2014). An important observation made by Jackson et al. (2014) was the relationship between $^{3}He/^{4}He$ and the distance from the common component region in Pb-isotope space, where $^{3}He/^{4}He$ decreases further away from the common component, approaching endmember compositions for EM I, EM II, and HIMU. The relationships shown by Dottin et al. (2020) (Chapter 2) between sulfur, lead, and helium suggest that $\Delta^{33}S$ would increase further away from the common component as the HIMU endmember is mixed with it. The data from the Vai trend collected by Dottin et al., 2020 and Labidi et al., 2015 are consistent with this suggestion, revealing $\Delta^{33}S$=0‰ at $D^{206/207/208Pb}$= 0.00 to 0.116 and $\Delta^{33}S$= +0.027‰ at $D^{206/207/208}Pb$ = 0.814 (Figure *17*) where $D^{206/207/208Pb}$ is a distance parameter from the common component in three-dimensional space (Jackson et al., 2014).

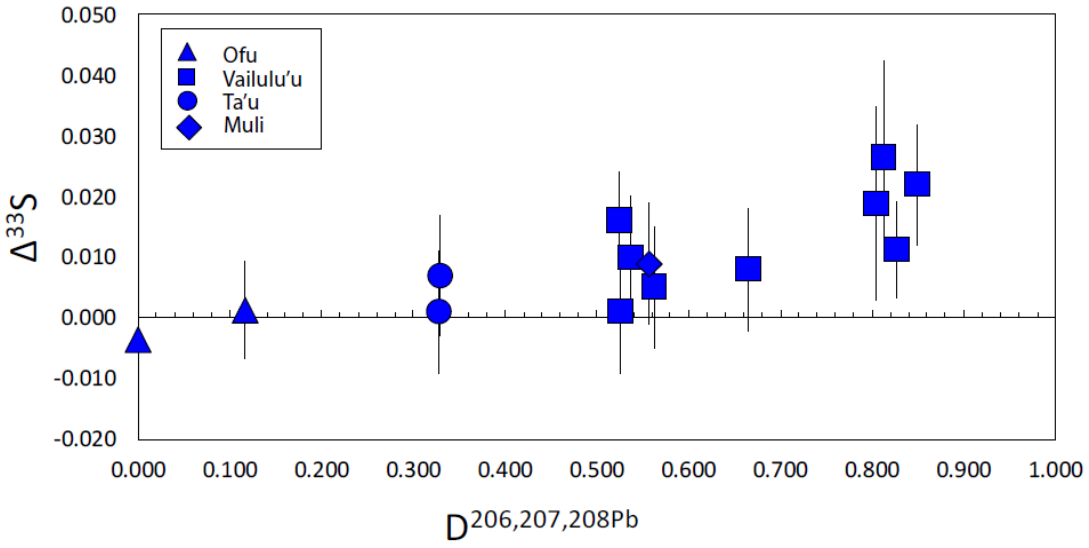

Figure 17. $D^{206,207,208Pb}$ vs. $\Delta^{33}S$ for basalts from the Vai trend illustrating an increase in $\Delta^{33}S$ with increasing distance from the common component. Data shown are from Dottin et al. (2020) and Labidi et al. (2015).

The relationship between $D^{206,207,208Pb}$ and $\Delta^{33}S$ is additional evidence of sulfur isotope mixing among samples in the Vai trend and shows that increased distance from the common component can result in a compositional influence on the S-isotope composition from HIMU related basalts. The positive correlation between $D^{206,207,208Pb}$ and $\Delta^{33}S$ also indicates that the HIMU component mixed in is potentially more positive than that seen by Dottin et al. (2020). In chapter 4, I present additional data from Mangaia, the type locality for HIMU related basalts and argue for an additional HIMU recycled endmember with positive $\Delta^{33}S$. Such may be an explanation for the slightly positive HIMU-related $\Delta^{33}S$ shown by Dottin et al. (2020) and in this chapter, but would be a component that contrasts with the negative $\Delta^{33}S$ presented on Mangaia (HIMU) basalts by Cabral et al. (2013), which ultimately points to multiple recycled S sources related to HIMU mantle components .

4.2.2 The Malu trend

An extensive data set from the Malu trend (mixing of C with EM II) has been published by Labidi et al. (2015). Additional samples are presented here with two additional analyses from Malumalu and two analyses from Malutut. The majority data collected are within the range of previously reported values from Malumalu (Labidi et al., 2015). One sample, ALIA 108-01 is an exception as it exhibits slightly positive $\Delta^{33}S$ (+0.028 ± 0.008) that matches the maximum $\Delta^{33}S$ of the Vai trend (Dottin et al., 2020) (Figure *15*). This slightly positive $\Delta^{33}S$ contrasts with the rest for the Malu related basalts that have $\Delta^{33}S$ values all within the origin ($\Delta^{33}S$=0).

On a plot of $D^{206/207/208Pb}$ vs. $\Delta^{33}S$, the data do not reproduce a relationship like that seen for the Vai trend where the most anomalous $\Delta^{33}S$ is associated with the furthest distance from the common component (Figure *18*). Given measurements of samples from the common component, $\Delta^{33}S$ is expected to trend towards 0 as the distance parameter decreases. This is observed, but because the majority of samples from the Malu trend plot within uncertainty of $\Delta^{33}S$ =0. One outlier (ALIA 108-01) was analyzed. The question is whether this outlier is part of this trend (reflecting heterogeneity in $\Delta^{33}S$ of EM II), or reflects some other sulfur source. In plots of $^{206}Pb/^{204}Pb$ vs. $^{208}Pb/^{204}Pb$ EM II is heterogenous. Thus, ALIA 108--01 may be illustrating the isotopic heterogeneity among recycled terrigenous sediment of marine origin in EM II mantle components.

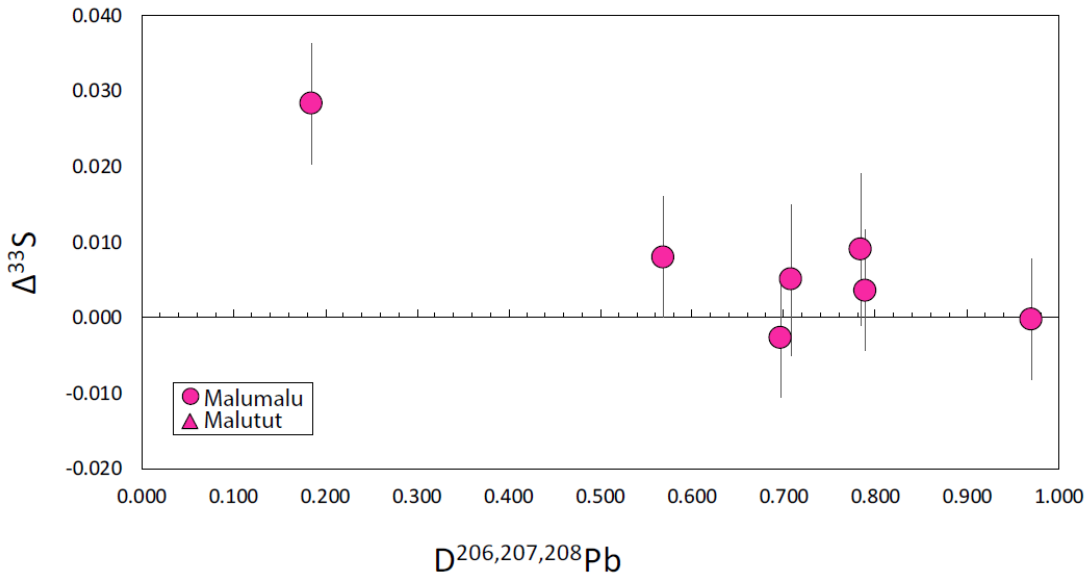

Figure 18. $D^{206,207,208Pb}$ vs. $\Delta^{33}S$ for Malu trend basalts that outlines essentially no trend among the samples with the exception of one outlier.

Interestingly, in plots of $^{206}Pb/^{204}Pb$ vs. $^{208}Pb/^{204}Pb$, ALIA108-01 plots low in both $^{206}Pb/^{204}Pb$ and $^{208}Pb/^{204}Pb$ relative to the majority of the samples from the Malu trend and plots in the data field better associated with diluted HIMU like that of the Vai trend, leaving the possibility that ALIA108-01 hosts $\Delta^{33}S$ that is linked to HIMU components rather than EM II. A problem with this suggestion is that this sample also does not fall on the relationship between $\Delta^{33}S$ and the distance parameter ($D^{206/207/208Pb}$) of the Vai trend. One possibility is that the HIMU component of the Vai trend has heterogeneous $\Delta^{33}S$ that has so far not been revealed. Another is that there is some other component, or possibly that the single sample is anomalous. Documentation of additional samples with similar characteristics will be needed to refine this interpretation.

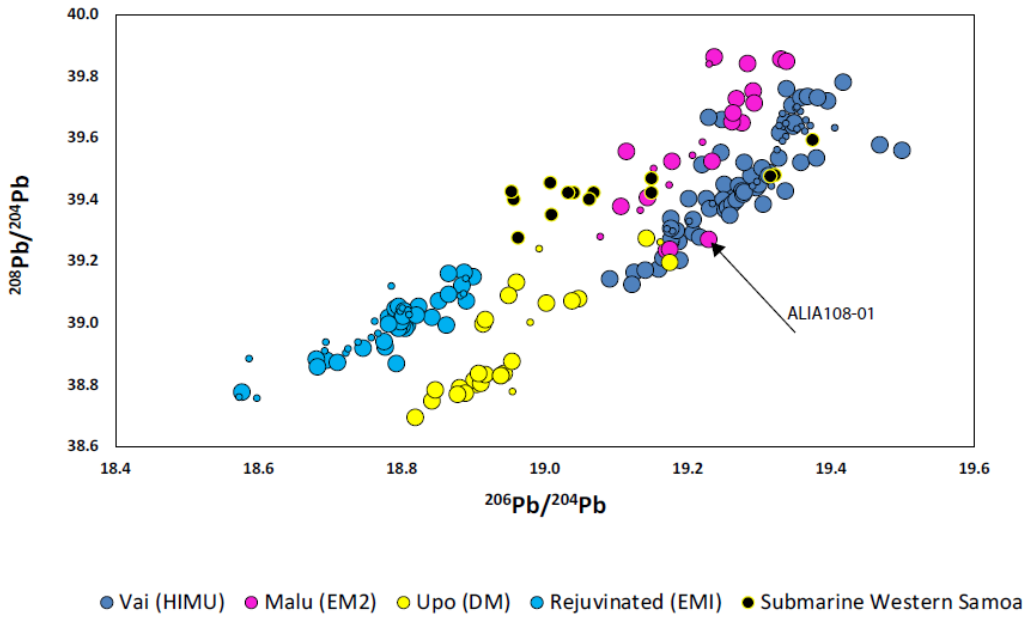

Figure 19. Pb isotope compilation of Samoan basalts from Jackson et al. (2014). In this figure ALIA108-01 is highlighted to illustrate that its compilation overlaps with that of the Vai trend. Large data symbols represent samples collected using Pb-spiked TIMS (thermal ionization mass spectrometer) methods and samples analyzed using Tl-addition by MC-ICP-MS methods, and small data symbols represent samples collected using unspiked-Pb isotope TIMS measurements.

4.2.3 Rejuvenated lavas

We present data on n=6 rejuvenated basalts from Samoa that are from the Savaii, Upolu, and Tutuila Islands. Volcanism at Samoa consists of a shield stage and a post-shield stage that is followed by a period of quiescence which is followed by rejuvenated volcanism. At Samoa, it is thought that rejuvenated volcanism was triggered by plate flexure of the lithosphere due to subduction at the Tonga Trench (Natland, 1980; Konter and Jackson, 2012). The rejuvenated basalts are characterized as having Sr-Nd-Pb isotope compositions that reflect a mixture between metasomatized

MORB and Rarotonga-type material, He-Ne that are linked to a metasomatic EM I-type mantle source (Konter and Jackson, 2012), and $^{206}Pb/^{204}Pb$ versus $^{208}Pb/^{204}Pb$ relationships that exhibit a diluted contribution from EM I type mantle (Jackson et al., 2014). The data from the rejuvenated lavas exhibit $\Delta^{33}S$ values that range from -0.018 ‰ to +0.015 ‰ and display the lowest $\Delta^{33}S$ recorded for Samoa (Figure *15*). In plots of $D^{206/207/208Pb}$ vs. $\Delta^{33}S$ the data reveal significant variation of $\Delta^{33}S$ for little variation of $D^{206/207/208Pb}$ (Figure *20*). This behavior is different than observed for sulfur associated with the Malu and Vai trends. The samples analyzed span a relatively limited range of $^{206}Pb/^{204}Pb$ and $^{208}Pb/^{204}Pb$ and therefore the distance parameter ($D^{206/207/208Pb}$). Like arguments made for the Malu trend and Vai trend data, mixing with a common component as was made for the Malu trend data, that any relationships should converge on $\Delta^{33}S=0$ at low values of distance parameter ($D^{206/207/208Pb}$). Thus, while the data may hint at the potential for a trend between $\Delta^{33}S$ and $D^{206/207/208Pb}$ the fact that it does not converge toward $\Delta^{33}S=0$ as the distance parameter decreases suggests that the EM I endmember has variable (positive and negative $\Delta^{33}S$). The remote possibility that a relationship exists for the small range of $D^{206/207/208Pb}$ for rejuvenated basalts should be investigated further to evaluate whether this assertion is justified.

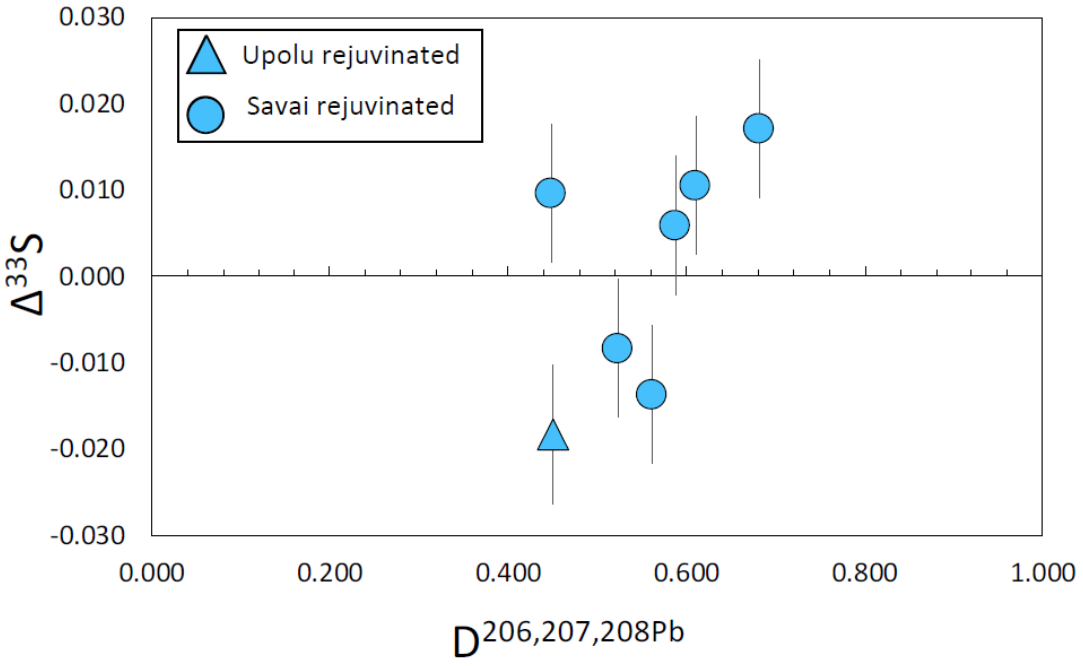

Figure 20. $D^{206,207,208Pb}$ vs. $\Delta^{33}S$ for rejuvenated basalts from Samoa illustrating a more steep relationship than that seen in Vai trend basalts.

Additional evidence that the rejuvenated lavas have variable $\Delta^{33}S$ is seen in plots of $\Delta^{33}S$ vs. $^{3}He/^{4}He$. The most negative $\Delta^{33}S$ (-0.018‰ ± 0.008) value in rejuvenated lavas is from the Upolu island. In addition to having an EMI (rejuvenated) type composition (Jackson et al., 2014), this sample has also been characterized as having a $^{3}He/^{4}He$ of 12 Ra, a value seen typically in OIB (Kurz et al. 2009). Samoan lavas with the highest $^{3}He/^{4}He$ are associated with near zero $\Delta^{33}S$ (Dottin III et al., 2020; Chapter 2). This sample expands the range of variability for $\Delta^{33}S$ of (typical) mantle with $^{3}He/^{4}He$ (8-12 Ra) from slightly positive to near zero $\Delta^{33}S$ (Dottin III et al., 2020; Chapter 2) to a range that also includes slightly negative $\Delta^{33}S$. The rejuvenated basalts from Savai'i hosts $\Delta^{33}S$ values that are similar to basalts previously

measured at Samoa and conform to arguments presented by Dottin et al. (2020) on S vs. He relationships. The rejuvenated basalt sample from Upolu does not conform to these arguments and illustrates mixing of a separate sulfur component (Figure *21*). The lack of conformity illustrates the uniqueness of the rejuvenated lava isotope composition and extends the range of potential recycled S-isotope compositions at Samoa to negative values.

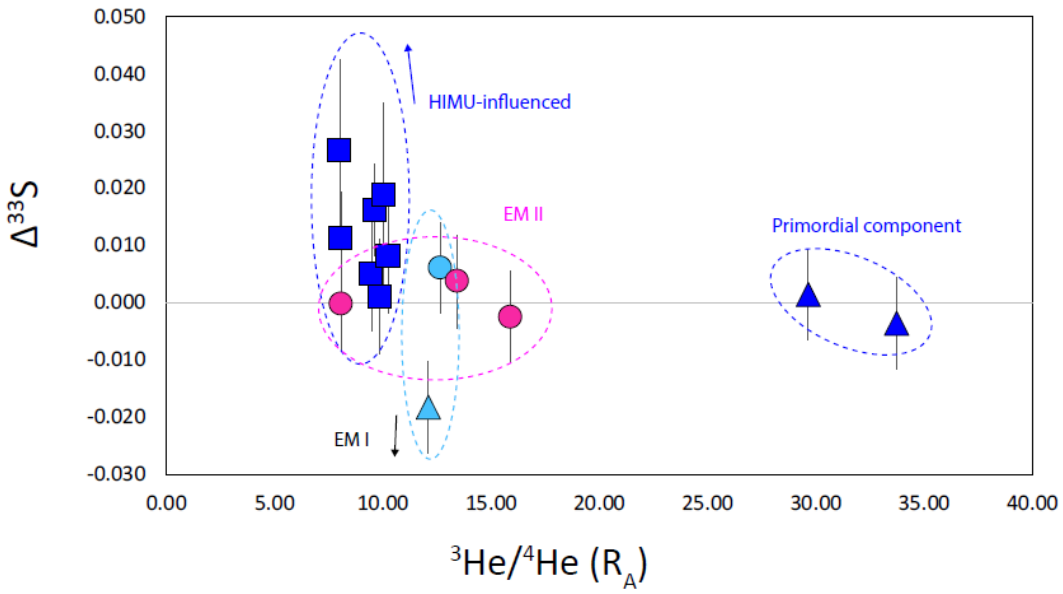

Figure 21. $^{3}He/^{4}He$ vs. $\Delta^{33}S$ for Samoan basalts. The data show a different mixing component for the rejuvenated basalts (EMI) from that previously shown by Dottin et al., (2020) in the Vai trend (HIMU). He isotope data are from Jackson et al. (2007a,b) and Jackson et al., (2014), and Workman et al. (2004)

Whether the rejuvenated composition observed at Upolu is related to the compositions at Pitcairn (the type locality for EM I basalts) for which negative $\Delta^{33}S$ has also been suggested (to -0.85 ‰ ± 0.13) via SIMS analyses reported by Delavault et al. (2016) remains an outstanding question. The $\Delta^{33}S$ deviation in UPO-7A is in the correct direction if trying to link to EM I components at Pitcairn, but the magnitude of

the $\Delta^{33}S$ is not sufficient to require a contribution from Archean sulfur, as is argued for Pitcairn and could reflect other materials of younger age (c.f., .Ono et al., 2012; Johnston et al., 2007).

The variance in $\Delta^{33}S$ may potentially be linked to the proposed metasomatized lithospheric mantle beneath these islands. Konter et al. (2016) argues that the elevated Fe isotope compositions at rejuvenated lavas is potentially due to a combination of partial melting and metasomatism of the lithospheric mantle. During metasomatism of the lithospheric mantle, anomalous $\Delta^{33}S$ can be transferred from the subducted slab to the lithospheric mantle. Thus, the composition seen may be one that is unique to the metasomatized lithospheric mantle beneath Samoa, differing from components likely subducted deeper and erupted elsewhere (e.g. Pitcairn). Question however remain in identifying how anomalous S isotope compositions are delivered to this metasomatized source. An Archean origin would likely require plume volcanism to deliver the S to the lithosphere beneath Samoa, as the Archean S mantle reservoir is hypothesized to be situated at base of the mantle (e.g. Farquhar and Jackson, 2016). Alternatively, the S may be contributed by biogenic sulfides which are known to host small $\Delta^{33}S$ variations and variable $\delta^{34}S$ (Rouxel et al., 2008a; Alt and Shanks, 2011; Ono et al., 2012). The modern sediments would be subducted at the tonga trench and upon further subduction into the mantle, the subducted slab would metasomatize the base of the lithosphere. The direction of subduction is, however, in the wrong direction that would allow for direct metasomatism. Instead, a sweeping mechanism that circulates subducted slab in the direction of Samoa would be required.

4.2.4 Upo Trend

Shield stage basalts from the Upolu Island and Tutuilla Pago represent samples from some of the oldest parts of the hotspot track and exhibit Pb isotope compositions that link them to DM-like components (Jackson et al., 2014). The S-isotope composition of MORB is estimated at $\delta^{34}S$= -0.9‰ and $\Delta^{33}S$=0‰ (Labidi et al., 2014). We analyzed three samples with these characteristics (U16, U19, and TUT 99-01). All samples with these characteristics have $\Delta^{33}S$ within uncertainty of that shown for the primordial mantle (Dottin et al., 2020) and MORB (Labidi et al. 2013;2014). $\delta^{34}S$ is variable, ranging from -0.29‰ to 1.76‰ (±0.3), but, as stated in section 4.1, is likely related a combination of mixing with recycled components and degassing. We note that the $\Delta^{33}S$ is also similar to the majority of EM II related material. Thus, without unaltered $\delta^{34}S$, no clear connection to DM components can be made. We can however argue that the lack of anomalous $\Delta^{33}S$ confirms the lack of exogenous sulfur which is expected for DM components and the $\Delta^{33}S$ is likely a representation of the S isotope compositions initially erupted at the Samoan islands. Furthermore, submarine basalts from Savai'i represent the oldest material erupted at Samoa (Koppers et al., 2008) and show near zero $\Delta^{33}S$ values. Although these samples are not associated with DM related components, the near zero $\Delta^{33}S$ from the Savai'i submarine samples affirm suggestions of a near zero $\Delta^{33}S$ associated with the oldest parts of the hotspot track.

4.4 Tutuila Island

Tutuila Island is an island that is characterized as a member of the Malu group. Tutuila is the cite of a drill core with radiogenic and major element data (Reinhard et

al., 2019) which here is used two samples to test whether the S-isotope composition is distinct between the earlier and later stages of volcanism of the Malu group. The core segments reflect1.45 million years of volcanism and show that the earliest eruptions were linked to EM II type mantle, followed by FOZO (Focal Zone), DMM, and lastly EM I from rejuvenated volcanism (Reinhard et al., 2019).

The isotopic analyses done here, reveal no difference in $\Delta^{33}S$ between the EM II related basalt and the rejuvenated EM I related basalt. A similar observation is seen between most samples from the Malu trend and rejuvenated lavas from Savai'i and suggests that the small $\Delta^{33}S$ variations seen at Malutut or in the rejuvenated lavas at Upolu are not widespread. Although the $\delta^{34}S$ values are distinct between the two samples we rule out significance due to the subaerial nature of these basalts and the susceptibility to alteration of the initial $\delta^{34}S$ from S degassing.

5. Conclusion

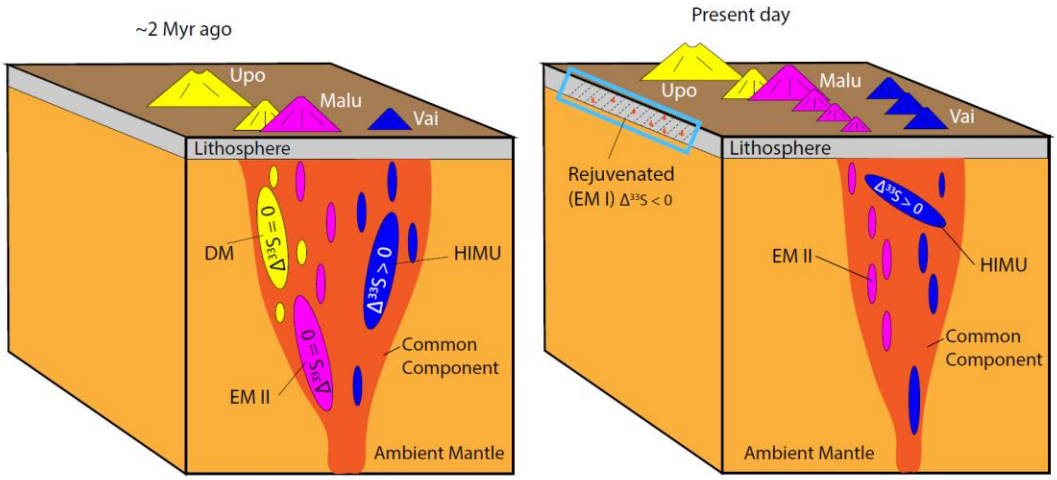

Figure 22. Schematic after Jackson et al., (2014) that illustrates hypothesis for geochemical geometry of the Samoan Plume as it pertains to the S-isotope compositions. Here, different components of the plume contribute variable proportions of mantle endmembers with unique $\Delta^{33}S$ characteristics, leading to the observed variability and geochemical relationships. On the left, the initial $\Delta^{33}S=0$ is erupted in DM related components associated with the Upo trend ~2 Myr ago. The beginning of the Malu and Vai trend also erupt $\Delta^{33}S=0$. At present day, rejuvenated volcanism erupts beneath the Upo trend (and partially beneath the beginning of the Malu trend) and contributed positive and negative $\Delta^{33}S$. The Vai trend receives components with slightly positive $\Delta^{33}S$ which potentially contaminates the melts erupted at the Malu trend that yields slightly positive $\Delta^{33}S$ erupted at Malutut (associated with the Malu trend).

We present S-isotope compositions (new data and data from Dottin et al. (2020) and Labidi et al. (2015)) on basalts from the Vai Trend, Malu Trend, Upo Trend, and rejuvenated basalts to test for unique S-isotope compositions associated with each islands' associated geochemical trend. Most data collected, including those with DM-like components, show $\Delta^{33}S$ values within uncertainty of the origin $\Delta^{33}S=0$. Exceptions are seen in two samples from the Vai trend (Dottin et al., 2020), one sample from the Malu trend, and one sample from rejuvenated lavas. The anomalous $\Delta^{33}S$ in the Vai trend is linked to recycled HIMU related sulfur that is mixed with sulfur associated with the common component ($\Delta^{33}S=0$). The origin of slightly positive $\Delta^{33}S$ of the sample from the Malu trend with is not clear. The data point is an outlier from other data from Malu trend and does not exhibit a relationship between sulfur and distance from the common component that would suggest that its recycled component is being mixed in a systematic way. The data collected on Rejuvenated lavas show slightly positive and slightly negative $\Delta^{33}S$ associated with diluted EM I compositions relative to $^{206}Pb/^{204}Pb$ vs. $^{208}Pb/^{204}Pb$. The small variations in $\Delta^{33}S$ leaves no way to unambiguously discern whether the compositions are linked to S-isotope compositions

measured in Pitcairn basalts (type locality for EM I) or whether the S-isotope variability is linked to a separate EM I related recycled component.. The composition is however indicative a different recycled component and highlights a previously unrecognized recycled compositional endmember for Samoan basalts. Altogether, the different compositional trends appear to have unique S-isotope characteristics, suggesting the proposed geochemical geometry of Samoa can have an influence on S-isotope compositions erupted at the specific compositional trends (Figure 22). The work presented establishes the basis for additional work needed at Samoa to test for unique $\Delta^{33}S$ at the various compositional trends. The data begin to outline specific compositional fields in S vs. Pb isotope space (see appendix Figure 34) however, more work is needed to establish increased definition of each compositional field.

Chapter 4: Bulk sulfur isotope characterization of HIMU mantle feeding the Mangaia mantle plume: Evidence for multiple recycled sulfur reservoirs

James W. Dottin III*[1], Jabrane Labidi[3], Matthew G. Jackson[4], James Farquhar[1,2]

*Corresponding author: jdottin@umd.edu
[1]Department of Geology, University of Maryland, College Park, MD 20742, United States
[2]Earth System Science Interdisciplinary Center, College Park, MD 201742, United States
[3]Université de Paris, Institut de physique du globe de Paris, CNRS, F-75005 Paris, France
[4]Department of Earth Science, University of California, Santa Barbara, CA 93106, United States

Abstract

Mangaia, an ocean island in the Cook-Austral suite, is the type locality for the HIMU mantle reservoir, and has also been shown to exhibit evidence for recycled sulfur with anomalous $\delta^{34}S$ and $\Delta^{33}S$ that has been attributed an Archean origin. Here we report bulk S isotope data from sulfide inclusions in olivine and pyroxene phenocrysts from one of the previously analyzed and four additional Mangaia basalts to further test for the prevalence of anomalous S in the HIMU mantle source feeding Mangaia. We document values that range from -5.13‰ to +0.21‰ (±0.3 2σ), +0.006‰ to +0.049‰ (±0.016 2σ), -0.81‰ to +0.69‰ (±0.3 2σ) for $\delta^{34}S$, $\Delta^{33}S$, and $\Delta^{36}S$ respectively. These data extend the range of measured values for HIMU lavas and

suggest S-isotope heterogeneity in the HIMU mantle source at Mangaia. We show that S-isotope compositions of bulk sulfide in olivine is not in isotopic equilibrium with bulk sulfide in pyroxene from the same samples and that samples from a confined area in the northern central part of the island show a distinct covariation for $\delta^{34}S$ and $\Delta^{33}S$. This isotopic variation (array) suggests mixing of sulfur from two sources that was captured at different stages of crystallization by phenocrysts in the Mangaia magma HIMU sulfur endmember.

1. Introduction

Covariations in the radiogenic isotope signature of strontium (Sr), neodymium (Nd) and lead (Pb) seen in various Ocean Island Basalts (OIB) and Mid-Ocean Ridge Basalts (MORB) have been used to identify distinct compositional reservoirs that exist in the mantle as a result of melt removal and recycling of oceanic and continental crust. These reservoirs have been termed Depleted MORB Mantle (DMM), Enriched Mantle I and II (EM I, EM II), and HIMU (high $\mu=^{238}U/^{204}Pb$). Depleted MORB mantle is characterized as having relatively low $^{206,207,208}Pb/^{204}Pb$ and $^{87}Sr/^{86}Sr$ but high $^{143}Nd/^{144}Nd$, and argued to have formed from the process of melt removal during crust formation (Salters and Stracke, 2004; Workman and Hart, 20u05). HIMU is characterized by high $^{206,207,208}Pb/^{204}Pb$, low $^{87}Sr/^{86}Sr$, and intermediate $^{143}Nd/^{144}Nd$. The HIMU reservoir is thought to have formed from the recycling of oceanic crust that experienced Pb loss from sulfides during subduction followed by the ingrowth of radiogenic Pb due to a high $^{238}U/^{204}Pb$ ('high μ') time integrated ratio (e.g Chauvel et al., 1992; Kelley et al., 2005) with a wide range of proposed formation ages of 550 Ma

to 3.0 Ga (Hauri and Hart, 1993; Thirlwall, 1997; Nebel et al., 2013; Mazza et al., 2019).

Mangaia, located in the Cook-Austral volcanic chain, is the type locality for the HIMU mantle reservoir that, together with Bermuda, preserve the highest reported radiogenic $^{206}Pb/^{204}Pb$ isotope compositions of any OIB locality suggesting an old and recycled source (Hauri and Hart, 1993; Woodhead, 1996; Mazza et al., 2019). This source also appears to have connections to recycling. Jackson and Dasgupta (2008) and Cabral et al. (2014) argue that HIMU basalts are associated with a carbonated mantle source on the basis of major element characteristics (low SiO_2 and high CaO/Al_2O_3) and elevated volatile contents of CO_2. Weiss et al. (2016) suggest the HIMU mantle source of Mangaia was metasomatized by carbonatitic fluids and imply a connection to recycling processes. The sulfur isotope composition of sulfides in sulfide inclusions from Mangaia basalts have been measured using Secondary Ion Mass Spectrometry (SIMS) and conventional bulk isotope methods, and show anomalous $\delta^{34}S$ and $\Delta^{33}S$ values in samples, suggesting a subducted component in the source of Mangaia melts that hosted Archean sulfur characterized by mass independent fractionation (Cabral et al., 2013a). What remains unanswered is whether anomalous Archean S is common in the HIMU mantle reservoir sampled by Mangaia, or whether other Mangaia basalts contain what might be considered more typical mass-dependent sulfur, with S-isotope compositions similar to that of the convective mantle or from recycled material that is post-Archean in origin.

Here, we present bulk S-isotope compositions ($\delta^{34}S$, $\Delta^{33}S$ and $\Delta^{36}S$) of sulfide inclusions within magmatic olivine and clinopyroxene phenocrysts from five Mangaia

samples. These olivine and clinopyroxene phenocrysts trap sulfide inclusions during their growth at depth in the magma chamber and, like melt inclusions (e.g. Sobolev and Shimizu, 1993), they may shed light on melt mixing of diverse sources. Our data provide new constraints on the various recycled components that dominate HIMU mantle melts feeding lavas at Mangaia.

2. Samples and Methods

We present new multiple sulfur isotope data on 5 basaltic samples from Mangaia: MGA-B-25, M4, M10, M12, and M13. Localities on Mangaia island are shown in Figure *23*: A road cut along the northeast side of the island (MGA-B-25), Vau Roa stream Valley (M4, M10, M12, and M13), a road cut adjacent to a stream north of Tamarua village on the south side of the island (MGA-B-47) and a small outcrop revealed by a road cut near a stream on the south side of the island (MG1001B). MG1001B, MGA-B-47 and MGA-B-25 were analyzed in Cabral et al. (2013). We analyzed newly prepared aliquots of minerals from MGA-B-25, while M4, M10, M12, and M13 (n=4) are samples that have not previously been analyzed for sulfur isotopes.

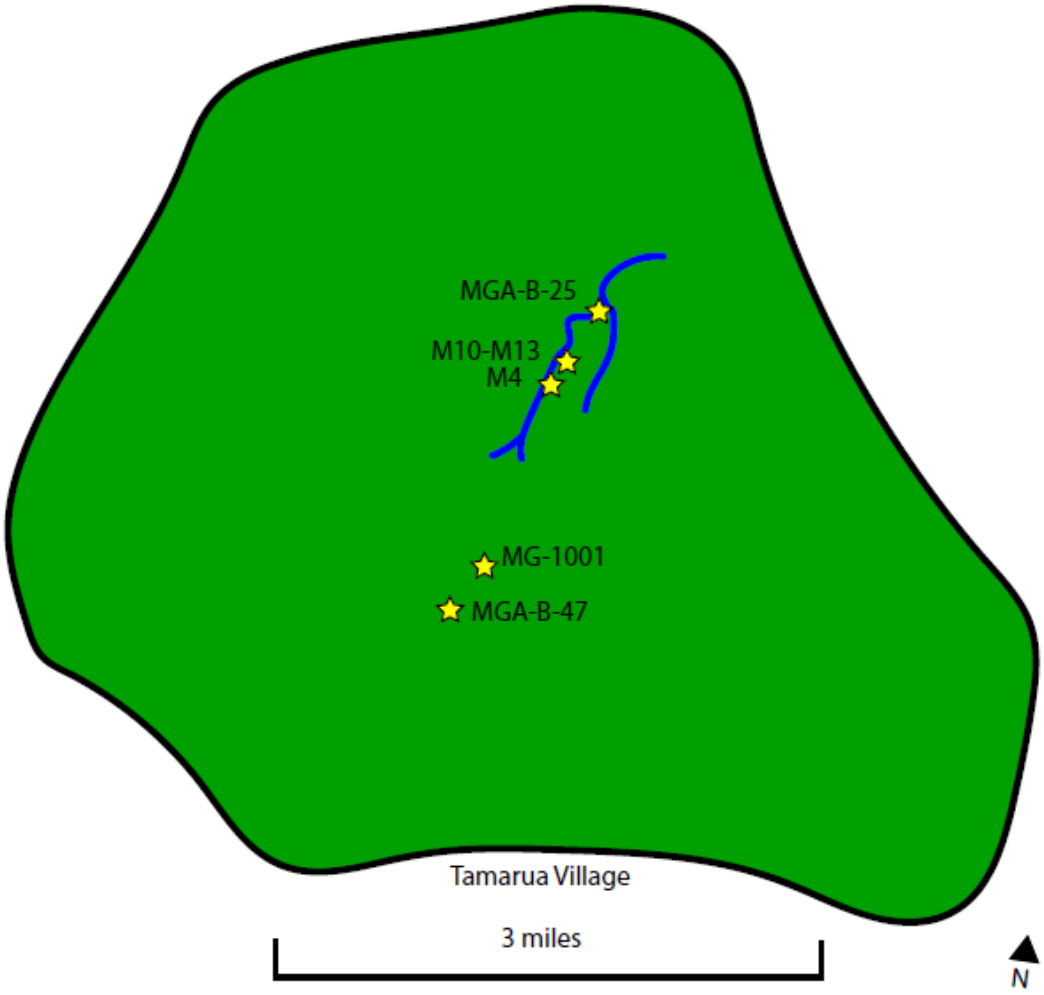

Figure 23. Sketch of Mangaia and the sampling localities (denoted with stars).

1.1 Acid digestion

All samples are olivine and clinopyroxene phenocryst separates that were hand-picked and cleaned by sonication in preparation for S isotope analyses. Crushed and weighed Ol and Px mineral separates were placed into Teflon reaction vessels for acid hydrofluoric digestion using methods developed by Labidi et al. (2012). The digestion apparatus was first purged for ~ 15 minutes with N_2. After purging, the samples were

acidified and digested in a heated solution (70-80˚C) of 3.2M $CrCl_2$, 12M HCl, and 29M HF in the amounts of 10 ml, 5 ml, and 5ml respectively. During this digestion, sulfide was released as H_2S, bubbled (~3-5 bubbles every ~1-2 seconds) through a water trap to remove acid vapors, before being bubbled and trapped in weakly acidic $AgNO_3$ where S is precipitated as Ag_2S. The Ag_2S was centrifuged and rinsed 3 times with Milli-Q water. After rinsing, the Ag_2S was dried at ~ 70 ˚C and subsequently weighed to determine sulfur concentration.

1.2 Fluorination

The weighed Ag_2S was wrapped in foil and placed into nickel reaction tubes 3-5 times excess F_2. Reactions between Ag_2S and F_2 occurred at ~250˚C for at least 12 hours. The product SF_6 was separated from residual F_2 by freezing into a liquid-nitrogen-cooled trap. Residual F_2 was passivated through a reaction with heated (~ 110˚C) KBr salt. After all fluorine was passivated, the liquid nitrogen trap was replaced by an ethanol slush (~-108 ˚C to -115˚C) to retain co-condensed HF and the SF_6 was sublimated into a separate liquid-nitrogen-cooled trap, from which it was injected into a gas chromatograph (GC) with a 1/8-inch diameter, 6-foot long Haysep-Q™ GC column and a 5A GC column using a helium flow rate of 20 mL/min. SF_6 was monitored while passing through the GC and captured in liquid nitrogen cooled metal coils. Once captured, the SF_6 was thawed to determine procedural yields as pressure and lastly, stored in individual glass manifolds.

1.3 Mass spectrometry

Isotopic variations of the four stable isotopes of sulfur (^{32}S (95.2%), ^{33}S (0.75%), ^{34}S (4.25%), and ^{36}S (0.02%)) were determined using gas source mass spectrometry of purified SF_6. Measurements were made by monitoring SF_5^+ ion beams at m/z of 127, 128, 129, and 131 of the purified SF_6. Each sample underwent three measurements that consists of eight 26-second cycles measuring the sample and the reference gas. Data are reported in per mil using the following notation:

$$\delta^{33}S = [(({}^{33}S/{}^{32}S)_{sample} / ({}^{33}S/{}^{32}S)_{CDT}) - 1]$$

$$\delta^{34}S = [(({}^{34}S/{}^{32}S)_{sample} / ({}^{34}S/{}^{32}S)_{CDT}) - 1]$$

$$\delta^{36}S = [(({}^{36}S/{}^{32}S)_{sample} / ({}^{36}S/{}^{32}S)_{CDT}) - 1]$$

$$\Delta^{33}S = [(({}^{33}S/{}^{32}S)_{sample} / ({}^{33}S/{}^{32}S)_{CDT}) - (({}^{34}S/{}^{32}S)_{sample} / ({}^{34}S/{}^{32}S)_{CDT})^{0.515}]$$

$$\Delta^{36}S = [(({}^{36}S/{}^{32}S)_{sample} / ({}^{36}S/{}^{32}S)_{CDT}) - (({}^{34}S/{}^{32}S)_{sample} / ({}^{34}S/{}^{32}S)_{CDT})^{1.9}]$$

Analyses are normalized to analyses of Canyon Diablo Troilite that place IAEA-S1 at a composition of $\delta^{34}S$ =-0.401, $\Delta^{33}S$ =0.116, $\Delta^{36}S$ =-0.796 (Antonelli et al. 2014). Uncertainties on measurements are estimated from the long-term reproducibility on measurements (including wet chemistry, fluorination, and mass spectrometry) of standard materials and are 0.3, 0.016, and 0.3 (2σ) for $\delta^{34}S$, $\Delta^{33}S$, and $\Delta^{36}S$ respectively.

3. Results

Bulk sulfur isotope compositions of sulfide minerals hosted in olivine and pyroxene mineral separates from Mangaia basalts are reported in Table *6* and illustrated

in Figure *24* and Figure *25*. We extracted 0.54 mg to 1.57 mg of Ag_2S from ~ 300 to 400 mg of sample resulting in sulfur concentrations that range from 96 to 333 ppm. S concentration in Ol and Px from the same sample do not match and no systematic relationship between S concentration and the mineral separates is observed.

The $\delta^{34}S$ values measured range from -5.13‰ to +0.21‰ (±0.3 2σ). Sulfide minerals hosted in olivine are not in isotopic equilibrium with sulfide minerals from pyroxene in the same sample showing -3.97‰ and -5.13‰ for MGA-B-25 Ol and MGA-B-25 Px respectively, -0.28‰ and -0.85‰ for M10 Ol and M10 Px respectively, - 2.35‰ and -1.57‰ for M12 Ol and M12 Px respectively, and -2.07‰ and 0.21‰ M13 Ol and M13 Px respectively. There is no relationship between the magnitude of the signal and type of mineral separate. There is also no systematic fractionation among the mineral separates from the same sample.

The $\Delta^{33}S$ and $\Delta^{36}S$ range from +0.002‰ to +0.049‰ and -0.81‰ to +0.69‰, respectively. $\Delta^{33}S$ values of sulfide in Ol and Px from the samples measured are similar for with exception of one sample (M13) showing $\Delta^{33}S$= 0.006 and 0.049 for Px and Ol respectively. Similarly, $\Delta^{36}S$ values are generally similar for sulfides in pyroxene and olivine. the mineral separates with the exception of M12 showing $\Delta^{36}S$= -0.24 and 0.70 for Px and Ol respectively. A subset of samples (M4, M10, M12, and M13) yield a negative correlation between $\delta^{34}S$ and $\Delta^{33}S$. With the exception of two data points (MGA-B-25 Ol, and M12 Ol), the $\Delta^{33}S$ vs. $\Delta^{36}S$ overlap previously published data from MORB (*Figure 25*).

Table 6. S-isotope compositions of bulk sulfide in Ol and Px separates from Mangaia Basalts

Sample	S (ppm)	$\delta^{34}S$	$\Delta^{33}S$	$\Delta^{36}S$	$^{206}Pb/^{204}Pb$	$^{207}Pb/^{204}Pb$	$^{208}Pb/^{204}Pb$
MGA-B-25 Px	290	-5.13	0.028	-0.05	21.678	15.807	40.512
MGA-B-25 Ol	333	-3.97	0.016	-0.26	21.678	15.807	40.512
M4 Px	185	-1.17	0.026	-0.15	21.668	15.828	40.565
M10 PX	112	-0.85	0.009	-0.16	21.718	15.837	40.583
M10 OL	161	-0.28	0.008	-0.20	21.718	15.837	40.583
M12 PX	127	-1.5716	0.030	-0.24	21.708	15.831	40.561
M12 OL	322	-2.3453	0.035	0.70	21.708	15.831	40.561
M13 PX	238	0.21	0.006	0.02	21.666	15.817	40.539
M13 OL	96	-2.069	0.049	0.45	21.666	15.817	40.539
MGA-B-47*		-3.28	-0.13		21.784	15.813	40.734

Table 6. Data compilation of S-isotope and radiogenic Pb isotope compositions presented. *S-isotope data from Cabral et al. (2013). Radiogenic Pb for M4 -M13 from Woodhead et al. (1996). Radiogenic Pb data for MGA-B-25 and MGA-B-47 from Hauri and Hart (1993).

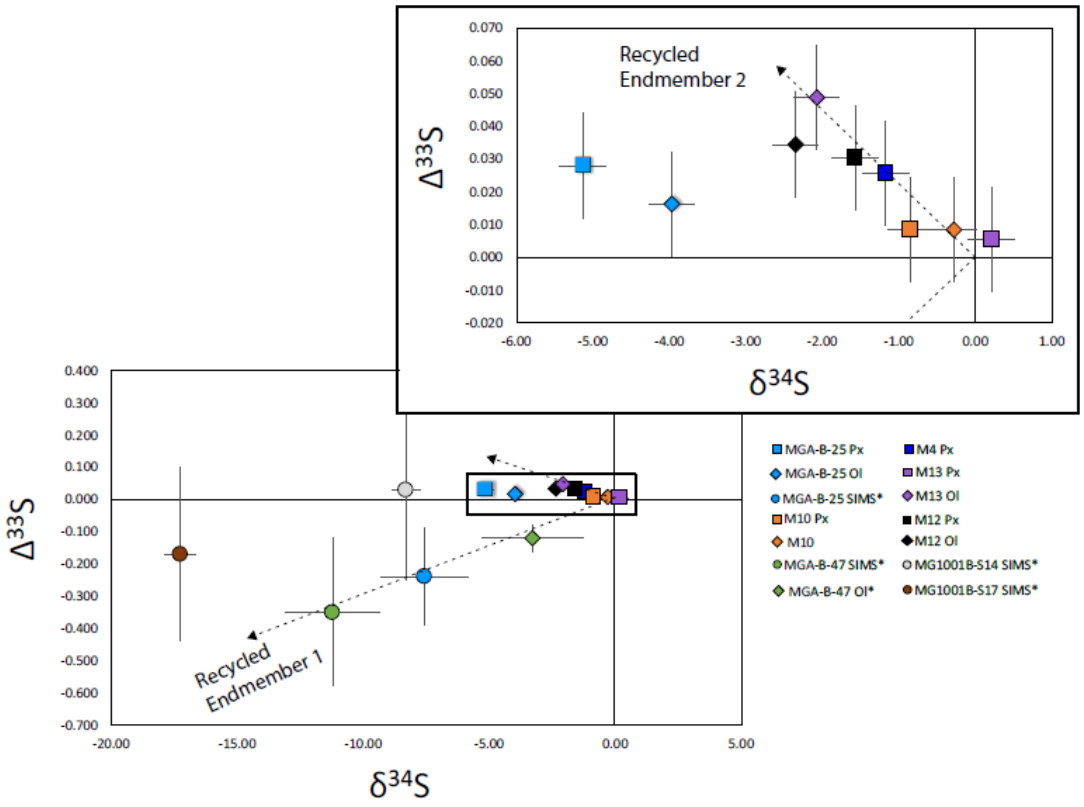

Figure 24. $\delta^{34}S$ vs. $\Delta^{33}S$ for bulk sulfide data from sulfide inclusions in olivine and pyroxene phenocrysts. The dotted line illustrates the proposed mixing between three S-isotope compositions introduced into the Mangaia mantle plume.

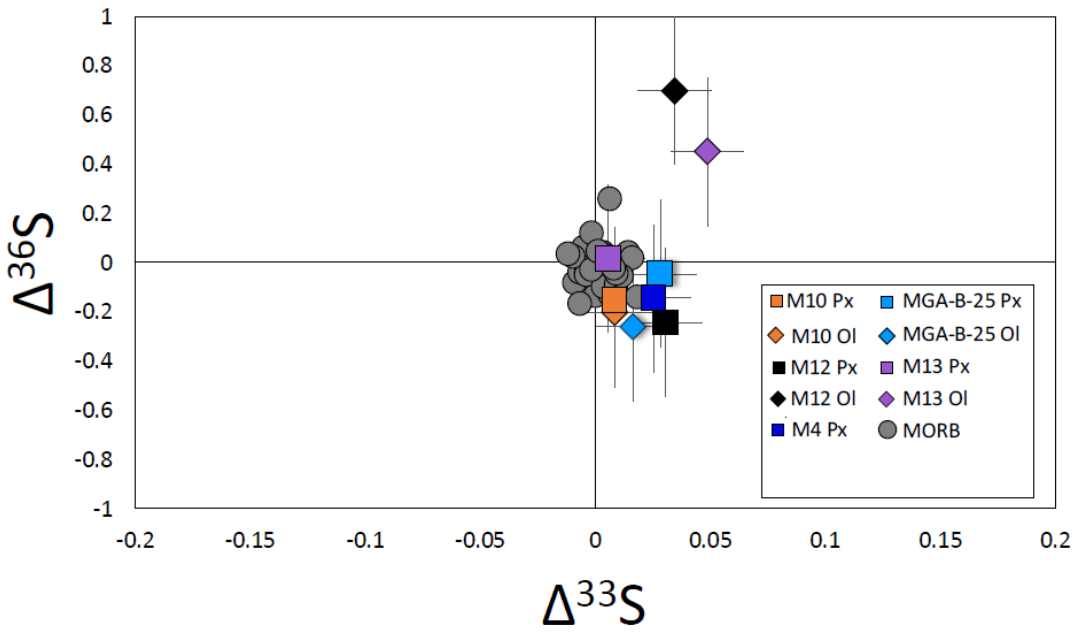

Figure 25. $\Delta^{33}S$ vs. $\Delta^{36}S$ for bulk sulfide data from sulfide inclusions in olivine and pyroxene phenocrysts. With the exception of two data points from sulfide in olivine (M12 Ol and M13 Ol), the data overlap with data from MORB (Labidi et al., 2013; 2014).

4. Discussion

A unique observation of HIMU mantle sampled at Mangaia made by Cabral et al. (2013), is the negative $\delta^{34}S$ and the presence of S-MIF observed in individual sulfides by SIMS and by SF_6 techniques similar to those used here. The signatures observed by Cabral yielded a field extending from $\delta^{34}S$ of -3.28 (±2‰) to -17.25 ‰ (±0.61‰) and with near-zero to negative $\Delta^{33}S$. The observation of samples with negative $\Delta^{33}S$ that were measured both by SIMS and with one measurement by SF_6 (-0.12±0.04‰, 2σ) done at UMD is interpreted to suggest the presence of subducted and recycled Archean components in the Mangaia source. The data collected in this study on sulfide inclusions in mineral separates of Ol and Px from Mangaia also shows a

range of $\delta^{34}S$, but not extending to as negative values (-5.13‰ to +0.21‰). Our data also lack the negative $\Delta^{33}S$ values seen in Cabral et al. (2013) and extend from to 0.006 to 0.049‰. Our data include analyses of sulfur from phenocrysts of one sample studied by Cabral et al. (2013) [MGA-B-25] for which they report a negative $\Delta^{33}S$, because this sample had not been analyzed using the SF_6 method by Cabral et al. (2013). Olivines from another sample reported by Cabral et al. (2013) as ^{33}S depleted using the SIMS method, MGA-B-47, were analyzed in our laboratory using the same fluorination and mass spectrometry as that described in the methods section of this manuscript, but a with a wet chemistry protocol involving hydrochloric acid and Cr(II) to digest sulfide minerals. This sample was not reanalyzed here due to lack of material available. The protocol we use here includes HF, in addition to HCl and Cr(II). The HF techniques are more efficacious at digesting silicate and thus can extract sulfides trapped within phenocrysts which may be missed by the HCl + Cr(II), but any exposed sulfide grains will be equally reactive. While the sulfide concentrations we observe (96 to 333 ppm) are higher than those reported in Cabral et al. (2013) for the SF_6 analysis of olivine from MGA-B-47 (~30 ppm), we cannot say whether this is due to some sulfide loss (or armoring- the trapping and preservation of sulfide and the associated conditions responsible), or whether this reflects a lower sulfide content for the material from MGA-B-47 compared to the samples studied here. Regardless, both datasets reveal significant variability for both $\delta^{34}S$ and $\Delta^{33}S$ that reflect some aspect of the history of these materials. We discuss below the arguments that support an origin associated with mixing of sulfur from different sources at the time of phenocryst formation.

4.1 Phenocrysts and links to sulfide concentration

A unique aspect of this work is that our samples are not whole rock samples or glasses, but rather phenocryst separates containing sulfide inclusions. For sulfide to be trapped as inclusions in phenocrysts, the associated melt must be sulfide saturated with coexisting sulfide (liquids) that have exsolved from the silicate melt and can be trapped by growing olivine and pyroxene phenocrysts. Note however that the sulfide concentration we measure within olivine and pyroxene separates likely reflects a variety of factors including the level of sulfide saturation and the behavior of sulfide liquids and phenocrysts at in the time leading up to entrapment. Thus, the links between the sulfide concentration reported here for mineral separates and sulfide concentration of the parent melt(s) are unlikely to follow a simple relationship. Melt inclusions in olivine phenocrysts from Mangaia record pressures of entrapment between 250 bar to 1.75 kbar that translates into approximately 0.9 to 6.4 km depth (Cabral et al., 2014). At these pressures, we safely discard sulfur degassing as a likely process (Gaillard et al., 2011; Burgisser et al., 2015). Thus, the phenocrysts insulate sulfide sulfur from processes such as degassing upon eruption and post-eruption weathering and provide snapshots of the diversity of magma chamber compositions prior to mixing and eruption. This process is analogous to the entrapment of melt inclusions which reveal heterogeneities inherited from mantle sources, before late mixing and eruption (e.g. Sobolev and Shimizu, 1993). Olivine phenocrysts from Mangaia demonstrate a range of forsterite compositions (e.g., forsterite 80.4 to 81.1 in MGA-B-25, and 80.3 to 86.1 in MGA-B-47; Cabral et al., 2014) that suggest chemical disequilibrium and the

likelihood for mixing of multiple magmas with distinct compositions at depth prior to eruption. Since we measure sulfide from different phenocrysts, there is the potential for them to capture diversity of the isotopic composition of this sulfide liquid, or to capture variability that was present for different sulfide liquids in the crystallizing silicate melt. We suggest that this aspect of phenocryst hosted sulfides allows the argument to be made that they capture isotopic variation produced by mixing of sulfur with different isotopic compositions. A similar argument was made by Saal et al. (1998), who observed Pb isotopic variability in individual olivine-hosted melt inclusions (but we acknowledge that subsequent studies (Paul et al., 2011; Cabral et al., 2014) have not identified the variability identified by Saal et al. (1998).

4.2 Covariation of $\delta^{34}S$ and $\Delta^{33}S$ in samples M4 and M10, M12, and M13

We observe covariation of $\delta^{34}S$ and $\Delta^{33}S$ for sulfide from bulk Ol and Px in samples M4, M10, M12, and M13. It is conceivable that the covariation is the result of a high temperature process that yields mass dependent fractionation. One may suggest that the Mangaia melts started with near-zero $\delta^{34}S$ and $\Delta^{33}S$ values, similar to MORB values (Labidi et al. 2014), and subsequently evolved towards low $\delta^{34}S$ and high $\Delta^{33}S$ as the result of a fractionation with a mass dependency exponent different from 0.515 (Hulston and Thode, 1965). One possible mechanism for mass fractionation at high temperature is degassing (Mandeville et al. 2009). The armoring of sulfides by phenocrysts likely makes them immune to effects of degassing. However, we explore and discuss this possibility further since degassing is common in basalts and, as such,

is a typical explanation for shifts to negative (or positive) $\delta^{34}S$ (Mandeville et al. 2009, de Moor et al. 2013, Beaudry et al., 2018). Given the mass fractionation scenario proposed by Fiege et al. (2015) at QFM (quartz-fayalite-magnetite) redox conditions, a loss of 85% of the sulfur as S(IV) during equilibrium (i.e. closed system) degassing would be required to achieve a $\delta^{34}S$ shift of ~-3 ‰. This is insufficient to account for the range of observed $\delta^{34}S$ in our dataset and also that observed by Cabral et al. (2013). Partitioning of sulfur to S(VI) (sulfate) also is known to shift the $\delta^{34}S$ of residual sulfide to negative values. A case has been made for the presence of sulfate in OIBs (Jugo et al., 2010; Labidi et al., 2015). Extrapolated data from Miyoshi et al. (1984) suggest the equilibrium fractionation between sulfide and sulfate for $\delta^{34}S$ is ~3‰ (e.g. Myoshi et al., 1984; Mandeville et al., 2009 and references within). The possibility that this accounts for a ^{34}S depletion of the magnitude we observe would again require a significant partitioning of sulfur to sulfate, and a sulfate/Σsulfur ratio much greater than the typical value of 0.2 seen in OIB (e.g Labidi et al., 2015). Both processes would require a mechanism to maintain sulfide saturation at the time of S loss to sulfate, evidence of which is not seen in Mangaia. In addition, we note that the fractionation would need to be associated with a mass dependency exponent different from 0.515 (Hulston and Thode, 1965). An exponent of 0.499±0.005 would be needed to fit the $\delta^{33}S$ - $\delta^{34}S$ data. This is far out of the range expected at high (magmatic) temperature (Cao and Liu, 2011) and is thus considered highly unlikely.

Altogether, we conclude that there is no reasonable process identified to explain the $\delta^{34}S$ and $\Delta^{33}S$ covariation among sample M4, M10, M12, and M13. We argue that instead, the covariation is rather likely caused by mixing processes in the mantle

sources prior to eruption, in agreement with previous arguments for mixing by Cabral et al. (2014) that is supported by 1) highly variable forsterite content of olivine from individual Mangaia lavas and 2) possible Pb isotopic variability in individual olivine-hosted melt inclusions in Mangaia lavas (Saal et al., 1998; but see Paul et al., 2011 and Cabral et al., 2014). The covariation requires mixing that involves trapping sulfide melts that sample at least two separate $\delta^{34}S$ and $\Delta^{33}S$ compositions: a mantle component with $\delta^{34}S=0$ and $\Delta^{33}S=0$, and a component with negative $\delta^{34}S$ and slightly positive $\Delta^{33}S$.

4.3 Nature and age of the recycled components

The HIMU mantle reservoir is generally thought to reflect mantle mixed with subducted oceanic crust that experienced Pb loss (e.g. Chauvel et al., 1992; Kelley et al., 2005); however, some proposals also call for a mantellic origin (Thirlwall, 1997), formation by recycled carbonate (Castillo, 2016), or carbonatitic metasomatism of the subcontinental lithospheric mantle that in turn delaminated and sank to the core-mantle boundary (Weiss et al., 2016). A wide range of ages have been proposed for the U/Pb fractionation that generated HIMU (~550 Ma to 3.0 Ga -- (Hauri and Hart, 1993; Thirlwall, 1997; Nebel et al., 2013; Mazza et al., 2019). Considering the U/Pb fractionation may be associated with sulfide loss (Chauvel et al., 1992), these different models for HIMU source generation have the potential to impact the sulfur isotopic composition of the HIMU endmember. Sulfur with negative $\delta^{34}S$ could be the result of a process associated with subduction. If the subducted crust started with ~1000 ppm S (Rouxel et al., 2008a; Alt and Shanks, 2011) with a $\delta^{34}S$ of +3‰ on average (Alt, 1995), and assuming Pb is hosted in sulfides (Kelley et al., 2003), Pb loss by sulfide

breakdown in the subduction results in 400-20 ppm S (i.e. 60% to 98% sulfide loss) in the HIMU mantle source (Labidi et al., 2014). A process resulting in the preferential loss of ^{34}S with 60% sulfide loss during slab devolatilization would require an average fractionation of ~14‰ between the fluid (preferentially partitioning ^{34}S) and the residual slab (preferentially partitioning ^{32}S) to explain our data, and a ~34 ‰ fluid-slab residue fractionation to explain the lowest $\delta^{34}S$ in Cabral et al. (2013). If 98% sulfide loss an average fractionation of ~9‰ between the fluid and the residual slab to explain our data, and a ~21 ‰ fluid-slab residue fractionation to explain the lowest $\delta^{34}S$ in Cabral et al. (2013).These fractionations are large for temperatures associated with slab dehydration, and are not observed in studies of metamorphism (Li et al., 2020). We note additionally that in other localities, in mantle sources and diamond sulfides, subducted components show no evidence for S isotopic fractionations (Farquhar et al., 2002; Thomassot et al., 2009; Labidi et al., 2013; Labidi et al., 2015; Beaudry et al., 2018; Smit et al., 2019), suggesting the subduction of crustal protoliths does not cause significant S isotope fractionation. We conclude that the unusually low $\delta^{34}S$ must rather be inherited from the composition of the protolith before it was subducted.

Jackson and Dasgupta (2008) suggest that the protolith of the HIMU endmember has two components, a mafic component and a peridotite component, and this package is carbonated. They suggest this could be a (proximal) mixture formed from a peridotite that was metasomatized by carbonated silicate melt or carbonatitic melt or as a more distinct physical mixture of peridotite and a mafic component enriched in CO_2 (Jackson and Dasgupta, 2008). Further, they argue that recycled crustal

component (the mafic component) could have been carbonated and would also have carried the elevated high U/Pb and Th/Pb that evolved to the HIMU endmember. Cabral et al. (2014) argue for a carbonated source at HIMU endmember Mangaia lavas on the basis of inferred (pre-degassing) high primary CO_2 in melt inclusions required to explain their elevated CaO/Al_2O_3 and low SiO_2, as well as the presence of carbonatite observed in Mangaia melt inclusions by Saal et al. (1998). Weiss et al. (2016) suggest an alternative mechanism for generating the carbonated HIMU source via carbonatitic metasomatism of subcontinental lithosphere that subsequently delaminated and ultimately was incorporated into the plume. The low $\delta^{34}S$ values at Mangaia (this study) support mixing of at least one component with a recycling origin that could be tied to a carbonatitic metasomatizing agent, or to a recycled carbonated mafic component. The isotopic composition of sulfur reflects the exogenic sulfur that was recycled, which in turn reflects the age of the subducted materials and also the processes that mobilized sulfur in the mantle.

The covariation of $\delta^{34}S$ and $\Delta^{33}S$ among samples M4, M10, M12, and M13 can be accounted for by mixing between 1) a recycled endmember with $\delta^{34}S$=-7.5 ‰ and $\Delta^{33}S$=+0.15‰, and 2) a convective mantle component with $\delta^{34}S$=0‰ and $\Delta^{33}S$=0‰. Note that MGA-B-25 does not fall along this array and is likely linked to a separate endmember previously identified in Cabral et al., (2013). Low $\delta^{34}S$ values are not typically observed in Archean rocks although they have been observed in some samples (e.g. Mojzsis et al., 2003; Hoffman et al., 2009). Low $\delta^{34}S$ values are not typically observed in Archean rocks although they have been observed in some samples (e.g. Mojzsis et al., 2003; Hofmann et al., 2009). In fact, there is a preponderance of

^{34}S-enriched material in the Archean (Farquhar and Jackson, 2016), which suggests an under-represented, possibly lost to recycling, reservoir of ^{34}S-depleted material existed. Further to this, Canfield (2004) suggests that recycling of ^{34}S-depleted sulfur in the middle Proterozoic could balance ^{34}S enrichments observed in the Proterozoic sedimentary S isotope record. Note, however, that sedimentary recycling was observed to be associated with positive δ^{34}S values in Discovery and Samoa (Labidi et al.. 2013; Labidi et al., 2015; Dottin III et al., 2020) These low δ^{34}S areubiquitous in post-Archean rocks (Johnston, 2011).While sedimentary pyrite commonly has negative δ^{34}S (lower than -40‰ for modern sediments (e.g. Strauss, 1997) and as low as -17‰ (e.g Strauss, 2003) in Archean sediments) and recycling of such material could contribute to the low values in δ^{34}S, a sedimentary source would also carry high ^{87}Sr/^{86}Sr, low ^{143}Nd/^{144}Nd, and low ^{206,207,208}Pb/^{204}Pb that do not match the HIMU signatures of the rocks analyzed (e.g. Chauvel et al., 1992). Modern altered oceanic crust has, on average, a δ^{34}S that is positive due to the widespread occurrence of massive hydrothermal sulfides that generally carry positive values (Alt, 1995). While such material is consistent with the positive δ^{34}S estimated for HIMU by (Labidi et al., 2014) and Labidi and Cartigny (2016)), it contrasts with the low δ^{34}S values observed here. Alternatively, the bulk δ^{34}S of the first kilometer of oceanic crust is estimated to at -6 to -7 ‰ (Rouxel et al., 2008b; Alt and Shanks, 2011), with positive Δ^{33}S up to +0.162‰ ± 0.014 (Ono et al., 2012) from sulfate reduction. We suggest that such an oceanic crustal component could altogether account for the Pb isotope signature of HIMU (e.g. Chauvel et al., 1992; Woodhead, 1996; Kelley et al., 2005), while also accounting for the S-isotope compositions observed for samples M4, M10, M12, and M13. Note that such a model

would consequently suggest the contribution of sulfur with negative $\delta^{34}S$ and slightly positive $\Delta^{33}S$ is from a relatively young crustal component dominated by biogenic sulfides, in addition to the Archean component previously proposed (Cabral et al., 2013). This contribution of a young crustal component dominated by biogenic sulfides would be unique considering both the Samoa (EM II) and Discovery (EM I) hotspots carry components with positive $\delta^{34}S$ values (Labidi et al., 2013; Labidi et al., 2015, Dottin III et al., 2020), and MORBs that incorporate variable amounts of HIMU components (Sobolev et al., 2007) may be influenced by a source with $\delta^{34}S = +3 \pm 2‰$ (Labidi et al., 2014; Labidi and Cartigny, 2016). If the contribution is in fact from biogenic sulfides, Mangaia may be a unique location where the upper section of the oceanic crust, affected by biological mediation of sulfides, contributes to a mantle source after it is subducted. It is noteworthy that this unique ^{34}S-depleted signature is present in the samples from Mangaia studied here and also in the samples studied by Cabral et al. (2013), but there is a distinction in $\Delta^{33}S$ that may be linked to the ages of the sources.

Additional constraints on the relative age of sulfur contributing slightly positive $\Delta^{33}S$ may be provided by the relationship between $\Delta^{33}S$ and $\Delta^{36}S$. Archean rocks typically show covariation of $\Delta^{33}S$ and $\Delta^{36}S$ with a slope of ~-1 (Farquhar et al., 2007). This means that if a $\Delta^{33}S$ 0.05‰ like that observed here results from the contribution of an Archean protolith in the Mangaia mantle source, the corresponding $\Delta^{36}S$ is predicted to be -0.05‰ which is not resolved with our uncertainty on $\Delta^{36}S$ (±0.3‰). Post-Archean rocks show covariation of $\Delta^{33}S$ and $\Delta^{36}S$ with a slope of ~-7, which

would result in a very small $\Delta^{36}S$ shift to -0.4‰, which would be marginally resolvable given our estimated uncertainty.

Our data generally plot below (more negative $\Delta^{36}S$) and to the right (more positive $\Delta^{33}S$) of typical MORB (*Figure 25*). The shift for $\Delta^{36}S$ of the data cluster is more consistent with a biological fractionation than a mass-independent (Archean) fractionation, but an Archean component with little to no mass-independent anomaly could satisfy our observations. However, we argue the most parsimonious explanation for the data here is that the material we measured is post-Archean. This would be in addition to recycled material of Archean age implied by the findings of Cabral et al. (2013).

4.4 Recycling two reservoir ages

With the samples presented here, the Pb isotope data of whole rock basalts from Woodhead (1996) and Hauri and Hart (1993) all show extreme $^{206}Pb/^{204}Pb$, indicating the endmember HIMU character of the Mangaia mantle source. Further constraints on the nature of the recycled components at Mangaia may be provided in relationships between $^{206}Pb/^{204}Pb$ and sulfur isotopes: both Pb and S isotopes reveal heterogeneity in whole rock Mangaia lavas. There is some Pb isotopic heterogeneity in the whole rocks, but the Pb isotope compositions of individual melt inclusions in Mangaia lavas reveal substantially more heterogeneity than the whole rock data (Saal et al., 1998), though recent reports of Pb-isotopic heterogeneity in Mangaia inclusions reveal substantially less heterogeneity (Paul et al., 2011; Cabral et al., 2014) (*Figure 26*a). Thus, greater S

isotopic heterogeneity in individual melt inclusions, as observed by Cabral et al. (2013), may not be surprising in this light.

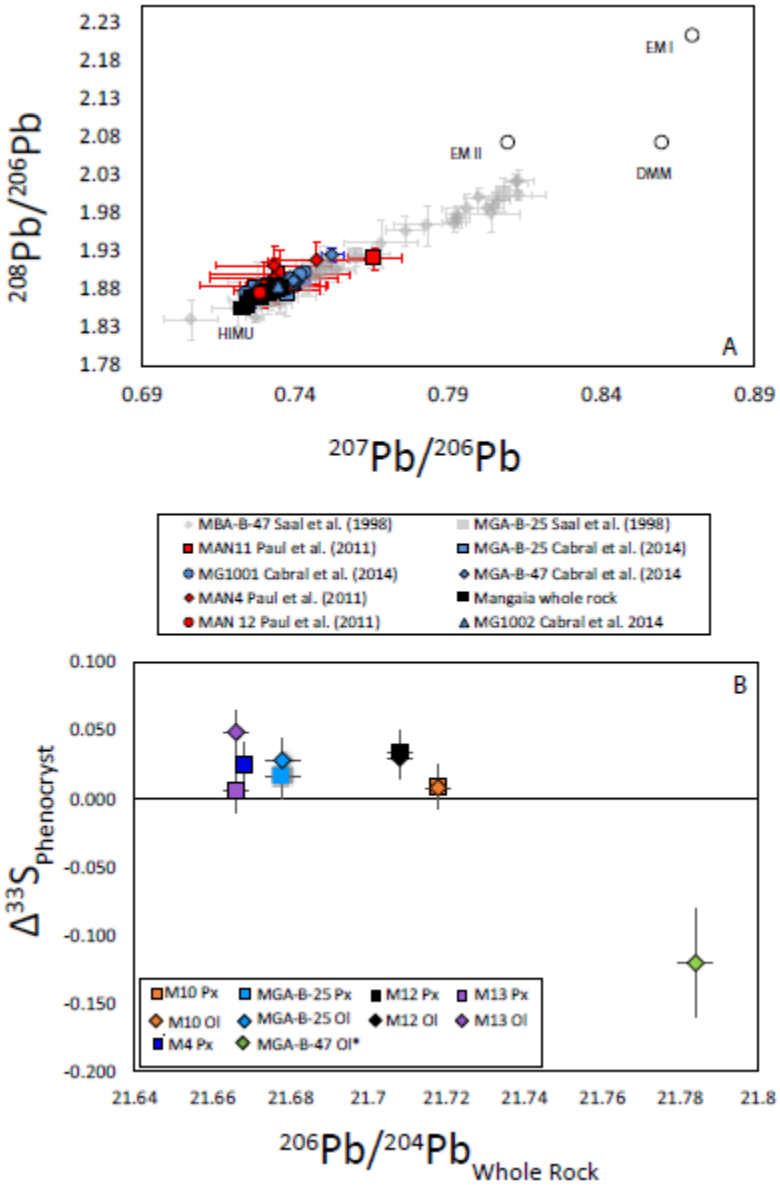

Figure 26. $^{207}Pb/^{206}Pb$ vs. $^{208}Pb/^{206}Pb$ for whole rock basalts from Mangaia (Woodhead et al. 1996; Hauri and Hart 1993) and melt inclusions from Paul et al. (2011), Cabral et al. (2014), and Saal et al. (1998). B. $^{208}Pb/^{204}Pb$ vs. $\delta^{34}S$. Sulfur data is as bulk sulfide from melt inclusions in olivine and pyroxene.

Our S isotope data are from mineral separates extracted from the same whole rocks presented in Woodhead et al. (1996) and Hauri and Hart (1993). Interestingly, the S isotope compositions presented in this study (and Cabral et al., 2013) from mineral separates show the potential for a relationship between whole rock Pb isotopes and bulk S isotopes from mineral separates (*Figure 26*b). We note however that the whole rock Pb isotope data use an older TIMS method that did not employ double or triple spike to track in-run mass fractionation. Thus, these older TIMS data are likely to have larger uncertainties than were originally reported by these authors (Hauri and Hart, 1993; Woodhead, 1996). The variability in Pb isotope compositions of melt inclusions is indicative of mixing of multiple compositions in the HIMU mantle source beneath Mangaia, suggesting the relationship we observe between bulk S isotope compositions from mineral separates and whole rock Pb isotope compositions, also reflects variability in the HIMU mantle source. If real, the data would reflect mixing between components of different ages, where the negative $\Delta^{33}S$ is associated with an older mantle component.

5. Conclusion

The data presented here on sulfide inclusions within olivine and pyroxene phenocrysts from Mangaia reveal a heterogeneous S-isotope composition. Values range from -5.13‰ to +0.21‰ (±0.3), +0.006‰ to +0.049‰ (±0.016), -0.81‰ to +0.69‰ (±0.3) for $\delta^{34}S$, $\Delta^{33}S$, and $\Delta^{36}S$ respectively. The $\Delta^{33}S$ values are different from those presented in Cabral et al. (2013) who generally show negative $\Delta^{33}S$ and indicate that some, possibly the preponderance, of HIMU sulfur sampled comes from a different reservoir, likely of younger post-Archean age. Both studies, however, report ^{34}S-

depleted sulfur, and this appears to be a characteristic of Mangaia HIMU that we attribute a crustal origin following observations by studies like Rouxel et al. (2008b) and Alt and Shanks (2011). Thus, there appears to be variability in the material derived from the same plume plumbing system at Mangaia.

This work focuses on S-isotope compositions of bulk sulfide in melt inclusions in Ol and Px from the same sample, and this sulfur is not in isotopic equilibrium but shows covariation in $\delta^{34}S$ and $\Delta^{33}S$ which we link to the capturing of S-isotope compositions of various melts as they are added to the magma chamber. The data for Mangaia presented here, and provided by Cabral et al. (2013), support mixing of melts with at least 3 distinct sulfur isotope endmembers: 1.) A convective mantle component with $\delta^{34}S=0$ and $\Delta^{33}S=0$; 2.) a component with negative $\delta^{34}S$ and slightly positive $\Delta^{33}S$; and 3.) a component with negative $\delta^{34}S$ and negative $\Delta^{33}S$. Below is a figure (Figure *27*) that illustrates the proposed models for the HIMU reservoir formation and ways the sulfur isotope composition can be affected.

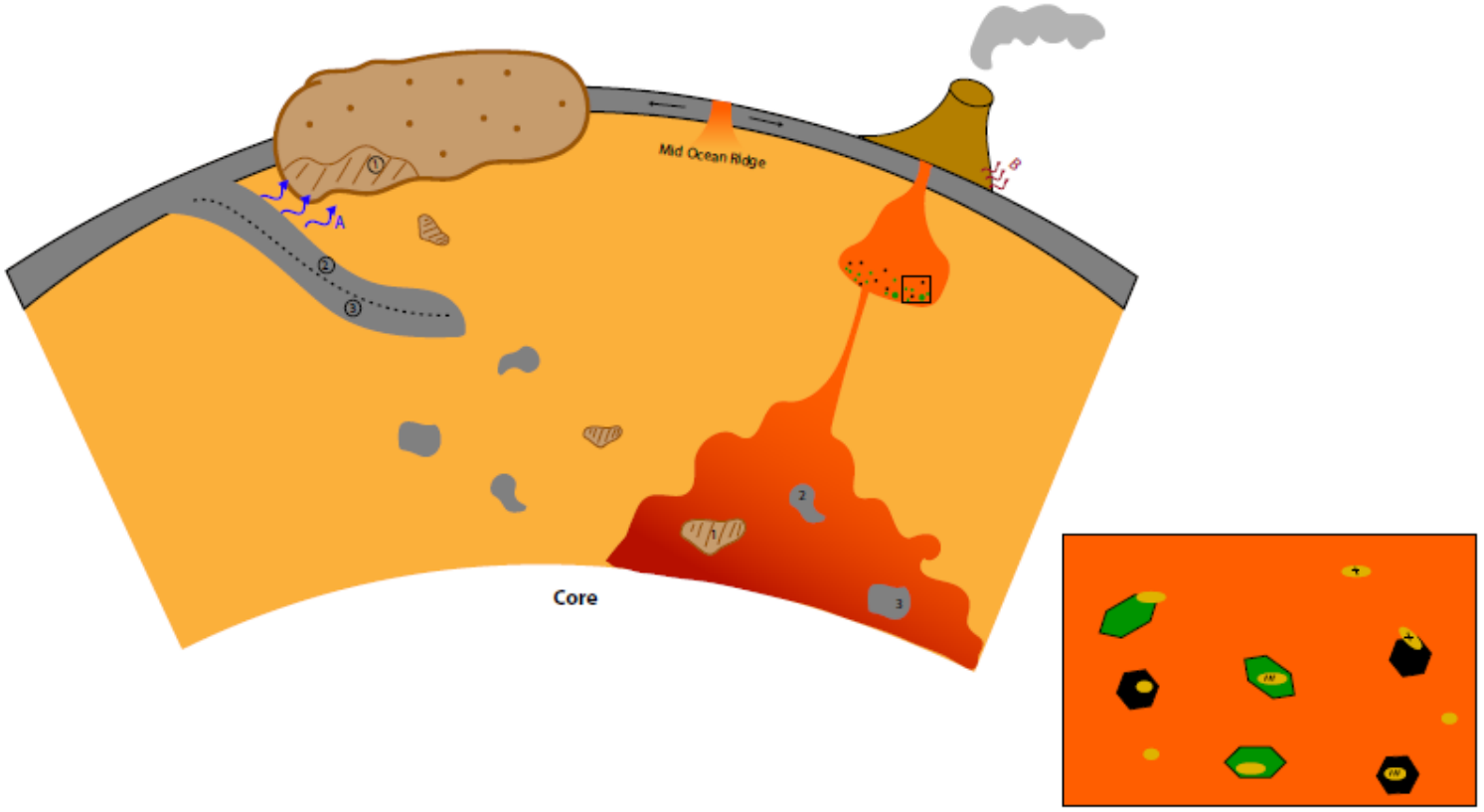

Figure 27. An illustration that outlines processes discussed that are related to the generation of the HIMU mantle source. A.) Metasomatism of upper oceanic crust; B.) Degassing of sulfur; 1.) metasomatized subcontinental lithosphere; 2.) Upper oceanic crust with biogenic sulfide- $\delta^{34}S$ in negative and $\Delta^{33}S$ is positive; 3.) Lower oceanic crust- $\delta^{34}S$ is positive; Inset: capturing sulfide of various composition in pyroxene (black) and olivine (green) within the magma chamber associated with Mangaia.

Chapter 5: Conclusions

Evidence from radiogenic isotope systems support the presence of recycled and primordial components at different ocean islands. The data presented in this dissertation were collected to characterize the sulfur isotope composition of deep Earth reservoirs and to understand how mantle evolution and the plumbing systems of mantle plumes play a role in the S-isotope compositions erupted and preserved in Ocean Island Basalts (OIB). Chapters 2, 3, and 4 describe three different aspects of sulfur geochemistry at ocean island volcanoes: chapter 2 describes connections between sulfur, tungsten, helium, and lead that inform about primordial reservoirs in the deep mantle; chapter 3 explores connections between sulfur and previously described heterogeneity in lead isotopes that defines heterogeneity among reservoirs in the plume feeding the Samoan islands; and chapter 4 revisits the question of very ancient sulfur hosted within the mantle plume feeding Mangaia using techniques on sulfide transported by phenocryst that crystalized deep in the magma chamber. The following subsections describe findings made in each of these chapters and concludes with a set of forward-looking questions.

5.1 Constraining primordial sulfur isotope compositions: insights from relationships between S, W, He, and Pb.

Samoa, the type locality for the Enriched Mantle II mantle endmember receives geochemical contributions from recycled and primordial components from a plume system associated with a Large Low Shear Velocity Province (LLSVP) and an Ultra-

Low Velocity Zone (ULVZ). Chapter 2 ["*Sulfur isotope characterization of primordial and recycled sources feeding the Samoan mantle plume"*] uses bulk rock sulfur isotope analyses from Samoan basalts to characterize the nature of sulfur in primordial and recycled mantle sources, revealed by $\mu^{182}W$ and $^{3}He/^{4}He$, erupted at the Samoan Islands of Ofu, Vailulu'u and Malumalu.

Research in chapter 2 reveals an array between $\Delta^{33}S$ and radiogenic isotope compositions of tungsten, helium, and lead. Primordial samples (negative $\mu^{182}W$, high $^{3}He/^{4}He$) define one endmember and are associated with $\Delta^{33}S \approx 0$, a value that supports assertions that Earth's primordial sulfur is similar to that of the majority of meteorites analyzed thus far and is indistinguishable from the composition of the Canyon Diablo Troilite reference. This value is also indistinguishable from the value measured for sulfur from the convective mantle. Given heterogeneities observed in the meteorite record, one implication of this finding is that sulfur was homogenized early in Earth's history.

The second endmember in this array indicates mixing with material having slightly positive $\Delta^{33}S$ (+0.027‰ ± 0.016). This component also has elevated $^{206}Pb/^{204}Pb$, linking it to an evolved HIMU mantle source. A second implication of the array between $\Delta^{33}S$ and radiogenic isotope compositions of tungsten, helium, and lead is that the anomalous $\Delta^{33}S$ points to recycled sulfur in the second endmember and that given the magnitude of the $\Delta^{33}S$ variation, the sulfur may be linked to either Archean or Proterozoic sulfur sources.

A third feature of the relationship between $\Delta^{33}S$ and $\mu^{182}W$, is what it implies for hypotheses related to the nature and origin of the reservoir that hosts the primordial

tungsten signature. The chemistry of tungsten suggests a link to the core, or to ancient metal in the deep mantle. Several hypotheses have been proposed to account for the observed ^{182}W depletion, including: (1) mixing with a mantle reservoir that has fully equilibrated with the core; (2) mixing directly with core material; (3) mixing with core material that has an exotic sulfur isotope composition; (4) or mixing with a dense basal reservoir with slightly negative $\mu^{182}W$ and high concentrations of W and S, such as that proposed for an Ultra-Low Velocity Zone. The sulfur isotope compositions rule out proposals #1-3 and are in support of hypothesis #4. The proposed contribution from a dense basal reservoir requires the reservoir to host $\mu^{182}W$ that is slightly negative (but, not as a negative as the core) and $\Delta^{33}S = 0$. The relationship cannot rule out a scenario in which the tungsten is contributed from the core and the sulfur is contributed from the mantle.

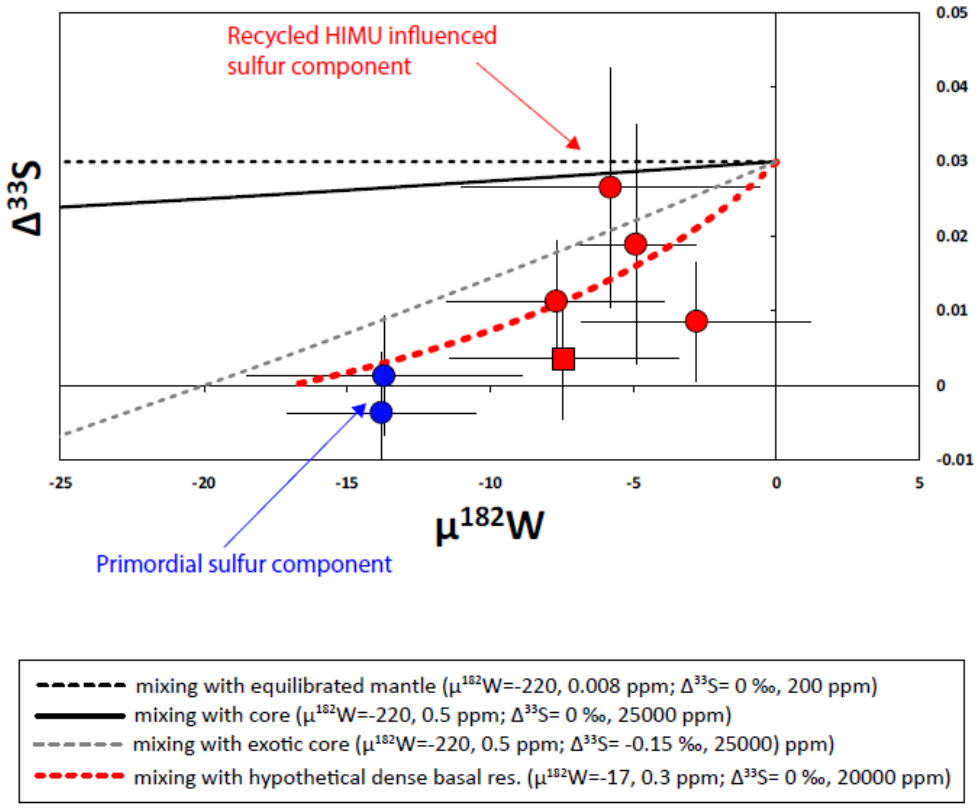

Figure 28. $\mu^{182}W$ vs. $\Delta^{33}S$ of Samoan basalts from Ofu (blue circles), Vailulu'u (red circles), and Malumalu (Red square). The data show a relationship between sulfur and tungsten that suggest mixing between a primordial component with near zero $\Delta^{33}S$ and a recycled component with slightly positive $\Delta^{33}S$. The recycled component is linked to a diluted HIMU related reservoir. Mixing models suggest the primordial sulfur and tungsten are sampled from a dense basal reservoir such as an Ultra-Low Velocity Zone (ULVZ).

5.2 Evidence for geochemical zonation: insights from Sulfur isotope characterization of Samoan geochemical trends

Research in chapter 3 [*Sulfur isotope evidence of geochemical geometry of the Samoan mantle plume*] considers sulfur in the context of a study that uses a distance parameter $D^{206,207,208Pb}$ that illustrates (in three dimensions) a geochemical distance from the primordial "common component" to resolve mixing trends (Vai, Malu, and Upo trends) produced by different endmembers in the mantle feeding the Samoan

islands. The distinct S-isotope composition associated with HIMU components from the Samoan "Vai trend" were described in Chapter 2 and are revisited in Chapter 3 along with sulfur in samples representing the two additional geochemical trends: the Malu trend, associated with EM II components, and the Upo Trend, associated with depleted MORB components. This research also examines a fourth relationship revealed by basalts from rejuvenated volcanism that illustrate a dilute contribution from EM I – type components. Given the unique isotope composition associated with basalts from the Vai trend, we test whether other mantle components erupted at Samoa host unique isotope compositions and evaluate how the complex plumbing system of the hotspot beneath Samoa plays a role in the S-isotope compositions erupted at specific islands. Furthermore, the S-isotope data presented in chapter 3 provide insight into the distribution of recycled mantle components in the mantle and their geochemical effect on basalts erupted globally.

The data from the Vai trend are correlated with a distance parameter $D^{206,207,208Pb}$ that illustrates (in three dimensions) a geochemical distance from the primordial "common component". As samples plot further away from the common component, the $\Delta^{33}S$ values increases, further supporting the presence of a recycled sulfur component in the Samoan HIMU endmember.

Volcanic glass associated sulfur from the Malu trend (EM II) has been studied previously by Labidi et al. (2015) and is shown to carry a recycled post-Archean signature. The $\Delta^{33}S$ analyses presented on samples from the Malu trend (EM II) in chapter 3 are generally consistent with this finding, however, one sample yields a $\Delta^{33}S$ value of +0.028‰ ± 0.008. Although the lead data overlap the Vai trend, this one

sample does not fall on the relationship between $\Delta^{33}S$ and $D^{206,207,208Pb}$ observed for the Vai trend samples. Thus, the sample may include HIMU sulfur, but the observation merits further investigation.

The rejuvenated basalts (EM I) from Savai'i and Upolu have $\Delta^{33}S$ values that range from -0.018‰ ±0.008 to 0.015‰ ± 0.008. $\Delta^{33}S$ values show scatter over a small range of $D^{206,207,208Pb}$ that suggests variability of $\Delta^{33}S$ in this EM I-influenced source. The $\Delta^{33}S$ values observed at the type locality for EM I (Pitcairn) have been determined by SIMS and extend to -0.85‰ (Delavault et al., 2016), suggesting a contribution from recycled Archean sulfur. The observations from rejuvenated lavas of Samoa also provide support for variable $\Delta^{33}S$ in an EM I endmember and may be linked to the source of sulfur erupted at Pitcairn or a more recently subducted component with similar radiogenic lead characteristics.

A drill core from Tutuila show a change in source composition with depth using radiogenic isotope compositions (Reinhard et al., 2019). We see no evidence for a change in $\Delta^{33}S$ with depth at this island. Finally, shield-stage basalts from Upolu and Tutuila (representing the Upo trend (DM)) all have $\Delta^{33}S$ values within uncertainty of the origin ($\Delta^{33}S=0$). This finding is in agreement with $\Delta^{33}S$ shown for MORB (e.g. Labidi et al., 2014). Note that the Upo trend represents some of the oldest parts of the hotspot track at Samoa. Such would suggest that the $\Delta^{33}S$ observed for the Upo trend is that of the original basalts erupted when forming the Samoan Islands.

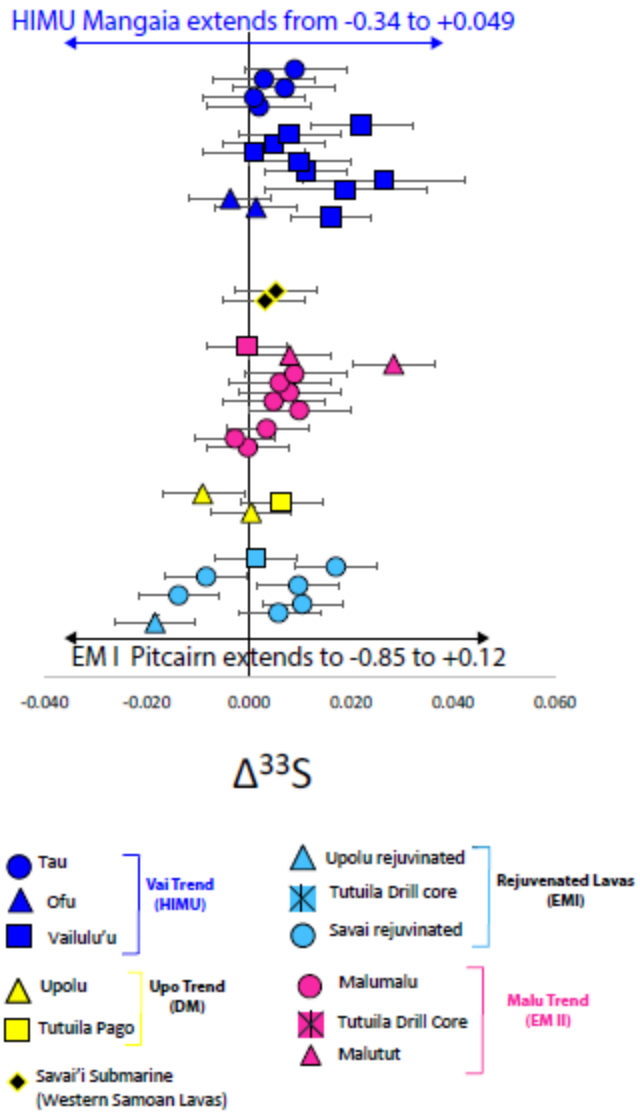

Figure 29. $\Delta^{33}S$ for all data collected for Samoan basalts highlighted by their associated geochemical trend. The Vai trend and rejuvenated basalts have unique $\Delta^{33}S$ that are likely do to influence from distinct recycled sources. Also highlighted is the range of compositions observed for HIMU and EM I at their type localities, Mangaia and Pitcairn respectively. The positive $\Delta^{33}S$ in the Vai trend may be linked to the new endmember identified in (chapter 4 see below). The negative $\Delta^{33}S$ in the rejuvenated basalts may be linked to EM I sulfur at Pitcairn as most sulfides exhibit negative $\Delta^{33}S$.

5.3 Sulfur from a crystalizing magma chamber: Characterization of HIMU sulfur at Mangaia

Mangaia, the type locality for the HIMU mantle endmember has been argued to host Archean related sulfide due to observations of S-MIF in a study by (Cabral et al. (2013). Research in chapter 4 revisits the question of Archean related sulfur at Mangaia through bulk sulfur isotope analyses of sulfide in melt inclusion from olivine and pyroxene phenocrysts. This method allows for analysis of sulfur trapped at depth in the magma chamber that avoids analysis of sulfur altered by post-magmatic processes. Trapping at depth also permits the sulfur from inclusions in phenocrysts to capture evidence for mixing of magmas with different sulfur isotopic compositions.

Several features of the Mangaia phenocryst data point to mixing of sulfur from at least three different sources. The exact nature of the material that produced the HIMU geochemical signatures, however, remains a subject of debate and may be linked to upper portions of subducted oceanic crust or a metasomatized subcontinental lithospheric component. The data presented do not show negative $\Delta^{33}S$ like that previously observed, but rather slightly positive $\Delta^{33}S$ (up to +0.049‰ ± 0.016), indicative of an exogenic source (connected to Earth's surface). Further, a subset of samples form an array among $\delta^{34}S$ vs. $\Delta^{33}S$. Among the data in this array is discrepancy between S-isotope compositions of sulfur in olivine and pyroxene from the same sample. The combination of this array and isotopic disequilibrium among phenocrysts from the same sample leads to arguments that the array illustrates the trapping of sulfur with an exotic composition during different stages of crystallization. This argument is in agreement with previous observations of heterogeneity in Pb isotope compositions

of melt inclusions from Mangaia and the forsterite compositions of the olivine in Mangaia basalts.

Pb isotope compositions also aid in determining a relative age difference among the sources contributing to the HIMU mantle source feeding Mangaia. The Pb isotope heterogeneity observed in whole rock analyses of Mangaia basalts demonstrate a potential relationship with $\Delta^{33}S$ from the phenocryst analyses. The relationship suggests the component that contributes slightly positive $\Delta^{33}S$ is relatively younger than the source that contributes negative $\Delta^{33}S$. Such invokes the potential need for an additional mantle reservoir that contributes recycled sulfur that is different from the slab graveyard at the base of the mantle that is thought to host the Archean related sulfur.

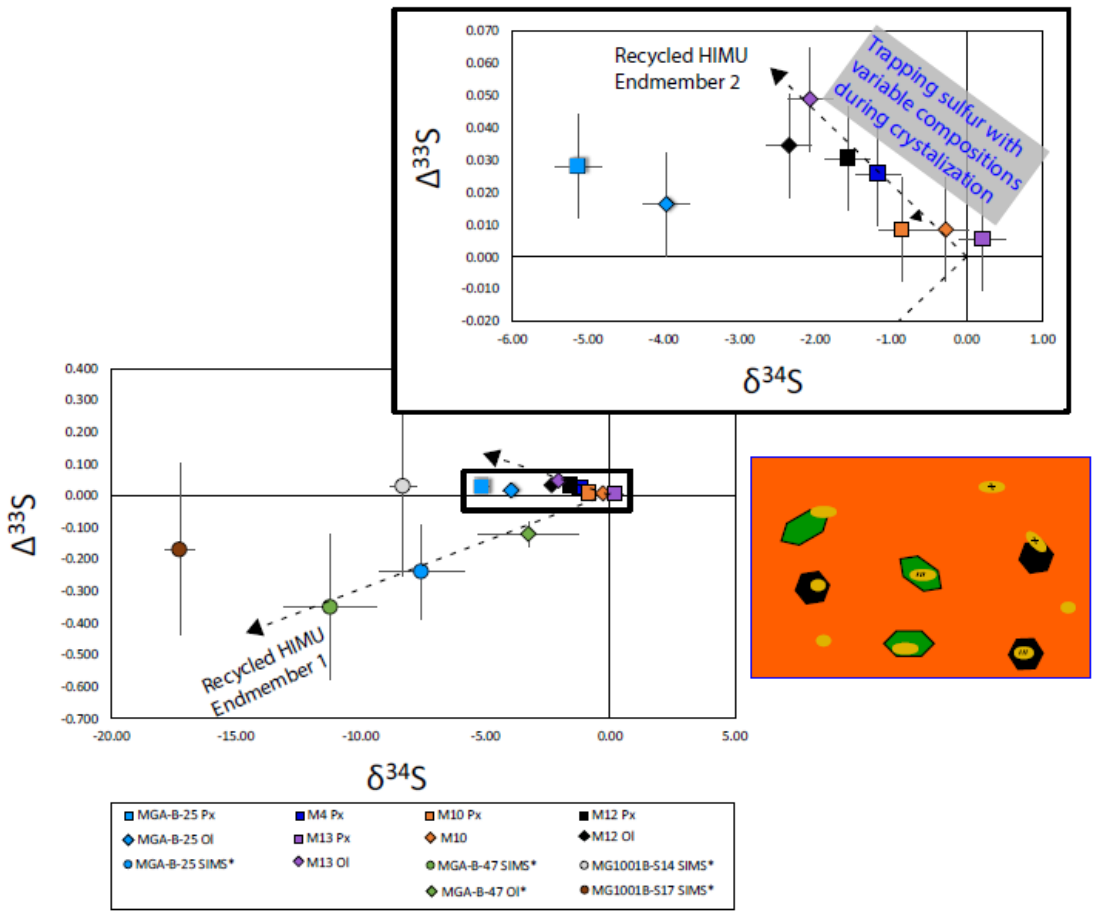

Figure 30. Compilation of S-isotope data collected at Mangaia with dotted mixing lines illustrating the two proposed recycled endmembers. Also included is a cartoon that illustrates how sulfur is trapped in olivine and pyroxene in the magma chamber.

5.4 Future Directions

5.4.1 Looking forward from chapter 2

The work in chapter 2 utilizes relationships between the isotopic compositions of sulfur, tungsten, helium, and lead, to place constraints on the primordial sulfur isotope composition of the mantle and identifies variable S sources that contribute to the overall isotopic heterogeneity seen at Samoa. One area in which the research can be expanded relates to the type of samples. The samples analyzed were bulk rock

powders that notoriously exhibit evidence of degassing. This process overprints signatures of primary mantle or core interaction and complicates detection of the mass dependent isotope composition of deep primordial reservoirs. Studies targeting unaltered, undegassed samples of basalt glass which are less susceptible to these effects present opportunity for future work.

Another opportunity for future work is through extension to a broader sampling of localities exhibit a similar W-He relationship (e.g. Hawaii) and W isotope anomalies (e.g. Baffin Island or OJP) indicative of contributions from primordial sources. Baffin Island and Ontong Java Plateau are particularly interesting targets because they exhibit positive ^{182}W anomalies instead of negative. An interesting project would be to test to see if there are compositional differences in S between the two localities. Any difference in the S isotope composition of primordial endmembers could provide constraints on processes that fractionate sulfur such as core formation, metal silicate partitioning, or core-mantle exchange.

The promise of information added by S isotopes has been realized by the work to date and as time progresses, more contributions from primordial reservoirs are being discovered. Our knowledge of the field is growing rapidly. In order to maintain the overall understanding of the origin of these reservoirs and their evolution, complementary S-isotope analyses has proven to be a critical addition.

5.4.2 Looking forward from Chapter 3

The work in chapter 2 identified a unique S-isotope composition associated with a HIMU influenced sample. The work in chapter 3 builds off of that observation

and tests whether the other geochemical trends host unique S-isotope compositions. A major observation from this study was the negative $\Delta^{33}S$ observed in a rejuvenated basalt from Upolu island that suggests rejuvenated lavas at Samoa with diluted EM I-like compositions host sulfur with negative $\Delta^{33}S$. With the data set presented, no clear links can be drawn between the sulfur at Pitcairn (EMI) and rejuvenated S at Samoa but it is worth pursuing further. An avenue of pursuit would be through the analysis of bulk rock powder of Pitcairn basalts in order to get a sense of the $\Delta^{33}S$ of bulk sulfide and compare that to rejuvenated basalts at Samoa, additionally it is worth analyzing bulk rock powders at other localities that demonstrate EM I characteristics. In chapter 2, we see that the $\Delta^{33}S$ of the HIMU influenced endmember is positive which contrasts with that observed by Cabral et al. (2013) but is in agreement with observations in chapter 4. A similar type of observation may be observed if other EM I type basalts are measured.

The research on this specific topic of geochemical geometry can be expanded to making more measurements to confirm the results observed. The data set is limited to one rejuvenated basalt from Upolu island. Additional analyses on rejuvenated basalts from Upolu would aid in constraining the $\Delta^{33}S$ of melt that feeds those lavas. Additional analyses should also be performed on samples from the Tutuila drill core. From the data set, it is very clear that anomalous $\Delta^{33}S$ is not prevalent in the Samoan samples. Considering only two samples were analyzed, the research could benefit from additional analyses from each section of the core, to confirm the lack of anomalous $\Delta^{33}S$.

5.4.3 Looking forward from Chapter 4

The work in chapter 4 revisits determining the S-isotope composition of basalts from Mangaia, the type locality for the HIMU mantle reservoir, through bulk S-isotope analyses of sulfide hosted in melt inclusions within olivine and pyroxene phenocrysts in order to determine the prevalence of Archean sulfides in the Mangaia mantle source. Research on this topic can be expanded to bulk rock powders using methods described in chapter 3. When trying to characterize the mixing endmembers relative to Pb isotope compositions, the interpretation was limited to comparing the bulk sulfide data from olivine and pyroxene to lead isotope data collected on bulk rock powders. Although some conclusions were able to be drawn, a better comparison would involve S-isotope analyses on a bulk rock powder.

An S-isotope analysis of the bulk rock powders would also aid in identifying any other sources of S-that was not trapped in olivine or pyroxene. The data presented represent a pristine, unaltered melt composition of the magma chamber. However, the specifics on sulfide entrapment circumstances remain poorly understood, leaving an entire fraction of uncaptured sulfide analyzed. Bulk rock data could provide insight into any other S-sources that may exist in the HIMU source at Mangaia.

The research topic could also benefit from a reanalysis of MGA-B-47, the critical sample studied by Cabral et al., 2013, using wet chemistry methods involving HF and mass spectrometry methods that involve longer analysis. With the alternative method, there is the potential to extract more S which would decrease the level of uncertainty on $\delta^{34}S$ from fluorinations and allow for longer analysis which would decrease the uncertainty on $\Delta^{33}S$.

A major observation in chapter 4 was the mismatch in S-isotope composition in MGA-B-25 between the SIMS method and the SF_6 method. As it stands, a concrete understanding of this observation has not been developed and is simply described as heterogeneity in the source that contributes sulfur to the melts associated with MGA-B-25. Given the mismatch, it is important that a SIMS study on sulfides from M4-M13 is conducted 1.) for completeness, and 2.) to test whether similar levels of heterogeneity exist or if the S-isotope compositions match. Such will aid in pinning down the various sources that contribute to HIMU at Mangaia and may also potentially identify isotopic endmembers that are mixed in.

5.4.4 Future directions for sulfur in OIB

The sulfur isotope data presented in this dissertation demonstrate that the sulfur isotope composition of the mantle is undoubtedly heterogenous. At both Mangaia and Samoa, $\Delta^{33}S$ is positive and negative and reflects a contribution of multiple recycled components. Such is a demonstration that the S-isotope composition of OIBs are unpredictable, and rather, reflects the complex mixing of melts that host multiple mantle components. As basalts from other ocean islands are analyzed, it is critical that the data are evaluated in the context of the variety of recycled components that exist in the mantle. As seen at Samoa, recycled components do not appear to be returned to a single locality and are rather dispersed throughout the mantle and incorporated into plumes in various proportions. Thus, future S-isotope data collected on OIB can benefit from evaluation in the context of other isotope systems, such as those of Sr, Nd, and Pb, to constrain the overall influence of recycled components globally in OIB.

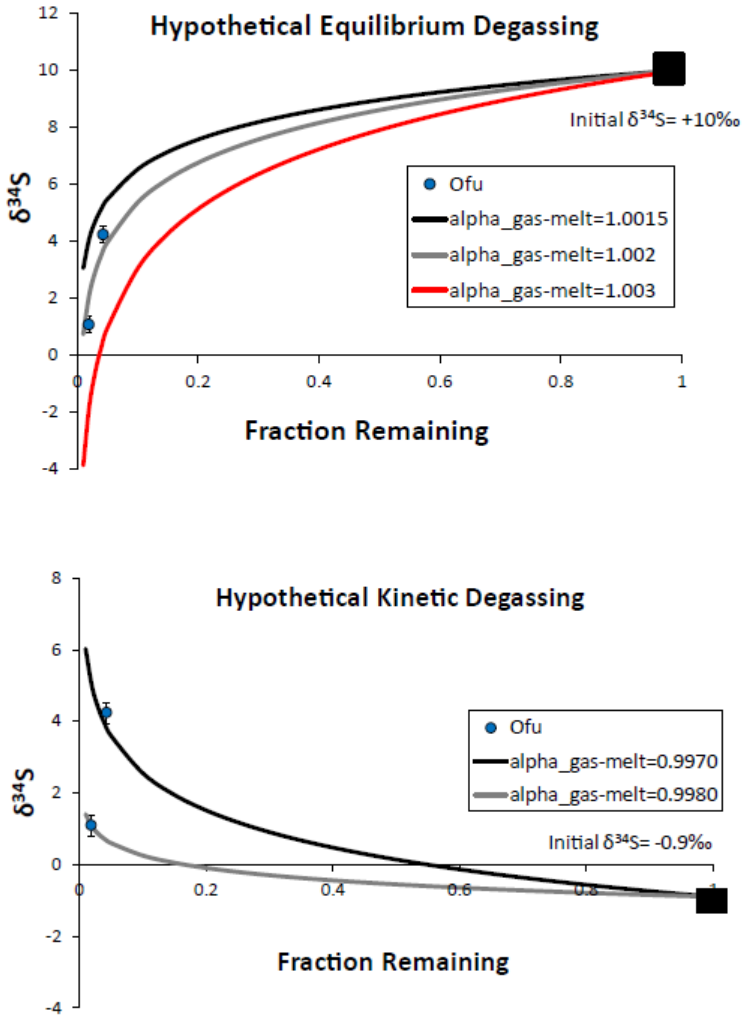

Figure 31. Plots of fraction remaining versus $\delta^{34}S$ illustrating hypothetical Rayleigh-type degassing for starting compositions with positive and negative $\delta^{34}S$ and equilibrium and kinetic isotope effects ($\alpha_{equilibrium} > 1.000 > \alpha_{kinetic}$). For equilibrium degassing, we use recycled endmember of $\delta^{34}S$ =+10‰ as suggested by Labidi et al. (2015). In the case of kinetic degassing, we use the inferred mantle composition of -0.9‰ (Labidi et al., 2014). In the case of both equilibrium and kinetic degassing, we cannot fit the data with a single fractionation factor. Equilibrium fractionation factors shown are those calculated and reported by Mandeville et al., 2009 for SO_2 degassing at 1200 ˚C. Kinetic fractionation factors shown are empirical where alpha_gas-melt= alpha_empirical/alpha_equilibrium (de Moor et al., 2013).

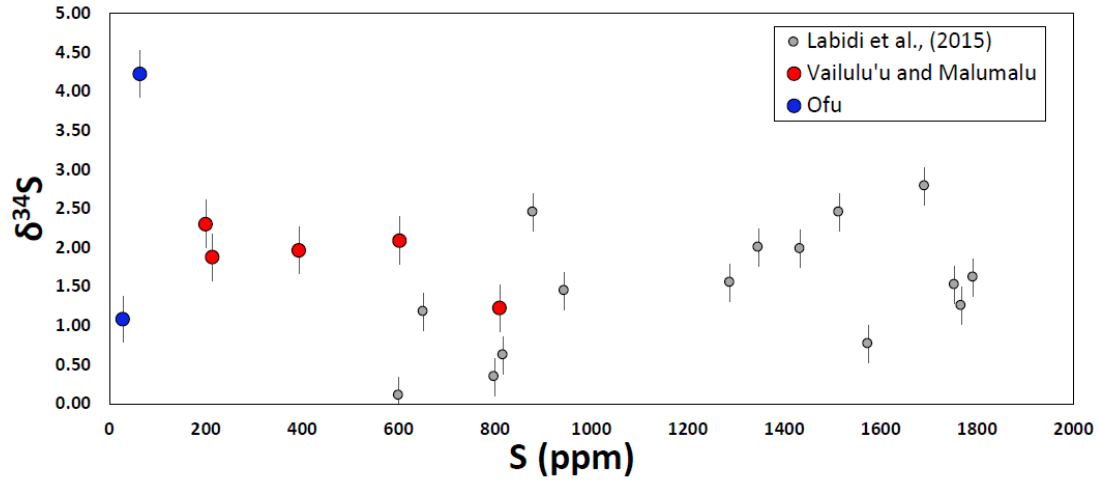

Figure 32**.** Plot of S concentration (ppm) vs. $\delta^{34}S$ for samples presented in chapter 3.

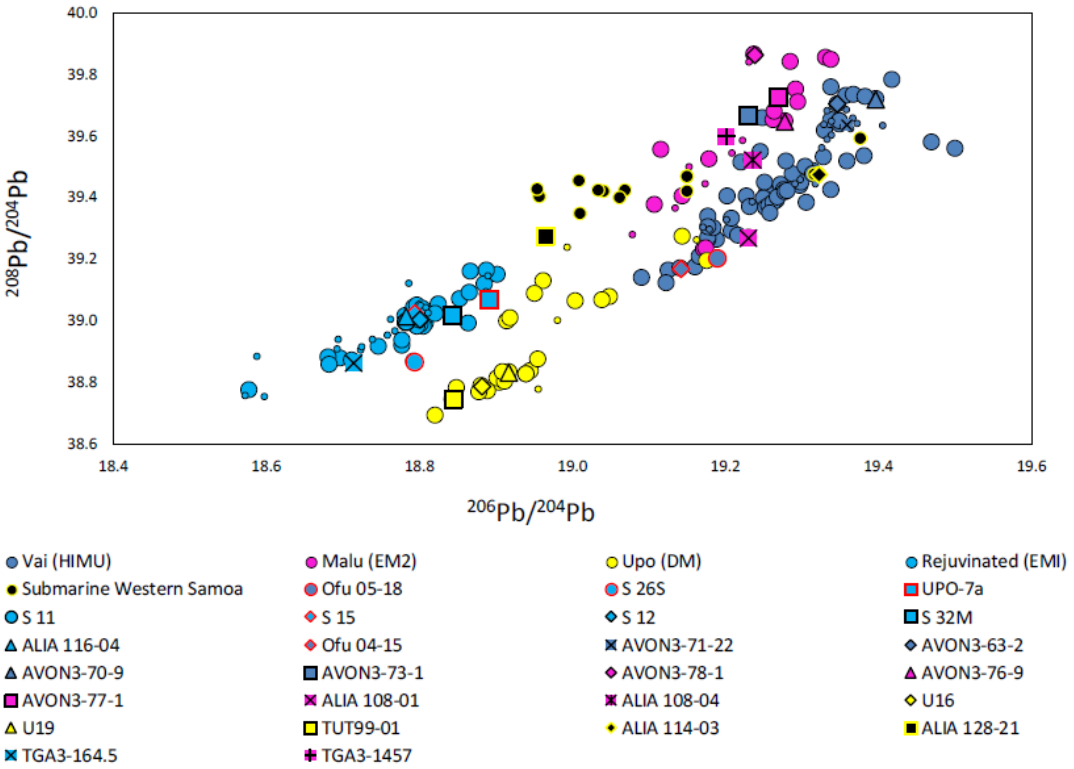

Figure 33. Data compilation from Jackson et al. (2014), highlighting the samples measured in chapter 2 and chapter 3.

Table 7. Model inputs for Bayesian Model selection

Sample	$\Delta^{33}S$ (1 σ)	$\mu^{182}W$ (1 σ)	$^{3}He/^{4}He$ (1 σ)	$^{206}Pb/^{204}Pb$ (1 σ)
AVON3-63-2	0.019	-4.9	10.06	19.3578
	0.008	1.05	0.05	0.0009
AVON3-70-9	0.027	-5.8	8.05	19.396
	0.008	2.6	0.1	0.0002
AVON3-71-22	0.009	-2.8	9.64	19.358
	0.004	2.0	0.1	0.0097
AVON3-73-1	0.01	-7.7	8.1	19.2299
	0.004	1.9	0.1	0.0001
AVON 3-77-1	0.004	-7.45	13.45	19.2683
	0.004	2	0.1	0.00015
OFU-04-15	0.001	-13.7	29.6	19.141
	0.004	2.4	0.2	0.00095
OFU-05-18	-0.004	-13.8	33.8	19.189
	0.004	1.7	0.2	0.00095

†Model Priors	$\Delta^{33}S$ vs. $\mu^{182}W$	$\Delta^{33}S$ vs. $^{3}He/^{4}He$	$\Delta^{33}S$ vs. $^{206}Pb/^{204}Pb$
Slope	(-0.0028 to 0.0028)	(-0.0014 to 0.0014)	(-0.1824 to 0.1824)
Y-intercept	(-0.0405 to 0.0405)	(-0.0405 to 0.0405)	(-3.1050 to 3.1050)

†Prior on slope and y-intercept are uniform. Data in table are from (Workman et al., 2004; Jackson et al., 2007b; Jackson et al., 2014; Mundl et al., 2017; Horan et al., 2018).

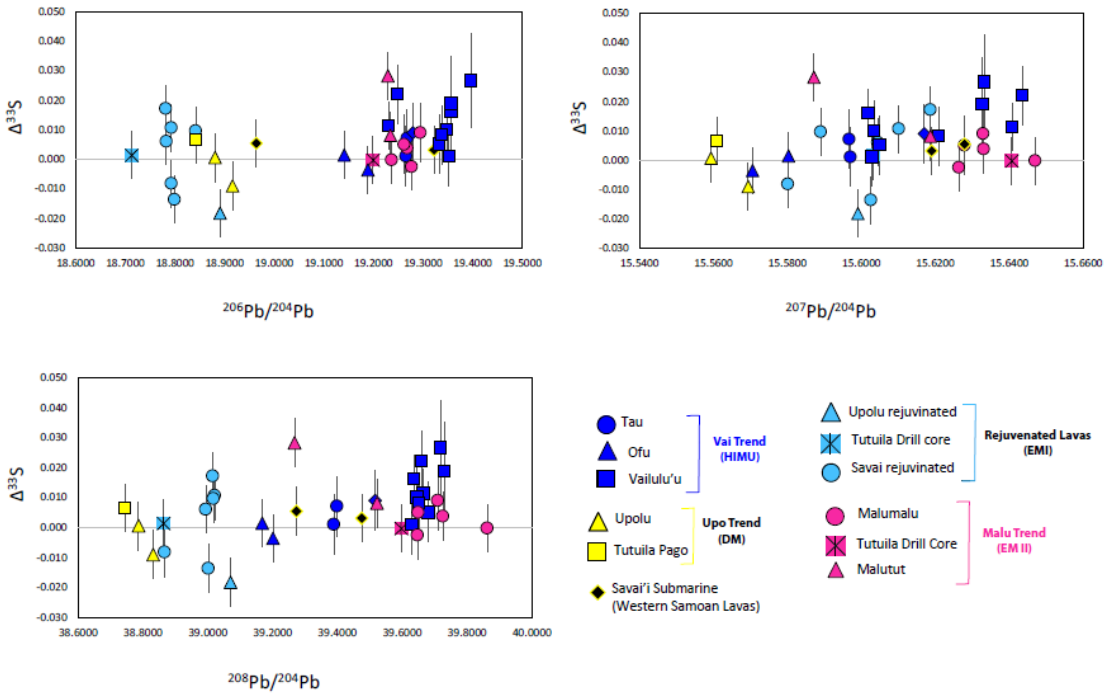

Figure 34. Panel plot of radiogenic Pb isotope compositions vs. $\Delta^{33}S$ for Samoan Basalts

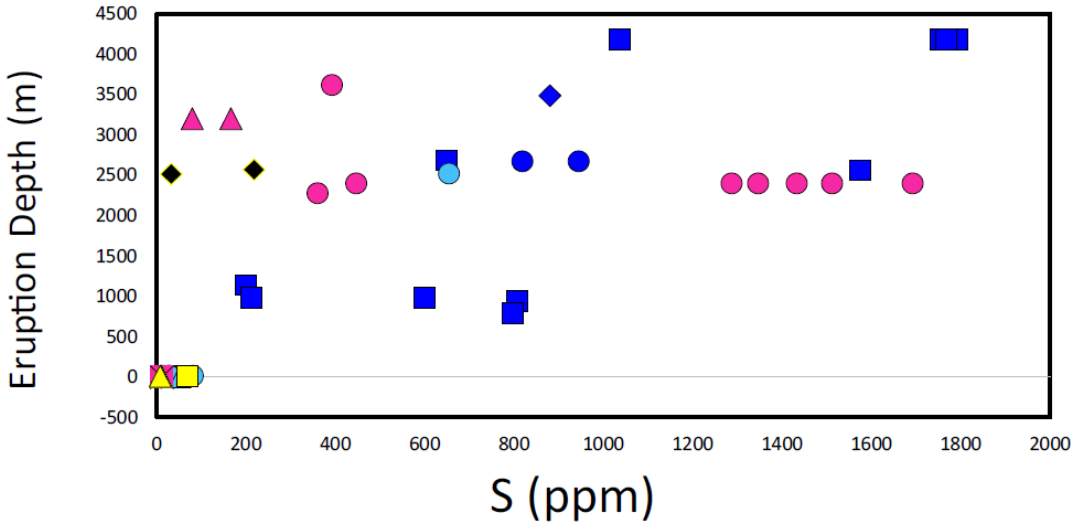

Figure 35. S (ppm) vs. eruption depth of Samoan Basalts from Chapter 3. The plots includes data from Dottin et al., (2020) and Labidi et al., (2015) Submarine basalts typically have higher S concentrations, however, the data show no clear relationship between the depth of eruption and the S concentration.

Bibliography

Alt J. C. (1995) Sulfur isotopic profile through the oceanic crust: Sulfur mobility and seawater-crustal sulfur exchange during hydrothermal alteration. *Geology* **23**, 585–588.

Alt J. C. and Shanks W. C. (2011) Microbial sulfate reduction and the sulfur budget for a complete section of altered oceanic basalts, IODP Hole 1256D (eastern Pacific). *Earth Planet. Sci. Lett.* **310**, 73–83.

Antonelli M. A., Kim S.-T., Peters M., Labidi J., Cartigny P., Walker R. J., Lyons J. R., Hoek J. and Farquhar J. (2014) Early inner solar system origin for anomalous sulfur isotopes in differentiated protoplanets. *Proc. Natl. Acad. Sci. U. S. A.* **111**, 17749–54. Available at: http://www.ncbi.nlm.nih.gov/pubmed/25453079.

Beaudry P., Longpré M.-A., Economos R., Wing B. A., Bui T. H. and Stix J. (2018) Degassing-induced fractionation of multiple sulphur isotopes unveils post-Archaean recycled oceanic crust signal in hotspot lava. *Nat. Commun.* **9**, 5093.

Bigeleisen J. (1996) Nuclear size and shape effects in chemical reactions. Isotope chemistry of the heavy elements. *J. Am. Chem. Soc.* **118**, 3676–3680.

Bigeleisen J. and Wolfsberg M. (1958) Advances in chemical physics. Vol. 1. *Intersci. Prlblishers Inc., New York*, 15.

Burgisser A., Alletti M. and Scaillet B. (2015) Simulating the behavior of volatiles belonging to the C–O–H–S system in silicate melts under magmatic conditions with the software D-Compress. *Comput. Geosci.* **79**, 1–14.

Cabral R. A., Jackson M. G., Koga K. T., Rose-Koga E. F., Hauri E. H., Whitehouse M. J., Price A. A., Day J. M. D., Shimizu N. and Kelley K. A. (2014) Volatile

cycling of H2O, CO 2, F, and C l in the HIMU mantle: A new window provided by melt inclusions from oceanic hot spot lavas at M angaia, C ook I slands. *Geochemistry, Geophys. Geosystems* **15**, 4445–4467.

Cabral R. A., Jackson M. G., Rose-Koga E. F., Koga K. T., Whitehouse M. J., Antonelli M. A., Farquhar J., Day J. M. D. and Hauri E. H. (2013a) Anomalous sulphur isotopes in plume lavas reveal deep mantle storage of Archaean crust. *Nature* **496**, 490–493.

Cabral R. A., Jackson M. G., Rose-Koga E. F., Koga K. T., Whitehouse M. J., Antonelli M. A., Farquhar J., Day J. M. D. and Hauri E. H. (2013b) Anomalous sulphur isotopes in plume lavas reveal deep mantle storage of Archaean crust. *Nature* **496**, 490–493. Available at: http://dx.doi.org/10.1038/nature12020.

Canfield D. E. (2004) The evolution of the Earth surface sulfur reservoir. *Am. J. Sci.* **304**, 839–861.

Canfield D. E. and Farquhar J. (2009) Animal evolution, bioturbation, and the sulfate concentration of the oceans. *Proc. Natl. Acad. Sci.* **106**, 8123–8127.

Cao X. and Liu Y. (2011) Equilibrium mass-dependent fractionation relationships for triple oxygen isotopes. *Geochim. Cosmochim. Acta* **75**, 7435–7445.

Castillo P. R. (2016) A proposed new approach and unified solution to old Pb paradoxes. *Lithos* **252**, 32–40.

Chauvel C., Hofmann A. W. and Vidal P. (1992) HIMU-EM: the French Polynesian connection. *Earth Planet. Sci. Lett.* **110**, 99–119.

Cottaar S. and Romanowicz B. (2012) An unsually large ULVZ at the base of the mantle near Hawaii. *Earth Planet. Sci. Lett.* **355**, 213–222.

Dauphas N. and Morbidelli A. (2014) Geochemical and planetary dynamical views on the origin of Earth'atmosphere and oceans. *Treatise Geochem* **6**, 1–35.

Delavault H., Chauvel C., Thomassot E., Devey C. W. and Dazas B. (2016) Sulfur and lead isotopic evidence of relic Archean sediments in the Pitcairn mantle plume. *Proc. Natl. Acad. Sci.* **113**, 12952–12956.

Domagal-Goldman S. D., Kasting J. F., Johnston D. T. and Farquhar J. (2008) Organic haze, glaciations and multiple sulfur isotopes in the Mid-Archean Era. *Earth Planet. Sci. Lett.* **269**, 29–40.

Dottin III J. W., Labidi J., Lekic V., Jackson M. G. and Farquhar J. (2020) Sulfur isotope characterization of primordial and recycled sources feeding the Samoan mantle plume. *Earth Planet. Sci. Lett.* **534**, 116073.

Dottin James W., Farquhar J. and Labidi J. (2018a) Multiple sulfur isotopic composition of main group pallasites support genetic links to IIIAB iron meteorites. *Geochim. Cosmochim. Acta* **224**, 276–281.

Dottin James W., Farquhar J. and Labidi J. (2018b) Multiple sulfur isotopic composition of main group pallasites support genetic links to IIIAB iron meteorites. *Geochim. Cosmochim. Acta* **224**, 276–281. Available at: https://doi.org/10.1016/j.gca.2018.01.013.

Dottin James W, Labidi J., Farquhar J., Piccoli P., Liu M.-C. and McKeegan K. D. (2018) Evidence for oxidation at the base of the nakhlite pile by reduction of sulfate salts at the time of lava emplacement. *Geochim. Cosmochim. Acta*. Available at: http://www.sciencedirect.com/science/article/pii/S0016703718304150.

Dreibus G. and Palme H. (1996) Cosmochemical constraints on the sulfur content in the Earth's core. *Geochim. Cosmochim. Acta* **60**, 1125–1130.

Farquhar J., Bao H. and Thiemens M. (2000) Atmospheric Influence of Earth's Earliest Sulfur Cycle. *Science (80-.).* **289**, 757–758.

Farquhar J. and Jackson M. (2016) Missing Archean sulfur returned from the mantle. *Proc. Natl. Acad. Sci.* **113**, 12893–12895.

Farquhar J., Johnston D. T. and Wing B. A. (2007) Implications of conservation of mass effects on mass-dependent isotope fractionations: influence of network structure on sulfur isotope phase space of dissimilatory sulfate reduction. *Geochim. Cosmochim. Acta* **71**, 5862–5875.

Farquhar J., Savarino J., Airieau S. and Thiemens M. H. (2001) Observation of wavelength-sensitive mass-independent sulfur isotope effects during SO2 photolysis: Implications for the early atmosphere. **106**, 32829–32839.

Farquhar J., Wing B. A., McKeegan K. D., Harris J. W., Cartigny P. and Thiemens M. H. (2002) Mass-independent sulfur of inclusions in diamond and sulfur recycling on early Earth. *Science (80-.).* **298**, 2369–2372.

Farquhar J., Zerkle A. L. and Bekker A. (2014) Geologic and geochemical constraints on Earth's early atmosphere.

Fiege A., Holtz F., Shimizu N., Mandeville C. W., Behrens H. and Knipping J. L. (2014) Sulfur isotope fractionation between fluid and andesitic melt: an experimental study. *Geochim. Cosmochim. Acta* **142**, 501–521.

Franz H. B., Kim S.-T., Farquhar J., Day J. M. D., Economos R. C., McKeegan K. D., Schmitt A. K., Irving A. J., Hoek J. and Dottin J. (2014) Isotopic links between

atmospheric chemistry and the deep sulphur cycle on Mars. *Nature* **508**, 364–8. Available at: http://www.ncbi.nlm.nih.gov/pubmed/24740066.

Franz H. B., Wu N., Farquhar J. and Irving A. J. (2019) A new type of isotopic anomaly in shergottite sulfides. *Meteorit. Planet. Sci.* **54**, 3036–3051.

French S. W. and Romanowicz B. (2015) Broad plumes rooted at the base of the Earth's mantle beneath major hotspots. *Nature* **525**, 95.

Frost D. J., Liebske C., Langenhorst F., McCammon C. A., Trønnes R. G. and Rubie D. C. (2004) Experimental evidence for the existence of iron-rich metal in the Earth's lower mantle. *Nature* **428**, 409.

Gaillard F. and Scaillet B. (2009) The sulfur content of volcanic gases on Mars. *Earth Planet. Sci. Lett.* **279**, 34–43.

Gaillard F., Scaillet B. and Arndt N. T. (2011) Atmospheric oxygenation caused by a change in volcanic degassing pressure. *Nature* **478**, 229–232.

Gao X. and Thiemens M. H. (1993a) Isotopic composition and concentration of sulfur in carbonaceous chondrites. *Geochim. Cosmochim. Acta* **57**, 3159–3169.

Gao X. and Thiemens M. H. (1993b) Variations of the isotopic composition of sulfur in enstatite and ordinary chondrites. *Geochim. Cosmochim. Acta* **57**, 3171–3176. Available at: http://www.sciencedirect.com/science/article/pii/001670379390301C [Accessed January 27, 2016].

Graham D. W., Christie D. M., Harpp K. S. and Lupton J. E. (1993) Mantle plume helium in submarine basalts from the Galápagos platform. *Science (80-.).* **262**, 2023–2026.

Graham D. W., Larsen L. M., Hanan B. B., Storey M., Pedersen A. K. and Lupton J. E. (1998) Helium isotope composition of the early Iceland mantle plume inferred from the Tertiary picrites of West Greenland. *Earth Planet. Sci. Lett.* **160**, 241–255.

Hanan B. B. and Graham D. W. (1996) Lead and helium isotope evidence from oceanic basalts for a common deep source of mantle plumes. *Science (80-.).* **272**, 991–995.

Hauri E. H. and Hart S. R. (1993) ReOs isotope systematics of HIMU and EMII oceanic island basalts from the south Pacific Ocean. *Earth Planet. Sci. Lett.* **114**, 353–371.

Hawkesworth C. J., Mantovani M. S. M., Taylor P. N. and Palacz Z. (1986) Evidence from the Parana of south Brazil for a continental contribution to Dupal basalts. *Nature* **322**, 356.

Heidel C., Tichomirowa M. and Junghans M. (2013) Oxygen and sulfur isotope investigations of the oxidation of sulfide mixtures containing pyrite, galena, and sphalerite. *Chem. Geol.* **342**, 29–43.

Hilton D. R., Grönvold K., Macpherson C. G. and Castillo P. R. (1999) Extreme 3He/4He ratios in northwest Iceland: constraining the common component in mantle plumes. *Earth Planet. Sci. Lett.* **173**, 53–60.

Hofmann A., Bekker A., Rouxel O., Rumble D. and Master S. (2009) Multiple sulphur and iron isotope composition of detrital pyrite in Archaean sedimentary rocks: a new tool for provenance analysis. *Earth Planet. Sci. Lett.* **286**, 436–445.

Hofmann A. W. (1988) Chemical differentiation of the Earth: the relationship

between mantle, continental crust, and oceanic crust. *Earth Planet. Sci. Lett.* **90**, 297–314.

Honda M., McDougall I., Patterson D. B., Doulgeris A. and Clague D. A. (1993) Noble gases in submarine pillow basalt glasses from Loihi and Kilauea, Hawaii: a solar component in the Earth. *Geochim. Cosmochim. Acta* **57**, 859–874.

Horan M. F., Carlson R. W., Walker R. J., Jackson M., Garçon M. and Norman M. (2018) Tracking Hadean processes in modern basalts with 142-Neodymium. *Earth Planet. Sci. Lett.* **484**, 184–191.

Hulston J. R. and Thode H. G. (1965) Cosmic-Ray-Produced S and S in the Metallic Phase of Iron Meteorites. *J. Geophys. Res.* **70**.

Jackson C. R. M., Bennett N. R., Du Z., Cottrell E. and Fei Y. (2018) Early episodes of high-pressure core formation preserved in plume mantle. *Nat. Publ. Gr.* **553**, 491–495. Available at: http://dx.doi.org/10.1038/nature25446.

Jackson M. G. and Dasgupta R. (2008) Compositions of HIMU, EM1, and EM2 from global trends between radiogenic isotopes and major elements in ocean island basalts. *Earth Planet. Sci. Lett.* **276**, 175–186.

Jackson M. G., Hart S. R., Konter J. G., Kurz M. D., Blusztajn J. and Farley K. A. (2014) Helium and lead isotopes reveal the geochemical geometry of the Samoan plume. *Nature* **514**, 355–358. Available at: http://dx.doi.org/10.1038/nature13794.

Jackson M. G., Hart S. R., Koppers A. A. P., Staudigel H., Konter J., Blusztajn J., Kurz M. and Russell J. A. (2007a) The return of subducted continental crust in Samoan lavas. *Nature* **448**, 684.

Jackson M. G., Kurz M. D. and Hart S. R. (2009a) Helium and neon isotopes in phenocrysts from Samoan lavas : Evidence for heterogeneity in the terrestrial high 3 He / 4 He mantle. *Earth Planet. Sci. Lett.* **287**, 519–528. Available at: http://dx.doi.org/10.1016/j.epsl.2009.08.039.

Jackson M. G., Kurz M. D. and Hart S. R. (2009b) Helium and neon isotopes in phenocrysts from Samoan lavas : Evidence for heterogeneity in the terrestrial high 3 He / 4 He mantle. *Earth Planet. Sci. Lett.* **287**, 519–528.

Jackson M. G., Kurz M. D., Hart S. R. and Workman R. K. (2007b) New Samoan lavas from Ofu Island reveal a hemispherically. **264**, 360–374.

Johnston D. T. (2011) Multiple sulfur isotopes and the evolution of Earth's surface sulfur cycle. *Earth-Science Rev.* **106**, 161–183. Available at: http://www.sciencedirect.com/science/article/pii/S0012825211000249.

Johnston D. T., Farquhar J. and Canfield D. E. (2007) Sulfur isotope insights into microbial sulfate reduction: when microbes meet models. *Geochim. Cosmochim. Acta* **71**, 3929–3947.

Jugo P. J., Wilke M. and Botcharnikov R. E. (2010) Sulfur K-edge XANES analysis of natural and synthetic basaltic glasses: Implications for S speciation and S content as function of oxygen fugacity. *Geochim. Cosmochim. Acta* **74**, 5926–5938.

Kanehira K., Yui S., Sakai H. and Sasaki A. (1973) Sulphide globules tholeiite and from sulphur isotope the Mid-Atlantic Ridge near 30'N latitude. *Geochem. J.* **7**, 89–96.

Kelley K. A., Plank T., Farr L., Ludden J. and Staudigel H. (2005) Subduction

cycling of U, Th, and Pb. *Earth Planet. Sci. Lett.* **234**, 369–383.

Kelley K. A., Plank T., Ludden J. and Staudigel H. (2003) Composition of altered oceanic crust at ODP Sites 801 and 1149. *Geochemistry, Geophys. Geosystems* **4**.

Killingsworth B. A., Sansjofre P., Philippot P., Cartigny P., Thomazo C. and Lalonde S. V (2019) Constraining the rise of oxygen with oxygen isotopes. *Nat. Commun.* **10**, 1–10.

Konter J. G. and Jackson M. G. (2012) Large volumes of rejuvenated volcanism in Samoa: Evidence supporting a tectonic influence on late-stage volcanism. *Geochemistry, Geophys. Geosystems* **13**.

Konter J. G., Pietruszka A. J., Hanan B. B., Finlayson V. A., Craddock P. R., Jackson M. G. and Dauphas N. (2016) Unusual δ56Fe values in Samoan rejuvenated lavas generated in the mantle. *Earth Planet. Sci. Lett.* **450**, 221–232.

Koppers A. A. P., Russell J. A., Jackson M. G., Konter J., Staudigel H. and Hart S. R. (2008) Samoa reinstated as a primary hotspot trail. *Geology* **36**, 435–438.

Kruijer T. S. and Kleine T. (2018) No 182W excess in the Ontong Java Plateau source. *Chem. Geol.* **485**, 24–31.

Kurz M. D., Curtice J., Fornari D., Geist D. and Moreira M. (2009) Primitive neon from the center of the Galápagos hotspot. *Earth Planet. Sci. Lett.* **286**, 23–34.

Kurz M. D. and Geist D. (1999) Dynamics of the Galapagos hotspot from helium isotope geochemistry. *Geochim. Cosmochim. Acta* **63**, 4139–4156.

Kurz M. D., Jenkins W. J. and Hart S. R. (1982) Helium isotopic systematics of oceanic islands and mantle heterogeneity. *Nature* **297**, 43.

Kurz M. D., Jenkins W. J., Hart S. R. and Clague D. (1983) Helium isotopic variations in volcanic rocks from Loihi Seamount and the Island of Hawaii. *Earth Planet. Sci. Lett.* **66**, 388–406.

Kurz M. D., Meyer P. S. and Sigurdsson H. (1985) Helium isotopic systematics within the neovolcanic zones of Iceland. *Earth Planet. Sci. Lett.* **74**, 291–305.

Labidi J. and Cartigny P. (2016) Negligible sulfur isotope fractionation during partial melting: Evidence from Garrett transform fault basalts, implications for the late-veneer and the hadean matte. *Earth Planet. Sci. Lett.* **451**, 196–207.

Labidi J., Cartigny P., Birck J. L., Assayag N. and Bourrand J. J. (2012) Determination of multiple sulfur isotopes in glasses: a reappraisal of the MORB δ 34 S. *Chem. Geol.* **334**, 189–198.

Labidi J., Cartigny P., Hamelin C., Moreira M. and Dosso L. (2014) Sulfur isotope budget (32S, 33S, 34S and 36S) in Pacific-Antarctic ridge basalts: A record of mantle source heterogeneity and hydrothermal sulfide assimilation. *Geochim. Cosmochim. Acta* **133**, 47–67. Available at: http://dx.doi.org/10.1016/j.gca.2014.02.023.

Labidi J., Cartigny P. and Jackson M. G. (2015) Multiple sulfur isotope composition of oxidized Samoan melts and the implications of a sulfur isotope 'mantle array' in chemical geodynamics. *Earth Planet. Sci. Lett.* **417**, 28–39.

Labidi J., Cartigny P. and Moreira M. (2013) Non-chondritic sulphur isotope composition of the terrestrial mantle. *Nature* **501**, 208–211. Available at: http://dx.doi.org/10.1038/nature12490.

Labidi J., Farquhar J., Alexander C. M. O., Eldridge D. L. and Oduro H. (2017) Mass

independent sulfur isotope signatures in CMs: Implications for sulfur chemistry in the early solar system. *Geochim. Cosmochim. Acta* **196**, 326–350. Available at: http://www.sciencedirect.com/science/article/pii/S0016703716305610 [Accessed June 26, 2017].

Lau H. C. P., Mitrovica J. X., Davis J. L., Tromp J., Yang H.-Y. and Al-Attar D. (2017) Tidal tomography constrains Earth's deep-mantle buoyancy. *Nature* **551**, 321.

Li Y., Yu H., Gu X., Guo S. and Huang F. (2020) Silicon isotopic fractionation during metamorphic fluid activities: constraints from eclogites and ultrahigh-pressure veins in the Dabie orogen, China. *Chem. Geol.* **540**, 119550.

Lyons J. R. (2007) Mass-independent fractionation of sulfur isotopes by isotope-selective photodissociation of SO2. *Geophys. Res. Lett.* **34**, 1–5.

Macpherson C. G., Hilton D. R., Day J. M. D., Lowry D. and Grönvold K. (2005) High-3He/4He, depleted mantle and low-δ18O, recycled oceanic lithosphere in the source of central Iceland magmatism. *Earth Planet. Sci. Lett.* **233**, 411–427.

Madureira P., Moreira M., Mata J. and Allègre C. J. (2005) Primitive neon isotopes in Terceira Island (Azores archipelago). *Earth Planet. Sci. Lett.* **233**, 429–440.

Mahoney J., Nicollet C. and Dupuy C. (1991) Madagascar basalts: tracking oceanic and continental sources. *Earth Planet. Sci. Lett.* **104**, 350–363.

Mandeville C. W., Webster J. D., Tappen C., Taylor B. E., Timbal A., Sasaki A., Hauri E. and Bacon C. R. (2009) Stable isotope and petrologic evidence for open-system degassing during the climactic and pre-climactic eruptions of Mt. Mazama, Crater Lake, Oregon. *Geochim. Cosmochim. Acta* **73**, 2978–3012.

Mazza S. E., Gazel E., Bizimis M., Moucha R., Béguelin P., Johnson E. A., McAleer R. J. and Sobolev A. V (2019) Sampling the volatile-rich transition zone beneath Bermuda. *Nature* **569**, 398–403.

McKenzie D. and O'nions R. K. (1983) Mantle reservoirs and ocean island basalts. *Nature* **301**, 229.

Melander L. C. S. and Saunders W. H. (1980) *Reaction rates of isotopic molecules*., John Wiley & Sons.

Milner S. C. and le Roex A. P. (1996) Isotope characteristics of the Okenyenya igneous complex, northwestern Namibia: constraints on the composition of the early Tristan plume and the origin of the EM 1 mantle component. *Earth Planet. Sci. Lett.* **141**, 277–291.

Mojzsis S. J., Coath C. D., Greenwood J. P., McKeegan K. D. and Harrison T. M. (2003) Mass-independent isotope effects in Archean (2.5 to 3.8 Ga) sedimentary sulfides determined by ion microprobe analysis. *Geochim. Cosmochim. Acta* **67**, 1635–1658.

de Moor J. M., Fischer T. P., Sharp Z. D., King P. L., Wilke M., Botcharnikov R. E., Cottrell E., Zelenski M., Marty B. and Klimm K. (2013) Sulfur degassing at Erta Ale (Ethiopia) and Masaya (Nicaragua) volcanoes: Implications for degassing processes and oxygen fugacities of basaltic systems. *Geochemistry, Geophys. Geosystems* **14**, 4076–4108.

Moulik P. and Ekström G. (2016) The relationships between large-scale variations in shear velocity, density, and compressional velocity in the Earth's mantle. *J. Geophys. Res. Solid Earth* **121**, 2737–2771.

Mukhopadhyay S. (2012) Early differentiation and volatile accretion recorded in deep-mantle neon and xenon. *Nature* **486**, 101.

Mundl-Petermeier A., Walker R. J., Fischer R. A., Lekic V., Jackson M. G. and Kurz M. D. (2020) Anomalous 182W in high 3He/4He Ocean Island Basalts: Fingerprints of Earth's core? *Geochim. Cosmochim. Acta* **271**, 194–211.

Mundl-Petermeier A., Walker R. J., Jackson M. G., Blichert-Toft J., Kurz M. D. and Halldórsson S. A. (2019) Temporal evolution of primordial tungsten-182 and 3He/4He signatures in the Iceland mantle plume. *Chem. Geol.* **525**, 245–259.

Mundl A., Touboul M., Jackson M. G., Day J. M. D., Kurz M. D., Lekic V., Helz R. T. and Walker R. J. (2017) Tungsten-182 heterogeneity in modern ocean island basalts. *Science (80-.).* **356**, 66–69.

Natland J. H. (1980) The progression of volcanism in the Samoan linear volcanic chain. *Am. J. Sci.* **280**, 709–735.

Nebel O., Arculus R. J., van Westrenen W., Woodhead J. D., Jenner F. E., Nebel-Jacobsen Y. J., Wille M. and Eggins S. M. (2013) Coupled Hf–Nd–Pb isotope co-variations of HIMU oceanic island basalts from Mangaia, Cook-Austral islands, suggest an Archean source component in the mantle transition zone. *Geochim. Cosmochim. Acta* **112**, 87–101.

Oduro H., Harms B., Sintim H. O., Kaufman A. J., Cody G. and Farquhar J. (2011) Evidence of magnetic isotope effects during thermochemical sulfate reduction. *Proc. Natl. Acad. Sci.* **108**, 17635–17638.

Ohmoto H., Watanabe Y., Ikemi H., Poulson S. R. and Taylor B. E. (2006) Sulphur isotope evidence for an oxic Archaean atmosphere. *Nature* **442**, 908–911.

Ono S., Keller N. S., Rouxel O. and Alt J. C. (2012) Sulfur-33 constraints on the origin of secondary pyrite in altered oceanic basement. *Geochim. Cosmochim. Acta* **87**, 323–340.

Ono S., Wing B., Johnston D., Farquhar J. and Rumble D. (2006) Mass-dependent fractionation of quadruple stable sulfur isotope system as a new tracer of sulfur biogeochemical cycles. *Geochim. Cosmochim. Acta* **70**, 2238–2252.

Paul B., Woodhead J. D., Hergt J., Danyushevsky L., Kunihiro T. and Nakamura E. (2011) Melt inclusion Pb-isotope analysis by LA–MC-ICPMS: assessment of analytical performance and application to OIB genesis. *Chem. Geol.* **289**, 210–223.

Reinhard A. A., Jackson M. G., Blusztajn J., Koppers A. A. P., Simms A. R. and Konter J. G. (2019) "Petit Spot" Rejuvenated Volcanism Superimposed on Plume-Derived Samoan Shield Volcanoes: Evidence From a 645-m Drill Core From Tutuila Island, American Samoa. *Geochemistry, Geophys. Geosystems* **20**, 1485–1507.

Rizo H., Andrault D., Bennett N. R., Humayun M., Brandon A., Vlastélic I., Moine B., Poirier A., Bouhifd M. A. and Murphy D. T. (2019) 182W evidence for core-mantle interaction in the source of mantle plumes. *Geochemical Perspect. Lett.* **11**, 6–11.

Rizo H., Walker R. J., Carlson R. W., Horan M. F., Mukhopadhyay S., Manthos V., Francis D. and Jackson M. G. (2016) Preservation of Earth-forming events in the tungsten isotopic composition of modern flood basalts. *Science (80-.).* **352**, 809–812.

Robinson B. W. (1995) Sulphur isotope standards. *Int. At. Energy Agency TECDOC 825*, 39–45.

Rouxel O., Ono S., Alt J., Rumble D. and Ludden J. (2008a) Sulfur isotope evidence for microbial sulfate reduction in altered oceanic basalts at ODP Site 801. *Earth Planet. Sci. Lett.* **268**, 110–123.

Rouxel O., Shanks III W. C., Bach W. and Edwards K. J. (2008b) Integrated Fe-and S-isotope study of seafloor hydrothermal vents at East Pacific Rise 9–10 N. *Chem. Geol.* **252**, 214–227.

Saal A. E., Hart S. R., Shimizu N., Hauri E. H. and Layne G. D. (1998) Pb isotopic variability in melt inclusions from oceanic island basalts, Polynesia. *Science (80-.).* **282**, 1481–1484.

Saal A. E., Kurz M. D., Hart S. R., Blusztajn J. S., Blichert-Toft J., Liang Y. and Geist D. J. (2007) The role of lithospheric gabbros on the composition of Galapagos lavas. *Earth Planet. Sci. Lett.* **257**, 391–406.

Sakai H., Casadevall T. J. and Moore J. G. (1982) Chemistry and isotope ratios of sulfur in basalts and volcanic gases at Kilauea volcano, Hawaii. *Geochim. Cosmochim. Acta* **46**, 729–738.

Sakai H., Marais D. J. D., Ueda A. and Moore J. G. (1984) Concentrations and isotope ratios of carbon, nitrogen and sulfur in ocean-floor basalts. *Geochim. Cosmochim. Acta* **48**, 2433–2441.

Salters V. J. M. and Stracke A. (2004) Composition of the depleted mantle. *Geochemistry, Geophys. Geosystems* **5**.

Schauble E. A. (2007) Role of nuclear volume in driving equilibrium stable isotope

fractionation of mercury, thallium, and other very heavy elements. *Geochim. Cosmochim. Acta* **71**, 2170–2189.

Siedenberg K., Strauss H. and Hoffmann E. J. (2016) Multiple sulfur isotope signature of early Archean oceanic crust, Isua (SW-Greenland). *Precambrian Res.* **283**, 1–12.

Smit K. V, Shirey S. B., Hauri E. H. and Stern R. A. (2019) Sulfur isotopes in diamonds reveal differences in continent construction. *Science (80-.).* **364**, 383–385.

Sobolev A. V, Hofmann A. W., Kuzmin D. V, Yaxley G. M., Arndt N. T., Chung S.-L., Danyushevsky L. V, Elliott T., Frey F. A. and Garcia M. O. (2007) The amount of recycled crust in sources of mantle-derived melts. *Science (80-.).* **316**, 412–417.

Sobolev A. V and Shimizu N. (1993) Ultra-depleted primary melt included in an olivine from the Mid-Atlantic Ridge. *Nature* **363**, 151–154.

Starkey N. A., Stuart F. M., Ellam R. M., Fitton J. G., Basu S. and Larsen L. M. (2009) Helium isotopes in early Iceland plume picrites: Constraints on the composition of high 3He/4He mantle. *Earth Planet. Sci. Lett.* **277**, 91–100.

Strauss H. (2003) Sulphur isotopes and the early Archaean sulphur cycle. *Precambrian Res.* **126**, 349–361.

Strauss H. (1997) The isotopic composition of sedimentary sulfur through time. *Palaeogeogr. Palaeoclimatol. Palaeoecol.* **132**, 97–118.

Stuart F. M., Lass-Evans S., Fitton J. G. and Ellam R. M. (2003) High 3 He/4 He ratios in picritic basalts from Baffin Island and the role of a mixed reservoir in

mantle plumes. *Nature* **424**, 57.

Suer T. A., Siebert J., Remusat L., Menguy N. and Fiquet G. (2017) A sulfur-poor terrestrial core inferred from metal–silicate partitioning experiments. *Earth Planet. Sci. Lett.* **469**, 84–97.

Sun T. and Bao H. (2011) Thermal-gradient-induced non-mass-dependent isotope fractionation. *Rapid Commun. Mass Spectrom.* **25**, 765–773.

Thirlwall M. F. (1997) Pb isotopic and elemental evidence for OIB derivation from young HIMU mantle. *Chem. Geol.* **139**, 51–74.

Thomassot E., Cartigny P., Harris J. W., Lorand J. P., Rollion-Bard C. and Chaussidon M. (2009) Metasomatic diamond growth: A multi-isotope study (13C, 15N, 33S, 34S) of sulphide inclusions and their host diamonds from Jwaneng (Botswana). *Earth Planet. Sci. Lett.* **282**, 79–90.

Thorne M. S., Garnero E. J., Jahnke G., Igel H. and McNamara A. K. (2013) Mega ultra low velocity zone and mantle flow. *Earth Planet. Sci. Lett.* **364**, 59–67.

Thornton E. K. and Thornton E. R. (1970) *ORIGIN AND INTERPRETATION OF ISOTOPE EFFECTS.*, Pennslyvania Military Coll., Chester. Univ. of Pennsylvania, Philadelphia.

Trieloff M., Kunz J., Clague D. A., Harrison D. and Allègre C. J. (2000) The nature of pristine noble gases in mantle plumes. *Science (80-.).* **288**, 1036–1038.

Valbracht P. J., Staudacher T., Malahoff A. and Allègre C. J. (1997) Noble gas systematics of deep rift zone glasses from Loihi Seamount, Hawaii. *Earth Planet. Sci. Lett.* **150**, 399–411.

Weiss Y., Class C., Goldstein S. L. and Hanyu T. (2016) Key new pieces of the

HIMU puzzle from olivines and diamond inclusions. *Nature* **537**, 666–670.

Wicks J. K., Jackson J. M. and Sturhahn W. (2010) Very low sound velocities in iron-rich (Mg, Fe) O: Implications for the core-mantle boundary region. *Geophys. Res. Lett.* **37**.

Willbold M., Elliott T. and Moorbath S. (2011) The tungsten isotopic composition of the Earth's mantle before the terminal bombardment. *Nature* **477**, 195.

Williams C. D., Mukhopadhyay S., Rudolph M. L. and Romanowicz B. (2019) Primitive Helium is Sourced from Seismically Slow Regions in the Lowermost Mantle. *Geochemistry, Geophys. Geosystems*.

Williams Q. and Garnero E. J. (1996) Seismic evidence for partial melt at the base of Earth's mantle. *Science (80-.).* **273**, 1528–1530.

Wing B. A. and Farquhar J. (2015) Sulfur isotope homogeneity of lunar mare basalts. *Geochim. Cosmochim. Acta* **170**, 266–280.

Woodhead J. D. (1996) Extreme HIMU in an oceanic setting: The geochemistry of Mangaia Island (Polynesia), and temporal evolution of the Cook—Austral hotspot. *J. Volcanol. Geotherm. Res.* **72**, 1–19.

Workman R. K., Eiler J. M., Hart S. R. and Jackson M. G. (2008) Oxygen isotopes in Samoan lavas: Confirmation of continent recycling. *Geology* **36**, 551–554.

Workman R. K. and Hart S. R. (2005) Major and trace element composition of the depleted MORB mantle (DMM). *Earth Planet. Sci. Lett.* **231**, 53–72.

Workman R. K., Hart S. R., Jackson M., Regelous M., Farley K. A., Blusztajn J., Kurz M. and Staudigel H. (2004) Recycled metasomatized lithosphere as the origin of the Enriched Mantle II (EM2) end-member: Evidence from the Samoan

Volcanic Chain. *Geochemistry, Geophys. Geosystems* **5**, 1–44.

Workman R. K., Hauri E., Hart S. R., Wang J. and Blusztajn J. (2006) Volatile and trace elements in basaltic glasses from Samoa: Implications for water distribution in the mantle. *Earth Planet. Sci. Lett.* **241**, 932–951.

Wu N., Farquhar J., Dottin J. W. and Magalhães N. (2018) Sulfur isotope signatures of eucrites and diogenites. *Geochim. Cosmochim. Acta* **233**, 1–13.

Young E. D., Galy A. and Nagahara H. (2002) Kinetic and equilibrium mass-dependent isotope fractionation laws in nature and their geochemical and cosmochemical significance. *Geochim. Cosmochim. Acta* **66**, 1095–1104.

Yuan K. and Romanowicz B. (2017) Seismic evidence for partial melting at the root of major hot spot plumes. *Science (80-.).* **357**, 393–397.

Zerkle A. L., Claire M. W., Domagal-Goldman S. D., Farquhar J. and Poulton S. W. (2012) A bistable organic-rich atmosphere on the Neoarchaean Earth. *Nat. Geosci.* **5**, 359.

Zhang Z., Dorfman S. M., Labidi J., Zhang S., Li M., Manga M., Stixrude L., McDonough W. F. and Williams Q. (2016) Primordial metallic melt in the deep mantle. *Geophys. Res. Lett.* **43**, 3693–3699.

Zindler A. and Hart S. R. (1986) Chemical Geodynamics. *Annu. Rev. Earth Planet. Sci.* **14**, 493–571.